Title

A Synapse-level Characterization of Gustatory Receptor Neurons in Drosophila melanogaster

Author

Engert, Stefanie M

Publication Date

2021

Peer reviewed|Thesis/dissertation

A Synapse-level Characterization of Gustatory Receptor Neurons in *Drosophila melanogaster*

By

Stefanie Maria Engert

A dissertation submitted in partial satisfaction of the

requirements for the degree of

Doctor of Philosophy

in

Molecular and Cell Biology

in the

Graduate Division

of the

University of California, Berkeley

Committee in charge:

Professor Kristin Scott, Chair
Professor David Bilder
Professor Gian Garriga
Professor Noah Whiteman

Fall 2021

A Synapse-level characterization of Gustatory Receptor Neurons in *Drosophila melanogaster*

By Stefanie Maria Engert

Abstract

A Synapse-level Characterization of Gustatory Receptor Neurons in *Drosophila melanogaster*

By

Stefanie Maria Engert

Doctor of Philosophy in Molecular and Cell Biology
University of California, Berkeley
Professor Kristin Scott, Chair

Animals utilize the rich variety of chemicals in their surroundings to identify and evaluate food sources, communicate with conspecifics and detect predators. These vital functions have led to the evolution of sophisticated sensory systems for the detection of volatiles and dissolved chemicals in the form of olfactory and gustatory systems, respectively. In a testament to the universality of many of these evolutionary pressures, remarkably diverse animals have adopted similar schemes to most efficiently extract relevant chemosensory information, even though key details such as receptor identity and mechanism vary widely. In this work, we provide an extensive overview of the sensory organs, chemoreceptors and sensory coding strategies underlying taste and smell in common model organisms.

An especially attractive model to study gustation is the fruit fly *Drosophila melanogaster*. Not only does *Drosophila* detect a wide range of food compounds with a relatively small number of easily accessible sensory neurons, but there is also a vast array of sophisticated tools available to the fly neurobiology community. One such resource is a recent electron microscopy dataset of the entire adult fly brain. We used this dataset to reconstruct the majority of gustatory sensory neurons of the outer mouthparts. We further annotated all synaptic sites on these neurons to elucidate their connectivity. We utilized a combination of our anatomical and connectivity data to identify which taste modality reconstructed sensory neurons are likely to detect. We found that connectivity between sensory neurons is a common circuit motif and occurs mostly between neurons of the same type. We further explored the significance of these direct synaptic connections of neurons of the same and different modalities using a combination of calcium and voltage imaging. While we were not able to show functional connectivity between sensory neurons of different taste modalities, we did find preliminary evidence suggesting that excitatory connections exist between neurons of the same subclass. Lastly, we identified a second order gustatory neuron in the EM dataset and characterized its taste response profile, which was congruent with our assignment of its inputs' taste modality identities. Our studies provide a valuable gateway to the further exploration of the gustatory circuitry of *Drosophila* at synaptic detail.

To my parents, who never doubted
I could make it this far

Table of Contents

Chapter 1: Introduction to Chemosensory Systems in Common Model Organisms

Abstract

Organisms detect a rich variety of chemical cues in the environment that indicate the presence of food sources, predators or conspecifics. In unicellular organisms, detection of the surrounding chemical environment is accomplished via chemosensitive extracellular receptors. In many animals, a distinction is made between volatiles, which are detected by olfactory organs, and chemicals in solution, which are detected by the gustatory system. Given the vital and diverse roles of these chemical signals in behavior, it is not surprising that the molecular and neuronal foundations of chemosensation have been explored in great detail in a wide range of species. These studies have revealed common motifs across different forms of life that provide insight into not only the evolution of chemosensation but also the differing sensory strategies underlying smell and taste.

Here, I provide an overview of the receptors and/or sensory organs contributing to chemosensation in common model organisms: bacteria, the nematode *Caenorhabditis elegans*, mammalian models, and the fruit fly *Drosophila melanogaster*. While these divergent organisms differ significantly in the receptors and transduction mechanisms utilized by their sensory systems, there are striking parallels in the neuronal organization of smell and taste. Generally, the olfactory system is optimized to discriminate individual smells, necessitating a relatively large number of highly specialized cells and complex information processing. In contrast, gustation is marked by the pooling of information into categories, leading to a more limited number of sensory cells and a quality assessment of the stimulus at the primary sensory level. This chapter details fundamental insights from studies of peripheral chemosensory processing, which provide an invaluable basis for the exploration of central gustatory and olfactory circuitry.

Chemosensation in single celled organisms: On the Origin of Smell and Taste

Chemotaxis behaviors in single-celled organisms

The use of chemosensory information to guide feeding decisions is vital for all animals due to the presence of both nutrients and toxins in the environment. Indeed, the detection of chemicals is not restricted to multicellular organisms with dedicated chemosensory systems. Rather, relatively simple signaling mechanisms that recognize environmental chemicals, usually with transmembrane receptors, are widespread in bacteria and archaea, indicating the ancient evolutionary origin of these sensory systems across all clades. These rudimentary chemosensory systems most commonly aid in a locomotor behavior called chemotaxis. In many unicellular organisms, this behavior takes the form of a run-and-tumble pattern, where periods of straight forward movement (runs) are interspersed with random turning motions (tumbles). While moving through a substrate, the sensory system detects changes in the concentration of either attractive or repulsive chemicals. If unfavorable changes in the environment are detected, the microbe terminates the run and reorients itself via a tumble before initiating a new run. This run-and-tumble cycle is repeated until the desired orientation along the gradient is achieved: toward an attractant or away from a repellent (Berg & Brown 1972, Sourjik & Wingreen 2012).

Not surprisingly, attractants are often associated with potential food sources, such as sugars and amino acids (Adler et al 1973, Lambert et al 2012, Melton et al 1978, Moulton & Montie 1979, Ordal & Gibson 1977, Ordal et al 1979). Conversely, repellents are often indicative of harmful environmental conditions, such as a high pH or toxic chemicals (Seymour & Doetsch 1973, Smith & Doetsch 1969, Tso & Adler 1974, Young & Mitchell 1973). The individual attractant or repellent does not have to be biologically significant itself. It may correlate with the presence of relevant chemicals or be simply structurally similar enough to engage a receptor, even though it itself is value-neutral. For example, some attractants do not have any inherent metabolic value, such as the non-metabolizable galactose analogue D-fucose (Adler 1969). In this case, binding of the receptor is completely decoupled from the consumption of a nutritive substance.

Beyond the evaluation of food sources, chemosensory information can be a powerful tool for communication with conspecifics. One example of a “social” signaling system can be found in the slime mold *Dictyostelium*, which uses G protein coupled receptors (GPCRs) on its surface to detect trace amounts of cyclic AMP released by other amoeba under starvation conditions. In another instance of chemotaxis behavior, slime molds will orient in the direction of the highest concentration of cAMP to congregate and form a loose group of individual microbes behaving in a coordinated manner often described as a slug. This slug, or pseudoplasmodium, seeks out a more favorable environment by forming a fruiting body for sporulation and dispersal (Grutsch & Robertson 1978, Loomis 2014, Schaap et al 1984).

For single-celled organisms, analysis of the chemical environment is first and foremost a means of orientation for goal-directed locomotion. They generate a snapshot of their current chemical environment and evaluate it to assess changes of interest using rudimentary short-term “memory”. While this is a striking level of information processing in an individual cell, it naturally pales in comparison to the complexities of chemosensation in multicellular organisms. Many animals possess the ability to reliably

detect, and often even discriminate, a staggering number of chemicals, which can form the basis of complex behaviors such as associative learning. Additionally, they also communicate extensively with conspecifics in a wide array of social situations. Chemical cues in the environment are so central to survival that animals generally have devoted intricate specialized chemosensory systems to their detection: olfaction for the perception of volatile compounds and gustation for that of soluble chemicals.

Chemosensation in *Caenorhabditis elegans*: Neurons of many Trades

Chemotaxis in *C. elegans*

The microscopic nematode *Caenorhabditis elegans* feeds on a variety of soil bacteria in the wild. Its hunt for prey is largely dependent on its sensitive chemosensory system, which aids in a mode of chemotaxis behavior not dissimilar to that of bacteria: bouts of long relatively straight crawls are disrupted by periods of pirouetting to change direction. As in the bacterium *Escherichia coli*, the length of crawls (and, conversely, the frequency of pirouetting) is dependent on the chemical environment detected by the nematode. If the animal moves up a gradient of a chemoattractant, pirouettes are significantly less likely, and crawls are much longer than when the animal moves down the gradient. In addition to the pirouette-mechanism, *C. elegans* employ a second, parallel orientation strategy to increase the efficiency of their targeted locomotion, described commonly as the weathervane strategy. Slight adjustments of the heading direction during crawling periods lead to curved trajectories to better travel up the gradient of a chemoattractant, without having to resort to large turning maneuvers (Iino & Yoshida 2009). It is thought that the worm detects minute concentration differences that occur during each head swing in its sinusoidal movement to achieve this optimized orientation behavior (Izquierdo & Lockery 2010, Kato et al 2014). In both modes of locomotion, the most salient aspect of the sensory stimulus is therefore not the absolute concentration of the attractant, but the relative change in its concentration, as was also observed in bacterial chemotaxis (Appleby 2014, Pierce-Shimomura et al 2005, Pierce-Shimomura et al 1999, Ward 1973).

Chemosensory Organs and Receptors of *C. elegans*

Chemosensory organs in *C. elegans* are located at both the head and the tail of the animal (**Figure 1-1**). At the anterior end, these nematodes have two bilaterally symmetrical amphid organs housing 12 sensory neurons each. The dendrites of 11 of these neurons are bundled and wrapped by a sheath cell and a socket cell, forming a contained hair-like structure beneath the cuticle of the animal. The distal tips of only eight of these neurons are not entirely shielded by support cells and can directly interact with dissolved environmental chemicals via a pore in the cuticle (Ware et al 1975, White et al 1986). They are thought to be predominantly gustatory due to this anatomical characteristic; in contrast, the three neurons whose dendrites terminate near the distal end of the sheath are thought to be predominantly olfactory sensory neurons; the single neuron whose dendrite terminates within the sheath is not chemosensory (Bargmann et al 1993, Mori & Ohshima 1995, Troemel et al 1995). Additional chemosensory neurons in the head of the worm are located in the six inner labial organs, which are structured similarly to the amphid organs, but are much simpler. They only contain two sensory

neurons each and are located close to the mouth opening of the animal (Ward et al 1975). At the tail of the worm, the two bilaterally symmetrical phasmid organs also only house two neurons each (White et al 1986). It is important to note that, in addition to their roles in chemosensation, a majority of these neurons also contribute to other sensory modalities, which complicates their role in sensory processing in fascinating ways (Metaxakis et al 2018).

Chemosensitivity is conferred upon these sensory neurons by the expression of receptor proteins. Even though only about 30 core chemosensory neurons common to both males and hermaphrodites have been described in *C. elegans*, around 1300 candidate chemoreceptors have been identified in its genome (Thomas & Robertson 2008). Most of these genes possess the characteristic seven transmembrane domains of GPCRs, and many of them are thought to be expressed in sensory neurons, strongly suggesting functionality as chemoreceptors even in the absence of clearly characterized ligands (Chen et al 2005, Colosimo et al 2004, Troemel et al 1995). It is obvious and yet important to note explicitly that the vast disparity between the receptor and cell number in the chemosensory system of *C. elegans* necessitates the extensive co-expression of receptors within individual olfactory *and* gustatory neurons. Indeed, potential expression of twelve GPCRs has been reported for the amphid olfactory neuron AWA, of 19 in AWB and 22 in AWC (Vidal et al 2018). Besides GPCRs, receptor Guanylyl Cyclases (rGCs) play a role in chemosensation (Yu et al 1997). While the number of these genes (27 to date) is much more limited than that of GPCRs, this presents an expanded repertoire compared to mammalian and insect rGCs (at 6 and 7 genes, respectively) (Maruyama 2016). While the number of chemoreceptors in *C. elegans* is staggering, the limited number of cells that are devoted to chemosensation in this nematode necessitates a high degree of pooling of information. How this impacts the discriminatory power of chemosensory neurons, as well as the integration with other sensory modalities detected by the same cells, is an area of active investigation.

Neurons mediating chemoattraction in *C. elegans*

Even though the pressure to assign nervous system capacity very economically is especially high in an animal as small as *C. elegans*, the nematode's chemosensory system differentiates between olfaction and gustation at the level of sensory neurons. Laser ablation studies, in which a cell of interest is destroyed in a fairly targeted manner, have implicated the amphid neurons AWA and AWC as crucial for chemotaxis towards some volatile compounds (Bargmann et al 1993). In animals lacking AWA, chemotaxis towards diacetyl and pyrazine was compromised; in those without AWC, orientation towards benzaldehyde and butanone was impacted; and both cell classes contribute to the detection of isoamyl alcohol and 2,4,5-trimethylthiazol. These behavioral findings suggest that the two classes of olfactory neurons are not specialized towards the detection of discrete odorants or even well-defined classes of chemicals. Nevertheless, there is a degree of functional discrepancy between the cell types, and consequently of discriminatory power of the chemosensory system. Even within cell type, there can be a degree of specialization: different sensitivities to odorants have been reported between the left and the right AWC neuron. Dependent on the stochastic expression of the STR-2 receptor, one of the AWC neurons (the one not expressing STR-2) is necessary for the

detection of 2,3-pentanedione and for the discrimination between benzaldehyde and butanone (Wes & Bargmann 2001).

Chemotaxis towards soluble compounds has been predominantly linked to a single amphid chemosensory neuron, the ASE. Laser ablation of this neuron impacts an animal's attraction to sodium and chloride ions, biotin, cAMP, and, to a lesser degree, lysine (Bargmann & Horvitz 1991). Again, as in the case of AWC, there is a functional difference between the two anatomically equivalent ASE neurons: the ASE in the left amphid organ (ASEL) is sensitive to sodium ions, whereas the right ASE (ASER) detects chloride and potassium ions. This functional difference is thought to be a consequence of the expression of the homeobox transcription factor LIM-6 in ASEL, which has been linked to the differential expression of some rGCs (Maruyama 2016, Pierce-Shimomura et al 2001, Yu et al 1997). Beyond their distinct tastant selectivity, ASEL and ASER also show a preferential response with respect to the direction of concentration changes. Increases in the concentration of sodium chloride induce a depolarization in ASEL, whereas ASER is specifically sensitive to a reduction of salt concentration (Suzuki et al 2008). Indeed, responsiveness to changes in concentration as opposed to absolute concentration is a response motif that has been reported in multiple *C. elegans* chemosensory sensory neurons (Thiele et al 2009). The encoding of the concentration change on the level of sensory neurons is very satisfyingly mirrored in the fact that this stimulus feature has the biggest impact on chemotaxis behavior in *C. elegans*. Even though ASE's role in positive chemotaxis has been best characterized, it must be noted that ADF, ASG, ASI, ASK, and ASJ contribute to this behavior and weak chemotaxis persists even when ASE is ablated (Bargmann & Horvitz 1991, Thiele et al 2009).

Neurons mediating Chemorepulsion in *C. elegans*

Chemosensation not only mediates approach behavior, but also alerts the animal to potentially dangerous environmental conditions, leading to immediate avoidance. This has been observed in the presence of specific soluble chemicals, such as heavy metals or alkaloids (many of which are perceived as "bitter" by other animals) as well as in response to high osmolality, amongst other potentially noxious stimuli (Culotti & Russel 1978, Hilliard et al 2004). A key neuron mediating this behavior is the polymodal nociceptor ASH- an amphid neuron that expresses a wide variety of chemoreceptors and is also essential for the response to noxious touch (Kaplan & Horvitz 1993). At first glance, this pooling of sensory information of multiple modalities in a single neuron suggests a unified behavioral avoidance program elicited by quite diverse environmental stimuli. It has, however, been shown that the stimulus modality can be conveyed to the downstream circuitry, as for example in the case of the interneuron AVA, which is directly downstream of ASH. In AVA, distinct glutamate receptor subunits are required to receive inputs conveying stimuli of different modalities: the NMDA receptor subunit NMR-1 as well as the non-NMDA receptor units GLR-1 and GLR-2 are required for proper responses to harmful osmotic stimuli, while only the non-NMDA receptor subunits are required for avoidance of noxious touch (Hart et al 1995, Mellem et al 2002, Metaxakis et al 2018). Complicating matters even further, ASH not only responds to physical stimuli and soluble chemicals, but it also mediates aversion to high concentrations of odorants, thus blurring the distinction between gustation and olfaction (Yoshida et al 2012).

In contrast, AWB is a predominantly olfactory amphid neuron that primarily mediates the detection of aversive volatiles such as 2-nonanone and 1-octanol (Troemel et al 1997). This neuron is complimentary to the other “amphid winged” neurons, AWA and AWC, which mediate chemoattraction as outlined above. In fact, it has been shown that misexpression in AWB of the ODR-10 receptor, which mediates detection of the attractant diacetyl and is normally expressed in AWA, results in an aversion to diacetyl in an *odr-10* null background, and in severe chemotaxis defects in a wildtype background (Troemel et al 1997). These findings indicate that it is not the odorant per se that is categorized by the nervous system, but it is instead the identity of the stimulated sensory neuron that leads to the interpretation of the odorant as aversive. Even though mediating the avoidance of odors seems to be the main function of AWB, it has also been reported to play a minor role in electrosensation and light sensitivity (Gabel et al 2007, Ward et al 2008).

Another set of chemosensory neurons that mediate chemorepulsion are the two phasmid organ neurons, PHA and PHB. When worms encounter a chemical repellent, for example sodium dodecyl sulfate (SDS), at their tail during a bout of backwards movement, phasmid neurons inhibit further retreat. This indicates that chemorepulsive neurons in the amphid organs (specifically ASH and AWB) and the phasmid sensory neurons act in antagonistic fashion upon the circuitry controlling locomotion in *C. elegans* to coordinate forward and backward movement with the detection of harmful substances in the immediate environment (Hilliard et al 2002). Overall, the chemosensory neurons of the phasmid organs remain largely uncharacterized; no functional differences between PHA and PHB have been described to date, and their sensitivity to chemicals beside SDS is largely unknown. It is unquestioned that PHA/B are likely to respond to a broad subset of chemicals: they express at least 51 and 49 different GPCRs, respectively (Vidal et al 2018). This is comparable in sheer number with the GPCRs shown to be expressed in the amphid ASH neuron, but it has to be noted that each of the three cell types expresses a distinct, if overlapping set of receptors.

As incomplete as the current understanding of the role of the phasmid neurons may be, they have been far better characterized than the neurons of the inner labial sensory organs. It has been suggested that of the two neurons housed in each inner labial organ, only IL-2 may be chemosensory as its dendrite is directly exposed to the outside environment (Ward et al 1975). These neurons have been implicated in a dispersal behavior called nictation: during food scarcity, *C. elegans* in the alternative dauer stage raise the anterior part of their body in the air, presumably to hitch a ride with a passing animal or for wind dispersal. In animals with laser-ablated IL-2 neurons, this behavior is much reduced (Lee et al 2011). No function for IL-2 neurons in non-dauer animals has been reported, even though there is some suggestion that they may be involved in ethanol sensing (Johnson et al 2017).

Despite the gaps in our current understanding of the chemosensory system of *C. elegans*, it is apparent that it has both the potential to detect a vast number of chemicals and also a surprising capacity to distinguish between them. What is, however, the most striking aspect of chemosensation in *C. elegans* is the multimodal nature of the sensory neurons. Not only is the line between olfaction and gustation blurred, but even other sensory modalities are detected by the same cells. The details of how this impacts the processing of sensory information both within individual neurons and between cell types

is under investigation. These efforts are further enriched by insights gained from the completed connectome of *C. elegans*: chemical and electrical synapses among sensory neurons, as well as with downstream circuits, have been thoroughly described, suggesting staggeringly complex interactions throughout the system (Cook et al 2019, Hall & Russel 1991, White et al 1986).

Chemosensation in Mammals: Of Rodents and Men

Olfactory Organs in Mammals

While the entire core chemosensory system of *C. elegans* consists of roughly 30 neurons, mice have millions of sensory neurons dedicated to olfaction alone (Kawagishi et al 2014). These neurons are organized into separate tissues in the nasal cavity: the main olfactory epithelium, the septal organ (or organ of Masera) and the vomeronasal organ (**Figure 1-2**). While these sensory organs are common to most mammals, a fourth olfactory organ, the Grüneberg Ganglion, has been most thoroughly described in mice and rats. It is thought to be present in other animals outside of the rodent order, but its exact prevalence remains subject of study (Grueneberg 1973, Marshall & Maruniak 1986, Su et al 2009).

The main olfactory epithelium houses the vast majority of the canonical olfactory sensory neurons (OSNs). Their cell bodies are embedded amongst support cells in the epithelial layer, while the single dendrite of each cell extends into the mucus lining the nasal cavity. These sensory dendrites terminate at the air-mucus interface, where they are decorated with multiple cilia, whose surfaces house the olfactory receptors (Barrios et al 2014, Frisch 1967). The chemosensory neurons in the vomeronasal organ have a similar morphology: they are embedded in mucus-coated tissue amongst support cells and have complex dendritic structures. However, instead of cilia, they extend microvilli into the mucosa (Vaccarezza et al 1981). The sensory neurons of the septal organ are thought to be very similar to the canonical OSNs found in the main olfactory epithelium, while the Grüneberg Ganglion houses unusually compact olfactory neurons lacking expansive dendritic structures (Brechbuhl et al 2008, Brechbuhl et al 2014, Ma et al 2003, Roppolo et al 2006, Weiler & Farbman 2003).

The first chemosensory receptors in mammals were identified 30 years ago (Buck & Axel 1991). As in *C. elegans*, the olfactory receptors in mice were found to be GPCRs: about 1200 genes in the main olfactory receptor (OR) family have been identified in the mouse genome, in addition to ~200 genes in the vomeronasal 1 receptor (V1R) and ~60 in the vomeronasal 2 receptor (V2R) family (Yang et al 2005, Zhang et al 2007). OR genes are expressed by OSNs in the main olfactory epithelium, as well as in the septal organ, where they mediate general odorant detection. It is generally the case that each olfactory sensory neuron expresses either a single receptor or at most a very small number of receptors. This is achieved by an elegant system of gene regulation. Based on the location within the epithelium, one of multiple arrays of ORs in the genome is activated (Ressler et al 1993). Of this array, one allele of a single OR gene is expressed stochastically due to interactions with specialized regulatory sequences, which may be located on a different chromosome and come into contact with OR genes due to DNA folding in the nucleus (Chess et al 1994, Lomvardas et al 2006). While each OSN

expresses only a single receptor, each OR can detect a number of odorants, even though they do vary in the specifics of their tuning (Krautwurst et al 1998, Malnic et al 1999).

How are the thousands of olfactory sensory neuron types, as defined by their expressed OR, arranged in the olfactory epithelium? Neurons express ORs according to a spatial pattern observed across animals, where each subfamily of OR is expressed predominantly in defined zones of the nasal cavity. Within each zone, there does not appear to be a set pattern of receptor expression, and cells expressing different ORs are stochastically distributed (Ressler et al 1993, Vassar et al 1993, Zapiec & Mombaerts 2020). This gives rise to an organizational system in the mouse main olfactory epithelium where similar chemical groups are detected by closely related, structurally similar receptors expressed in cells grouped in the same tissue section (Ma & Shepherd 2000, Ressler et al 1993, Strotmann et al 1994). A spatial distribution pattern has not only become apparent in OR expression, but also in the morphology of the cilia which house the receptors. While it had long been thought that OSNs are morphologically relatively homogenous, it has now been shown that OSNs located antero-dorsal in the nasal cavity tend to have overall longer cilia. These cells present more receptors due to their increased surface area, which is presumably the root for their increased sensitivity to odorants. This pattern does not depend on odor-dependent neuronal activity, but it remains unclear if the same mechanisms governing the spatial distribution of ORs also accounts for the observed morphological patterning (Challis et al 2015).

The vomeronasal organ (VNO) is predominantly dedicated to the detection of chemical signals originating from conspecifics, such as pheromones (Leinders-Zufall et al 2000). Rodents lacking a functional VNO have a wide variety of deficits in social behaviors, including aggression and maternal care (Del Punta et al 2002, He et al 2008, Kimoto et al 2005). The VNO is vestigial in humans, in accordance with their relative de-emphasis of pheromonal communication (D'Aniello et al 2017). The VNO can be broadly divided into two zones based on the receptor types expressed by the OSNs: V1R expressing neurons are found in the apical zone, while V2R positive neurons localize to the basal surface (Dulac & Axel 1995, Herrada & Dulac 1997, Matsunami & Buck 1997, Rodriguez et al 2002). It is thought that V1Rs are expressed in a monogenic, monoallelic manner similar to canonical ORs, but their tuning seems much narrower: each V1R responds to a single pheromone, and no additional neurons are recruited upon increasing the pheromone concentration (Leinders-Zufall et al 2000, Rodriguez et al 1999). In contrast, V2R positive neurons have been shown to co-express a small number of receptors (Ishii & Mombaerts 2011, Martini et al 2001). While the classical model of the olfactory system postulates a clear distinction between the main olfactory system, which detects general smells, and the vomeronasal system, there is evidence of functional overlap between the two: some cells in the VNO respond to odorants, and there are some pheromone-sensing cells in the main olfactory epithelium (Karunadasa et al 2006, Trinh & Storm 2003, Wang et al 2006).

The roles of the septal organ and the Grüneberg ganglion are largely unclear. The septal organ contains olfactory neurons expressing classical ORs, but they are arranged in fewer layers compared to the main olfactory epithelium (2-4 and 6-8, respectively), and their dendrites are shorter with larger dendritic knobs (Kaluza et al 2004, Ma et al 2003, Pedersen & Benson 1986, Tian & Ma 2004, Weiler & Farbman 2003). Although huge strides have been made with respect to the anatomical characterization of the septal

organ, its behavioral function remains stubbornly elusive and subject to intensive study. The Grüneberg ganglion houses neurons expressing the olfactory gene OMP as well as V2R83 (Fleischer et al 2006, Fleischer et al 2007, Fuss et al 2005). Consistent with the expression of a vomeronasal receptor, the Grüneberg Ganglion has been implicated in the detection of alarm pheromones (Brechbuhl et al 2008). Additional aversive responses to cooling have been tied to the Grüneberg Ganglion, leading to the intriguing hypothesis that it plays a role in the avoidance of danger by confining pups to the warm nest and facilitating social communication in mature animals (Schmid et al 2010).

Encoding of Odorant Identity in Mammals: Combinatorial Coding

The projection targets of the OSNs in the brain are determined by the receptors they express. The olfactory bulb consists of a group of glomeruli, anatomical structures formed by the axonal terminals of the OSNs, the dendrites of projection neurons, and local interneurons. OSNs expressing the same receptor all project to one glomerulus per hemisphere in the olfactory bulb, so that each odor is represented by a topographical activity map in the brain based on the receptors it binds to (Mombaerts et al 1996, Ressler et al 1994, Vassar et al 1994, Wachowiak & Cohen 2001). Each glomerulus is furthermore composed of the dendrites of dedicated mitral cells, the main projection neurons of the olfactory bulb, which do not receive direct excitatory input from other glomeruli (Aungst et al 2003, Kishi et al 1982). This ensures the convergence of a single population of OSNs, defined by a common OR, onto a restricted population of mitral cells, thus creating a dedicated neuronal circuit for each receptor. OSNs of the septal organ and the Grüneberg Ganglion similarly project to dedicated glomeruli in the main olfactory bulb (Fleischer et al 2006, Fuss et al 2005, Ma et al 2003, Pedersen & Benson 1986).

The position of individual glomeruli in the main olfactory bulb is largely stereotyped between animals (Bressel et al 2016). Their correct development is at least partially dependent on both the identity and the functionality of the OR in a given OSN type: the deletion of receptors leads to acute axon misguidance phenotypes where axons fail to coalesce on a single glomerulus (Feinstein et al 2004). Additionally, the impairment of cAMP generation downstream of ORs leads to similar axon guidance defects, indicating that neuronal activity plays a role in the wiring of the olfactory bulb (Imai et al 2006). Complementary studies have also shown that the replacement of an OR with an olfactory receptor gene of a different species leads to the formation of seemingly functional ectopic glomeruli (Belluscio et al 1999). The thus carefully arranged spatial organization of the olfactory bulb itself seems to be integral to the efficient extraction of pertinent olfactory information, even though olfactory projection neurons have been shown to target a wide variety of brain regions. Specifically, ablation of regions of the olfactory bulb has been shown to adversely impact the innate response to smells associated with predators, but not to impede learned responses to the same smells. This suggests that higher olfactory circuitry may not necessarily consider the entirety of the distributed representation of a smell in the olfactory bulb, but be biased towards relevant landmark glomeruli (Kobayakawa et al 2007).

The organization of the accessory olfactory bulb, the projection target of sensory neurons residing in the VNO, is less clear-cut. OSNs expressing the same receptor innervate multiple glomeruli instead of converging on a single one per hemisphere, and the positioning of these target glomeruli within the accessory olfactory bulb is less

stereotyped between individuals (Belluscio et al 1999, Del Punta et al 2002, Rodriguez et al 1999). Interestingly, the mitral cells of the accessory olfactory bulb contact the glomeruli innervated by OSNs expressing the same VR, thus establishing a labeled circuit for each receptor not dissimilar to the those observed for the ORs in the main olfactory bulb (Del Punta et al 2002). The establishment of a topographical map based on olfactory receptors enables the organization of sensory inputs across all olfactory subsystems. This ensures that smells can be correctly identified based on their unique activity signatures in the olfactory bulbs, which are analyzed further in other brain regions, such as the olfactory cortex and the amygdala.

Gustatory Organs in Mammals

Taste sensory organs in mice are located on the tongue, the soft palate, the larynx, pharynx and epiglottis in the form of taste buds (**Figure 1-3**). Each taste bud is composed of tightly packed sensory cells and has an opening to allow the entry of chemicals from the environment (Delay et al 1986, Kinnamon et al 1993). Taste buds contain on average between 25 and 51 sensory cells, depending on their location (Ogata & Ohtubo 2020, Ohtubo & Yoshii 2011). They are embedded in the surrounding epithelium, which forms distinct ultrastructures on the tongue: at the anterior part of the tongue, taste buds are concentrated in fungiform papillae, at the sides in foliate papillae and at the back of the tongue in circumvallate papillae (Kobayashi 1989, Kobayashi 1994). Taste buds not located on the tongue are not grouped and occur individually in the epithelium (Yarmolinsky et al 2009).

Remarkably, mammalian taste receptor cells (TRCs) differ from the other sensory cells discussed in this chapter in that they are not neurons; instead, the surrounding epithelium gives rise to TRCs (Stone et al 1995). Despite this fundamental distinction, their morphology is most similar to vomeronasal sensory cells: both cell types form extensive microvilli at their apical surface, which house densely packed receptors. In mice and other mammals, the number of taste receptors, and thus the amount of possible different types of TRCs, is paltry compared to the plethora of olfactory receptors. There are only about 35 taste receptor genes in mice, in addition to sensors for salts and acids (Adler et al 2000, Matsunami et al 2000, Nelson et al 2002, Nelson et al 2001). These taste receptors are, like ORs and VRs, seven transmembrane domains containing GPCRs, even though they are not closely related to either (Nelson et al 2001). This indicates that the sensory detection and coding approach in the gustatory system has a limited discrimination capacity compared to olfaction. Indeed, TRCs in mice and other mammals generally come in the five distinct flavors known to most by personal experience: sweet, bitter, salty, sour and umami.

Encoding of Tastant Quality in Mammals: The Labelled Line Model

The receptors that detect different taste qualities have been well described. Sweet sensing TRCs express two receptor subunits of the taste 1 receptor (T1R) family that form a heterodimeric functional GPCR: T1R2 and T1R3. This receptor complex is responsible for the detection of a surprising variety of compounds that register as “sweet”, from the expected sugars to a number of amino acids as well as artificial sweeteners (Li et al 2002, Nelson et al 2001). This versatility is due to multiple binding pockets on the receptor, which show different affinities for distinct chemicals (Assadi-Porter et al 2010, Jiang et al

2004, Masuda et al 2012, Xu et al 2004). While this swiss-army-knife-approach is certainly efficient in terms of receptor-to-ligand ratio, it comes at the cost of discriminatory power. While some compounds may be more intensely sweet, there are no distinct types of sweetness per-se, which makes it impossible to differentiate between, for example, sucrose and glucose. Arguably, the distinction between these tastants is of little consequence to the animal, as their biological value lies in their nutritious potential, not in their exact identity. Similar to the sweet-sensing GPCR, savory or umami taste is detected by a heterodimeric receptor complex of the T1R family, in this case T1R1 and T1R3. This receptor responds to most L-amino acids as well as some monophospho-nucleotides, most notably IMP (Li et al 2002, Nelson et al 2002). Structural studies indicate that T1R1 and T1R2 play a larger role in ligand binding compared to the shared T1R3 subunit, which is in keeping with sweet and umami as distinct taste categories (Nuemket et al 2017). It has been reported, however, that T1R3 is also expressed without the other T1Rs, and can act as a receptor for high sugar concentrations and calcium (Nelson et al 2001, Tordoff et al 2012, Zhao et al 2003). T1R3 homodimers have also been implicated as possible glucose sensors in human pancreatic beta cells (Kojima et al 2015).

Bitter sensing cells, in contrast, have been adapted to address a very different problem. A vast array of potentially harmful substances has to be detected even at very low concentrations to ensure the survival of the animal. Indeed, the majority of taste receptors in mice are bitter detecting Taste 2 Receptors (T2Rs), which are coexpressed in the same cells (Adler et al 2000, Matsunami et al 2000). This expression pattern suggests an even more extreme pooling of information than is observed in sweet and umami cells. As not all bitter cells express all T2Rs and consequently don't respond to all bitter stimuli, however, there may be some underlying degree of specialization amongst bitter cells (Caicedo & Roper 2001). It is unclear what, if any, the functional relevance of the distribution of receptors across bitter cells is. Individual T2Rs are thought to differ widely with respect to their selectivity. In humans, some T2Rs have been reported to respond to single chemicals, as in the case of, for example, T2R5, which only shows responses to cycloheximide (Chandrashekar et al 2000). Other T2Rs show a high degree of promiscuity and respond to a multitude of tastants (Behrens et al 2009, Brockhoff et al 2007, Meyerhof et al 2010). While these studies are intriguing, it has to be mentioned that the sheer number of compounds thought to be potential bitters precludes truly comprehensive tests. Some receptors may appear to be highly selective simply due to the restricted number of compounds tested. Complicating the matter further, it is a fairly common phenomenon that tastants which do not register as bitter at low concentrations are detected by the receptors at high concentrations. This accounts for the bitter aftertaste of many artificial sweeteners, such as saccharine (Kuhn et al 2004, Pronin et al 2004).

While the exact mechanism of sour taste remains debated, PKD2L1, a member of the TRP channel superfamily has been implicated, along with the TRP related protein PKD1L3 (Huang et al 2006, Ishimaru et al 2006). Both are present in sour-specific TCRs, and expression of these two proteins has been shown to be sufficient to confer acid sensitivity in heterologous expression experiments (Inada et al 2008, Ishimaru et al 2006, Kataoka et al 2008). Additionally, knock out of these genes leads to an impaired response to acids, even though the result is not complete sour blindness (Horio et al 2011). Undermining the central role of PKD2L1/1L3, studies have shown that a stimulus-dependent proton influx is crucial to acid responses in sour taste cells- and that the

PKD2L1/1L3 complex is not required for this conductance (Chang et al 2010). Using *PKD2L1* as a marker gene for sour taste cells, transcriptomic studies have recently identified the proton-selective channel Otopetrin1 as a likely candidate for this sour-sensing pathway (Tu et al 2018, Zhang et al 2019). Interestingly, members of the *otopetrin* family are also widely expressed in non-taste tissues, so that a shared otopetrin-dependent mechanism for acid sensing in many physiological contexts seems likely (Tu et al 2018).

Salt taste differs from the other four taste modalities in its qualitative ambiguity: low salt concentrations are perceived as attractive, especially in salt-starved animals, while high concentrations of salt are aversive (Lindemann 2001). These two opposing responses to salt of differing concentrations are mediated by distinct mechanisms: the response to low salt is in fact specific to sodium ions and can be inhibited by the application of amiloride (Heck et al 1984). In contrast, different taste receptor cells respond to high concentrations of multiple ions in an amiloride-independent manner (Ninomiya 1998, Ninomiya et al 1989). This observation implicated the amiloride-sensitive sodium channel ENaC in the detection of low salt concentrations (Yoshida et al 2009). Indeed, it has since been shown that the ENaC-expressing subpopulation of TRCs not only responds to low sodium, but that these cells are required for low salt attraction (Chandrashekar et al 2010). High salt concentrations, however, do not activate a dedicated population of TRCs- instead, this aversive taste is mediated via activation of both sour and bitter TRC populations (Oka et al 2013). How these TRCs detect high salt concentrations remains a subject of study.

As outlined above, taste sensory cells fall into distinct categories that are generally dedicated to the detection of a single taste modality. A tastant is assigned an inherent quality by virtue of the sensory cell type it activates. This conclusion is supported by ectopic expression experiments, where bitter T2Rs are expressed in normally sweet detecting cells, i.e. cells naturally expressing T1R2 and T1R3. In mice with this abnormal expression pattern, exposure to bitter compounds leads to anomalous acceptance behaviors. The reverse is also true, so that ectopic expression of receptors (even non-taste receptors) in bitter cells leads to aversion responses upon ligand exposure (Mueller et al 2005). These studies support the hypothesis that dedicated cell populations exist in the periphery which encode attractive tastes such as sweet and umami, as well as those that encode aversive taste categories like bitter and sour or, more ambiguously, salt. This model is generally referred to as the “labelled line” model, and while it is widely accepted as the processing mode at the level of sensory cells, it has been controversial how far exactly into the higher gustatory circuit this modality specificity is conserved. There is increasing evidence, however, that taste modality specific circuits may be maintained all the way to the gustatory cortex (Chen et al 2011, Jin et al 2021)

How taste information from the taste sensory cells, which are epithelial in nature, is funneled into the nervous system also remains debated. Only sour sensory cells have been shown to form classical synapses, as they are observed commonly elsewhere in the nervous system (DeFazio et al 2006, Yang et al 2000). Nevertheless, a number of classical neurotransmitters are expressed in taste buds, whose exact roles are only imperfectly understood (Cao et al 2009, Huang et al 2005, Oliveira-Maia et al 2009). It has also been suggested that TRCs release ATP via pannexin channels, which could in turn activate the ATP-gated cation channels P2X2 and P2X3, which are known to be

expressed on gustatory nerve endings (Bo et al 1999, Huang et al 2007, Romanov et al 2007). Regardless of the exact molecular mechanisms, it seems extremely likely that the labelled line model holds up at the level of these primary afferent fibers.

Chemosensation in *Drosophila melanogaster*

Chemosensory organs in adult *D. melanogaster*

Adult *Drosophila melanogaster* have hair like chemosensory sensilla which house sensory neurons on multiple body surfaces. Olfactory sensilla are localized on the third antennal segment and on the maxillary palps (**Figure 1-4**). There are three main morphological classes of olfactory sensilla: trichoid, basiconic and coeloconic, each with several morphologically distinct subtypes (Stocker 1994, Venkatesh & Singh 1984). Trichoid sensilla, which are readily identifiable by their cylindrical base structure and the sharply tapering shape of the main sensillum, house between one and three olfactory receptor neurons (ORNs). They are concentrated in the disto-lateral zone of the third antennal segment. Basiconic sensilla show only slight tapering towards the tip of the sensillum, lacking the distinctive basal structure of trichoid sensilla, and house either two or four ORNs, depending on their subtype. These sensilla are distributed proximo-laterally in a pattern complimentary to the trichoid sensilla, so that the opposing distribution gradients of the two subtypes divide the third antennal segment roughly diagonally. The third subtype, coeloconic sensilla, are small and pin like. They house either two or three sensory neurons and are distributed across the surface of the third antennal segment. Ranking the subtypes in prevalence, basiconic sensilla are the most common, with between ~190 and ~230 sensilla per antenna and ~60 on each maxillary palp, followed by trichoid sensilla with ~115 per antenna, and rarest being coeloconic sensilla with ~55 per antenna. The wall of each sensillum contains a multitude of pores that allow environmental volatiles to enter into its lumen, where they interact with the receptor-packed dendrites of the sensory neurons (Riesgo-Escovar et al 1997a, Riesgo-Escovar et al 1997b, Shanbhag et al 1999a, Stocker 1994).

In adult *Drosophila*, gustatory sensory organs can be found on the proboscis, pharynx, legs, wing margins and, in females, the ovipositor (**Figure 1-5**) (Stocker 1994). These sensilla are open to the outside environment via a single taste pore at their tip, which allows for the entry of chemicals into the lumen of the taste hair, where they can interact with the dendrites of gustatory receptor neurons (GRNs) (Nayak & Singh 1983, Shanbhag et al 2001). Owing to the fact that the gustatory organs of the inner and outer mouthparts have been most fully described, both in anatomy and function, this discussion will be focused on them. Taste bristles on the proboscis are restricted to its most distal section, the labella, where they are arranged in a stereotyped pattern with respect to both location and subtype. The 31 labellar gustatory sensilla on each labellar palp can be sorted into three types based on their length and the number of sensory neurons they house (Ray et al 1993, Shanbhag et al 2001): small sensilla contain four GRNs as well as one mechanosensory neuron; both large and intermediate sensilla contain two chemosensory neurons and one mechanosensory neuron, but their GRNs detect different tastant classes (see below). In addition to the taste bristles, smaller structures called taste pegs are also located on the fly labellum. These pegs each house two neurons, one

mechanosensory and one chemosensory neuron (Falk et al 1976, Fischler et al 2007, Ray et al 1993, Shanbhag et al 2001, Thorne et al 2004).

The taste sensilla of the inner mouthparts are grouped into three different taste organs. The most distal of these is the labral sense organ (lso), which contains 9 sensory sensilla. Six of these, which are associated with a sensory hair, are mechanosensory, while two of the three hairless sensilla contain two GRNs each, with the third containing 8 (Gendre et al 2004, Nayak & Singh 1983, Stocker & Schorderet 1981). These hairless sensilla strongly resemble mammalian taste buds, even though the number of sensory neurons is of course much reduced in comparison. The dorsal and ventral cibarial sense organs (dcso and vcso, respectively), are smaller than the lso: the dcso consists of two sensilla housing three GRNs each, while the vcso contains three sensilla, two with a pair of GRNs and one with four GRNs (Gendre et al 2004, Nayak & Singh 1983, Stocker & Schorderet 1981).

Olfaction in *D. melanogaster*

The best studied chemosensory receptors expressed by ORNs are, not surprisingly, the 62 olfactory receptors (ORs), which arise from 60 genes via alternate splicing (Clyne et al 2000, Robertson et al 2003, Vosshall et al 1999, Vosshall et al 2000). The identification of these receptors was heavily dependent on the assumption that, like *C. elegans* and mammalian odorant receptors, they would be GPCRs. While bioinformatic searches for candidate chemoreceptors with the characteristic seven transmembrane domains did indeed lead to the identification of members of the OR family, their transduction mechanism has been unexpectedly controversial. Surprisingly, *Drosophila* ORs not only lack some of the usual domains necessary for GPCRs to function, but their topology with an intracellular N-terminus is also inverted compared to confirmed GPCRs (Benton et al 2006). This, as well as the observation that no G-protein dependent signaling cascades are required for odorant-evoked responses in ORNs, indicates that insect ORs act in fact as ligand gated ion channels (Sato et al 2008, Wicher et al 2008). Further support for this hypothesis has come from the Cryo-EM structure of Orco (also known as OR83b), which strongly suggests that receptor proteins assemble as tetramers to form a ligand gated cation channel (Butterwick et al 2018).

As a rule, individual *Drosophila* ORNs express two OR genes- the broadly expressed olfactory coreceptor *Orco*, as well as one additional odorant binding OR (Jafari et al 2012, Larsson et al 2004, Vosshall et al 1999, Vosshall et al 2000). These two proteins form a heteromeric receptor complex essential to the detection of a vast array of diverse odors (Larsson et al 2004, Neuhaus et al 2005, Sato et al 2008, Wicher et al 2008). Even though the vast majority of ORNs adheres to this one receptor plus the coreceptor paradigm, exceptions have been reported: *Or22a* and *b* are coexpressed in the same antennal ORN in addition to *Orco*, even though rescue experiments in double mutant backgrounds suggest that only OR22a may be functional (Dobritsa et al 2003). Additionally, *Or33c* and *Or85* are coexpressed in the same maxillary palp ORN (Goldman et al 2005). ORNs are arranged according to a stereotyped pattern on the antennal surface based on the OR they express: it has been shown that ORNs with characteristic OR expression and consequently stereotyped response profiles to panels of odors are grouped together in certain sensilla, which in turn are distributed in well-defined zones

across the third antennal segment (Couto et al 2005, de Bruyne et al 2001, Hallem et al 2004).

In addition to the classic ORs, the repertoire of olfactory receptors in *Drosophila* includes other channel families. Ionotropic Receptors (IRs) are a family of roughly 60 three transmembrane domains containing receptors (Benton et al 2009). They are most closely related to ionotropic Glutamate Receptors (iGluRs) and are thought to act similarly as ligand-gated ion channels (Croset et al 2010). Mounting evidence suggests that IRs assemble as heteromeric functional receptor complexes, with IR8a, IR25a and IR76b acting as co-receptors similar to Orco (Abuin et al 2011, Ai et al 2013, Silbering et al 2011). A small niche role in olfaction is also played by Gustatory Receptors (GRs, also see below), specifically in the detection of CO_2. *Gr21a* and *Gr63a* are co-expressed in CO_2 sensitive ORNs of the antenna, where they are both necessary and sufficient for a response to CO_2 (de Bruyne et al 2001, Jones et al 2007, Kwon et al 2007). Interestingly, homologues of these two genes are also co-expressed in olfactory neurons of the mosquito *Anopheles gambiae,* whose reliance on CO_2 for prey detection is well established (Jones et al 2007). It is in fact a complex of three related GRs that is thought to confer CO_2 sensitivity to specialized neurons of *A. gambiae's* maxillary palp (Lu et al 2007, Robertson & Kent 2009).

Antennal ORNs project their axons along the antennal nerve to two symmetrical structures in the anterior part of the fly brain, the antennal lobes. Maxillary palp ORNs project to this brain region via the maxillary nerve and through the subesophageal zone (SEZ) of the lower brain. Each antennal lobe consists of 43 distinct glomeruli, which contain the axons of ORNs and the dendrites of olfactory projection neurons (Laissue et al 1999, Stocker et al 1990). Remarkably, all ORNs expressing the same receptor converge onto the same glomerulus, creating a topographical map in the brain, analogous to the patterning of the olfactory bulb in rodents (Ai et al 2013, Gao et al 2000, Grosjean et al 2011, Silbering et al 2011, Vosshall et al 2000). Consequently, odorants are encoded in the *Drosophila* brain with a combinatorial code, where each distinguishable odorant is associated with a specific activity pattern in the antennal lobe (Bhandawat et al 2007, Hallem & Carlson 2006, Silbering & Galizia 2007, Wilson et al 2004). Each glomerulus is innervated by a subset of olfactory projection neurons according to a well-defined pattern, so that specific projection neuron types receive stereotyped input from a subset of ORNs (Bates et al 2020, Couto et al 2005, Fishilevich & Vosshall 2005). These projection neurons then relay olfactory information to the main centers of learning and memory in the fly brain: the lateral horn, thought to be a hub mediating innate behaviors; and the mushroom body, the site of associative learning (Heimbeck et al 2001, Jefferis et al 2007, Marin et al 2002, Wong et al 2002).

Gustation in *D. melanogaster*

The best described family of receptors expressed by GRNs are the aptly named Gustatory Receptors (GRs), a family of 60 genes encoding 68 seven transmembrane domains containing proteins via alternate splicing (Clyne et al 2000, Dunipace et al 2001, Robertson et al 2003, Scott et al 2001). The GRs are mostly closely related to ORs: GRs are thought to be evolutionarily older while the ORs evolved relatively more recently. This suggests that GRs may similarly act as ligand gated ion channels. Although GRs are predominantly studied in the context of gustation, some of them are also expressed

outside of the gustatory system, where they have been proposed to play a role in CO_2 sensing as described above, and humidity detection, among other possible functions (Thorne & Amrein 2008).

There are multiple genetically defined GRN populations that detect distinct taste modalities (Cameron et al 2010, French et al 2015b, Jaeger et al 2018, Wang et al 2004). Each of the 31 gustatory sensilla of the labellar palp houses one sweet sensing GRN. *Drosophila* express 8 genes that encode receptors for sweet tastants: *Gr5a*, *Gr61a* and *Gr64a-f* (Dahanukar et al 2001, Miyamoto et al 2013, Robertson et al 2003, Slone et al 2007). The first of these, *Gr5a*, was identified based on its linkage to a known gene locus associated with trehalose taste (Tanimura et al 1982, Tanimura et al 1988, Ueno et al 2001). While these receptors are generally coexpressed within the same cells, *Gr64f* and *Gr5a* are expressed in all sugar GRNs, whereas the other GRs show expression in subsets of sugar cells, hinting at possible functional diversity (Dahanukar et al 2007, Fujii et al 2015). This has led to the hypothesis that GR64f and GR5a act as coreceptors in heteromeric receptor complexes (Jiao et al 2008, Slone et al 2007). Although sweet GRNs express receptors exclusively dedicated to the detection of sweet tastants, it has been observed that many bitter tastants interact with those receptors and inhibit the activity of the sugar sensory cells (French et al 2015b, Meunier et al 2003).

The vast majority of the remaining GRs participates in the detection of bitter compounds. The first of those, GR66a, has proven to be an invaluable marker for the exploration of bitter sensitive cells in *Drosophila*. GR66a was initially identified as a significant receptor for caffeine detection and has since been deemed a candidate coreceptor in bitter GRNs, as it is expressed in all 18 sensilla per labellar palp with known bitter sensory neurons (French et al 2015b, Moon et al 2006, Wang et al 2004). That expediency, however, masks some of the diversity suspected amongst bitter GRNs. Indeed, bitter receptors are expressed according to a complex combinatorial code that is consistent between animals (French et al 2015a, Weiss et al 2011). Consequently, it has been proposed that distinct subgroups of bitter neurons have specialized functions determined by the contingent of receptors they express (Sung et al 2017). If so, this peripheral bitter code will open exciting new avenues to explore behavioral discrimination of different bitter compounds.

In addition to these relatively classical chemoreceptors, the Pickpocket (ppk) family of Deg/ENaC channels has also emerged as a major player in gustation, namely in the taste of water and high salt. Each labellar palp of the proboscis contains 21 water sensory cells- one GRN in each large and small sensillum- which are distinct from both sugar and bitter sensory cells (Inoshita & Tanimura 2006). PPK28 was identified as the key protein for water detection in flies. Indeed, PPK28 was not only shown to be necessary for normal taste responses to water, but its ectopic expression in bitter GRNs was sufficient to induce water aversion (Cameron et al 2010). Another member of the ppk family, *ppk23*, has been implicated in salt taste. PPK23 positive GRNs have been shown to play a role in the avoidance of high concentrations of sodium, potassium and calcium ions (Jaeger et al 2018, Lee et al 2018). Intriguingly, *ppk23* is also expressed in a subset of bitter GRNs, which also show a response to high concentrations of salt. PPK23 positive, GR66a negative cells do retain their high salt response, but do not respond to bitters (or other tastants), indicating that, while there may be some functional overlap with bitter GRNs, high salt responsive GRNs represent a unique subpopulation of cells (Jaeger et al 2018).

While the role of IRs in chemosensation has been best described in the context of olfaction, there is mounting evidence indicating that they are important in gustation as well. Members of the *Ir20a* clade, which contains 28 receptors thought to be functional and 7 pseudogenes, are expressed in GRNs. Characterization of expression patterns using Gal4 driver lines suggests that *Ir56a* is expressed in bitter neurons, while *Ir56b* and *d* are expressed in sugar sensory neurons (Koh et al 2014). This, together with the observation that IRs are expressed in gustatory neurons with no known function, suggests diverse roles for this class of sensory receptors. Indeed, IR76b positive neurons have variously been reported to play a role in sour, salt and amino acid taste (Chen & Amrein 2017, Croset et al 2016, Lee et al 2017, Zhang et al 2013). Even though those observations are intriguing, the relatively broad expression pattern of *Ir76b* has limited its usefulness as a genetic marker for distinct GRN subpopulations. In the case of salt taste, it has also been proposed that *Ir94e* expression is more tightly restricted to low salt sensing GRNs, but its functional relevance remains to be established more firmly (Jaeger et al 2018).

All GRNs of the inner and outer mouthparts project to the subesophageal zone (SEZ) of the fly brain, where their axons terminate in characteristic patterns depending on the body part and the taste modality they represent. GRNs originating in the inner mouthparts arborize anterior to those from the labella, and the two populations do not overlap (Wang et al 2004). The taste modality map is somewhat less well defined, but it is discernible in the case of labellar GRNs: while bitter neurons terminate in a characteristic ring structure in the center of the SEZ, the GRNs of other taste modalities arborize more laterally in largely overlapping patterns (Marella et al 2006). This indicates that there is at least some anatomical separation between aversive and appetitive taste inputs. To date, it is unclear to what degree and where in the gustatory circuit the processing of different taste modalities converges. It is important to note, however, that the motor neurons innervating the muscles of the proboscis are also located in the SEZ, as are many interneurons known to impact feeding behavior, so that a local core feeding circuit is extremely likely (Flood et al 2013, Gordon & Scott 2009, McKellar et al 2020, Miyazaki et al 2015, Schwarz et al 2017).

Concluding Remarks

It is becoming increasingly apparent that there are common motifs in the sensory coding underlying taste and smell across diverse organisms, as well as consistent differences between olfaction and gustation. The overarching organization of the peripheral olfactory system is remarkably similar between *Drosophila* and mammalian models, even though the exact molecular mechanism of odorant detection is vastly different. In both models, large arrays of sensory neurons are defined by the singular receptors they express, which determine their exact projection targets. The result in both cases is a topographical map in the brain that is based on receptors, not the actual odorants. In contrast, in both vision and hearing, the sensory stimuli can be analyzed based on one key characteristic of the stimulus: the wavelength of light and the frequency of a sound, respectively. In olfaction, there is no obvious single variable that could serve as a foundation to conclusively categorize all odors. In this case, a system based on the excited receptors, where the actual odorant identity is represented via the distributed

activity patterns in the olfactory bulb or antennal lobe, seems to have emerged as the best option. The olfactory system is clearly optimized towards the precise identification of many odors, and both *Drosophila* and mammals dedicate large parts of their brains towards that goal. In the fly, it is especially apparent why this effort is of value: olfactory processing in this system is intricately linked with learning and memory formation. It is exceedingly powerful to use smells to make complex, experience-based decisions considering that they can represent long-range indicators of both desirable and undesirable environmental conditions. The value of these memories depends to a large part on their specificity, so the more odors can be reliably differentiated, the less memories linked to them are misleading.

The case is quite different in gustation, where the ultimate purpose is less geared towards the identification of individual chemical components of a food source, but towards a quality judgment of the whole. It is therefore economical to pool information into relevant modalities that reflect the diverse nutritious needs of an animal. Depending on their internal state, animals may require their food to contain more carbohydrates, amino acids or salt, while still wanting to avoid potentially toxic or spoiled food, so that these different broad categories need to be weighed against each other. Considering these universal pressures, it is not very surprising that *Drosophila* and mammalian models show broadly similar taste preferences, even though the details of taste detection with respect to individual chemicals may differ. Interestingly, the olfactory system of *C. elegans* is striking in its similarity to gustation, especially considering the large number of receptors per single neuron. This may be a consequence of the limited number of cells such a small animal can devote to sensory processing. Perhaps *C. elegans* does not have the luxury of precisely identifying an odor and must instead make a quality assessment as quickly as possible, which would lend itself to a taste-like processing scheme.

The striking parallels between taste and smell in mammals and fruit flies further highlight the strength of *D. melanogaster* as a model system for the discovery of fundamental principles in neuroscience. The same broad coding rules that underlie mammalian chemosensation can be studied in a system that boasts superior genetic tools, imaging capabilities and accessibility of sensory organs. Additionally, the numbers of receptor genes and sensory cells, especially in the context of olfaction, are several orders of magnitude smaller than in rodents and consequently pose a more manageable problem. While *C. elegans* is of course also famous for its prowess as a genetic model organism and well mapped nervous system, its chemosensory system is more constrained, especially with regards to odor discrimination. It is, however, a perhaps better model of signal transmission, considering that insect chemosensory receptors are not related to their mammalian equivalents. *Drosophila* is an overall excellent model to examine the circuitry and common logic underlying taste and smell processing, which can potentially be extrapolated to a large number of animals. These insights are of interest not only in human health, but also in agriculture and pest control, thus impacting many areas of economic and social interest.

Figures and Figure Legends

Figure 1-1

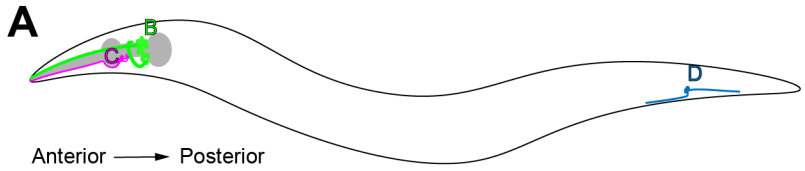

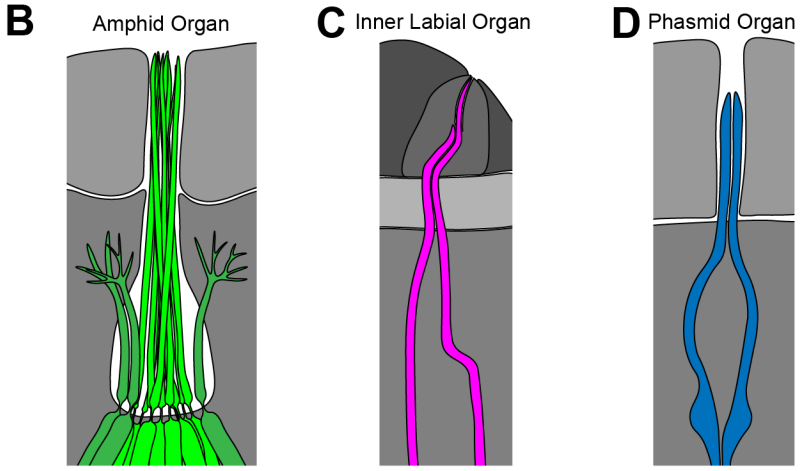

E

Chemosensory Cilia	Neuron	Function	GPCRs
Amphid	AWA	Olfaction - Chemoattraction	12
	AWB	Olfaction - Chemorepulsion	19
	AWC	Olfaction - Chemoattraction	22
	ASE	Gustation - Chemoattraction	5
	ASH	Gustation - Chemorepulsion Mechanosensation	51
	ASK	Gustation(?) - Chemoattraction	41
	ADL	Gustation(?) - Chemorepulsion	72
	ASI	Gustation(?) - Chemoattraction	99
	ASG	Gustation(?) - Chemoattraction	4
	ASJ	Gustation(?) - Dauer exit	39
	ADF	Gustation(?) - Dauer entry	9
Inner Labial Organ	IL-2	Gustation(?) - Chemorepulsion	5
Phasmid	PHA	Gustation(?) - Chemorepulsion	51
	PHB	Gustation(?) - Chemorepulsion	49

Figure 1-1. Cemosensory Organs in *C. elegans*

(A) Position of chemosensory cilia in *C. elegans*. One of two amphid organs (green), one of six inner labial organs (pink), and one of two phasmid organs (blue) are shown. (B) The distal section of an amphid organ. The dendrites of chemosensory neurons (light green: gustatory neurons; dark green: olfactory neurons) are wrapped in a sheath (grey) and a socket cell (light grey). (C) The distal section of an inner labial organ. The dendrites of both chemosensory neurons (pink) are wrapped in a sheath and socket cell (like B), but IL-1 terminates within the subcuticle (dark grey), while IL-2 is exposed to the external environment. The cuticle is indicated in anthracite (D) The distal section of a phasmid organ. The dendrites of both PHA and PHB (blue) are not entirely shielded by the sheath and socket cell (like B). (E) Summary table of core chemosensory neurons in *C. elegans*.

(A-D adapted from Ward et al 1975 and Perkins et al 1986; E adapted from Inglis et al 2007 and Vidal et al 2018)

Figure 1-2

A

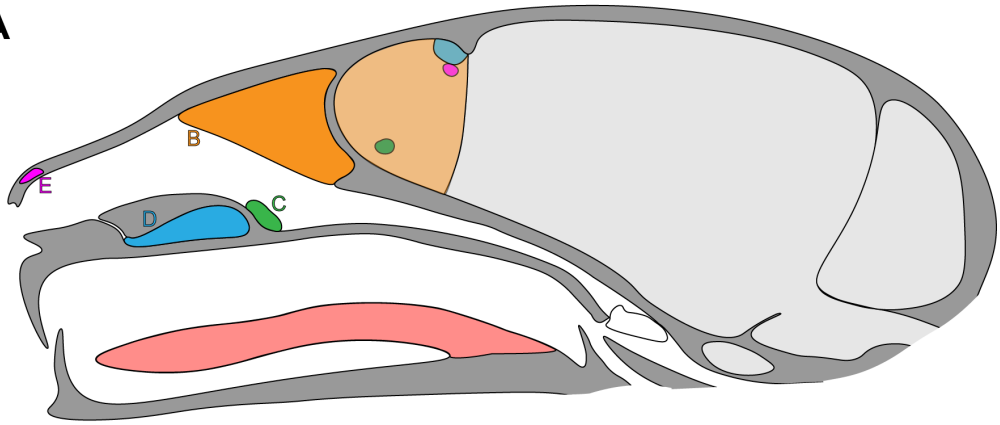

B Main Olfactory Epithelium

C Septal Organ

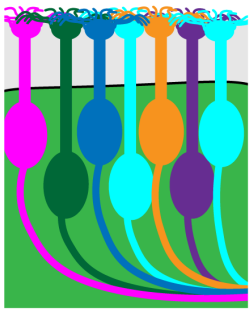

D Vomeronasal Organ

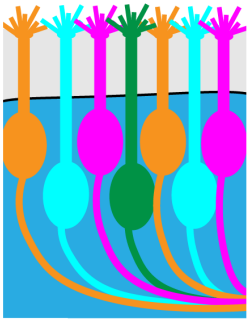

E Grüneberg Ganglion

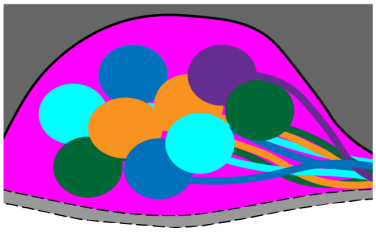

F

Olfactory Tissue	Estimated Number of Sensory Neurons in Mice	Receptors
Main Olfactory Epithelium	~10 000 000	ORs V1Rs
Vomeronasal Organ	~140 000	V1Rs V2Rs ORs
Septal Organ	~10 000 (highly variable)	ORs
Grüneberg Ganglion	~300-500	ORs V2R83

Figure 1-2. Olfactory Organs in Mice

(A) Localization of the main olfactory tissues in the nasal cavity and their projection targets in the brain. Sensory neurons of the main olfactory epithelium (B, orange) project to the main olfactory bulb (light orange); OSNs of the vomeronasal organ (D, blue) project to the accessory olfactory bulb (light blue); olfactory neurons of the septal organ (C, green) and the Grüneberg Ganglion (E, pink) project to small regions of the main olfactory bulb (light green and light pink, respectively). (B) Cross-section of the main olfactory epithelium. Four layers of mature OSNs expressing different ORs are embedded in the surrounding epithelium (orange) and extend their dendrites through the mucosa (light grey) before forming extensive ciliated terminal structures. (C) Cross-section of the septal organ epithelium. The morphology of the sensory neurons and the overall tissue architecture are similar to the main olfactory epithelium except for the lower number of cell layers. (D) Cross section of the vomeronasal organ epithelium. Two layers of sensory neurons are embedded in the epithelium (blue) and extend their dendrites through the mucosa (light grey), before forming a dendritic knob decorated with microvilli. (E) Cross section of the Grüneberg Ganglion. Compact sensory neurons lacking comprehensive dendritic structures reside in a pocket between the skull (dark grey) and a layer of keratinated epithelium (light grey) (F) Summary table of the main olfactory organs in mice.

(A-D adapted from Munger et al 2009; E adapted from Brechbuhl et al 2008 F Adapted from Brechbuhl et al 2008, Kawagishi et al 2014, Munger et al 2009, Wilson & Raisman)

Figure 1-3

A

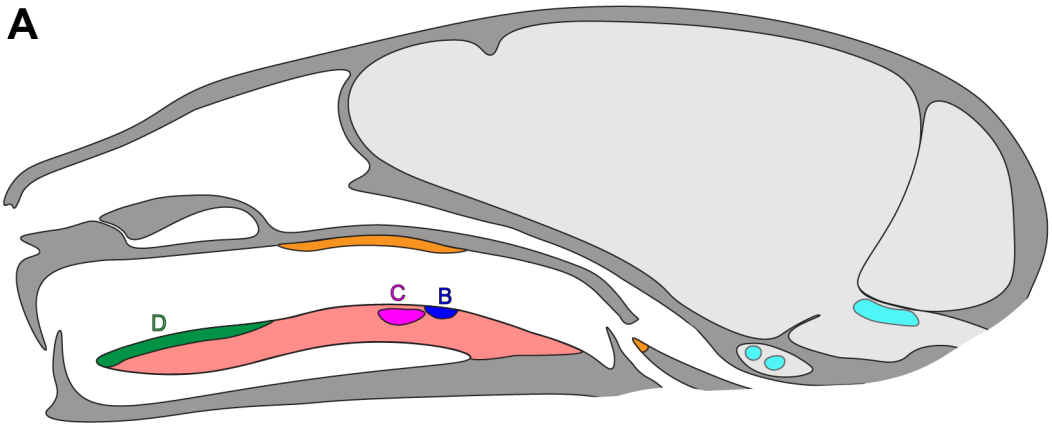

B

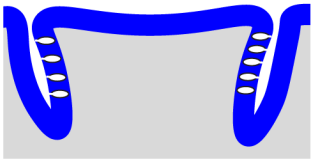

C

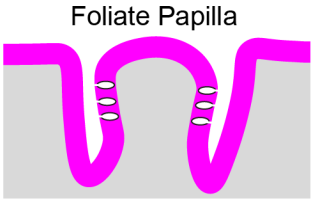

D

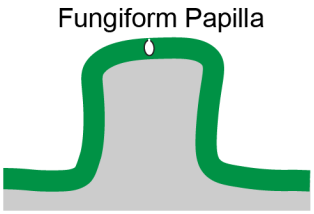

E

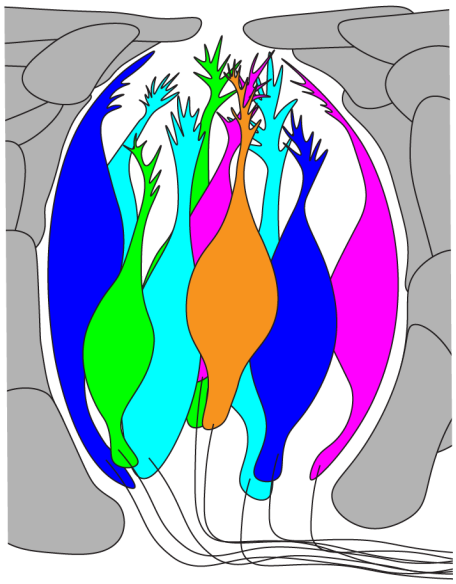

F

Lingual Papilla Type	Number of Papillae	Number of Taste Buds per Papilla
Circumvallate Papilla	1	~200
Foliate Papilla	~100	10-24
Fungiform Papilla	~90	1-3

Figure 1-3. Gustatory Organs in Mice

(A) Localization of gustatory epithelial tissues in the oral cavity and their projection targets in the brain. Taste buds on the tongue are housed in circumvallate (B, blue), foliate (C, pink) and fungiform papillae (D, green). Taste buds of the soft palate and epiglottis occur individually (orange). The neurons innervating the taste buds reside in peripheral ganglia (light blue) and project to the nucleus of the solitary tract (light blue within brain). (B) Cross section of a circumvallate papilla. Individual taste buds are indicated by white ellipses (C) Cross section of a foliate papilla (Taste buds like in B) (D) Cross section of a fungiform papilla (Taste buds like in B) (E) Cross section of a taste bud. Taste receptor cells are grouped and almost completely couched within the surrounding epithelium (grey), but are exposed to the environment via a pore. Gustatory neurons (black) relay taste information to the brain. (F) Summary table of gustatory organs in mice.

(A adapted from Yarmolinsky et al 2009; B and C adapted from Chandrashekar et al 2010; E adapted from Mistretta et al 1999; F adapted from Liu & Lee 1982, Mistretta & Baum 1984, Mistretta et al 1999)

Figure 1-4

A

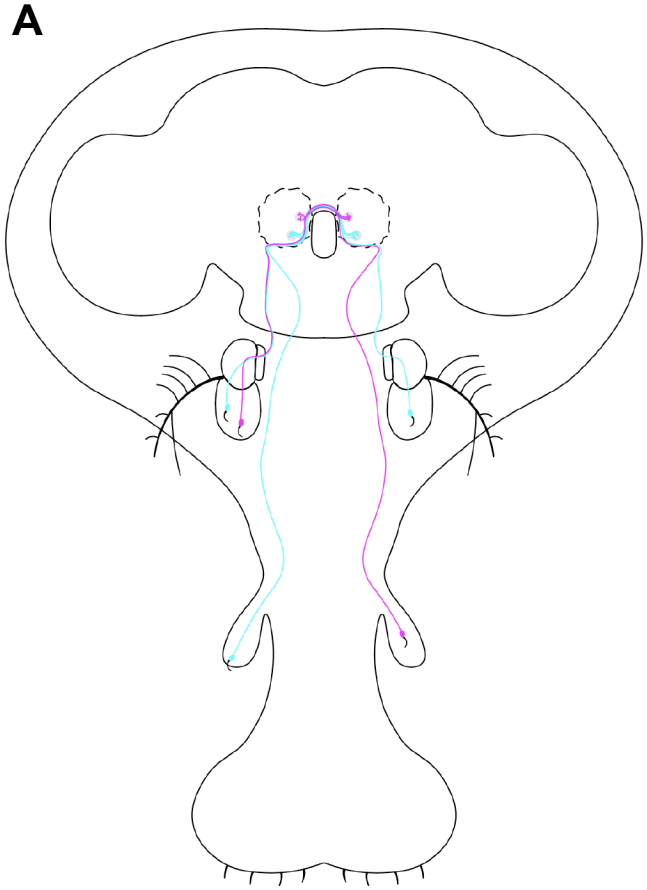

B Basiconic Sensillum

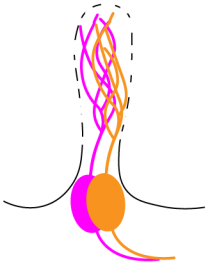

C Trichoid Sensillum

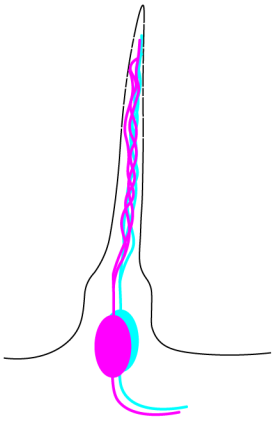

D Coeloconic Sensillum

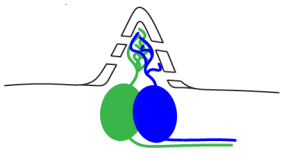

E

Body Part	Receptors	Sensillum Type	Sensillum Number	Neurons per Sensillum
Third Antennal Segment	ORs IRs	Trichoid	~115	1-3
		Basiconic	~200	2 or 4
		Coeloconic	~55	2-3
Maxillary Palp	ORs IRs GR21a, GR63a	Basiconic	~60	2

Figure 1-4. Olfactory Organs in *D. melanogaster*

(A) Localization of olfactory bristles on the third antennal segment and the maxillary palp. ORNs expressing the same receptor (indicated by colors) converge onto the same glomerulus (grey circle) in the antennal lobe of the brain, irrespective of the body part of their origin. (B-D) Types of olfactory bristles: a basiconic (B), a trichoid (C) and a coeloconic bristle (D). Multiple pores allow the entry of volatiles into the lumen, where they can interact with the dendrites of ORNs. (E) Summary table of olfactory sensilla.

(A adapted from Komiyama & Luo 2006; B-D adapted from Shanbhag et al 1999b, Stocker 1994, Venkatesh & Singh 1984 E adapted from Shanbhag et al 1999a, Stocker 1994, Benton et al 2009, Vosshall et al 1999, Jones et al 2007)

Figure 1-5

A

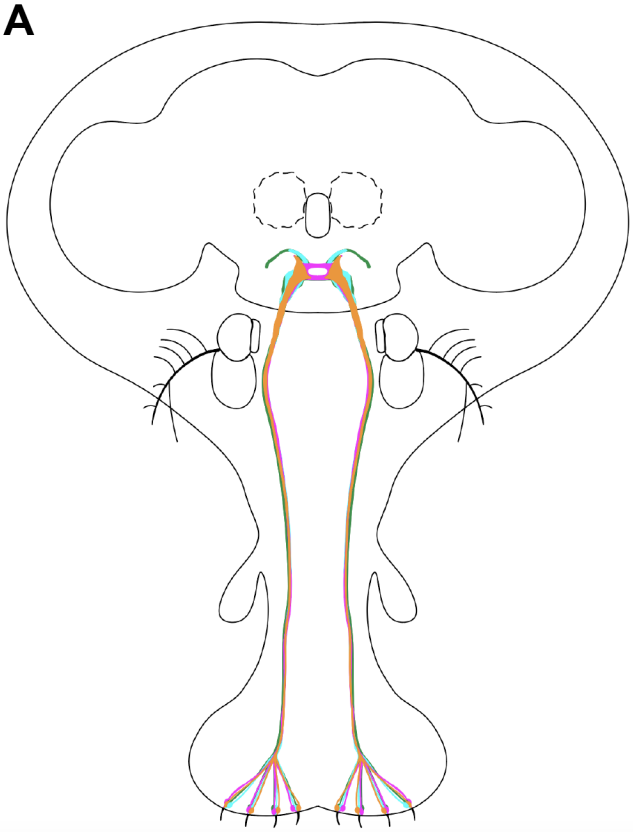

B Large Sensillum

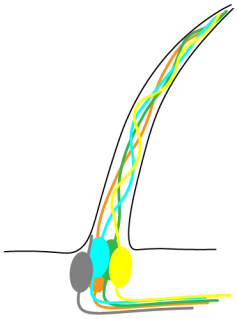

C Intermediate Sensillum

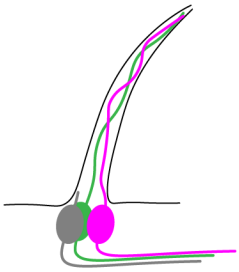

D Small Sensillum

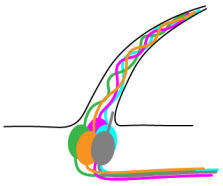

E

Taste Modality	Sensillum Type	Cell Number per Labellar Palp	Receptor
Sweet	Small Intermediate Large	31	GR64f (co-receptor?) GR5a Gr61c GR64a-e
Bitter	Small Intermediate	18-20	GR66a (co-receptor?) Remaining GRs (?)
Water	Small Large	15-21	PPK28
High Salt	Small Large	15	PPK23
Low Salt	Large	10	IR76b (co-receptor?) IR94e

Figure 1-5. Gustatory Organs in *D. melanogaster*

(A) Gustatory Organs of the outer mouthparts of *Drosophila*. GRNs project from the labellar palps at the distal tip of the proboscis along the labial nerve to the SEZ in the brain, where they terminate in characteristic patterns depending on the taste modality they encode. Bitter GRNs (pink) form a central ring structure, while the other modalities arborize more laterally. (B-D) The three main types of gustatory bristles: a large (B), an intermediate (C), and a small bristle (D). Tastants enter each bristle through a single pore at the tip of the sensillum. (E) Summary table of labellar gustatory sensilla and GRNs.

(A adapted from Kendroud et al 2018 and Wang et al 2004, B-D adapted from Nayak & Singh 1983 and Stocker 1994, E adapted from Jaeger et al 2018, Wang et al 2004, Weiss et al 2011)

References

Abuin L, Bargeton B, Ulbrich MH, Isacoff EY, Kellenberger S, Benton R. 2011. Functional architecture of olfactory ionotropic glutamate receptors. *Neuron* 69: 44-60

Adler E, Hoon MA, Mueller KL, Chandrashekar J, Ryba NJ, Zuker CS. 2000. A Novel Family of Mammalian Taste Receptors. *Cell* 100: 693-702

Adler J. 1969. Chemoreceptors in Bacteria. *Science* 166: 1588-97

Adler J, Hazelbauer GL, Dahl MM. 1973. Chemotaxis Towards Sugars in Escherichia coli. *J Bacteriol* 115: 824-47

Ai M, Blais S, Park JY, Min S, Neubert TA, Suh GS. 2013. Ionotropic glutamate receptors IR64a and IR8a form a functional odorant receptor complex in vivo in Drosophila. *J Neurosci* 33: 10741-9

Appleby PA. 2014. The role of multiple chemotactic mechanisms in a model of chemotaxis in C. elegans: different mechanisms are specialised for different environments. *J Comput Neurosci* 36: 339-54

Assadi-Porter FM, Maillet EL, Radek JT, Quijada J, Markley JL, Max M. 2010. Key amino acid residues involved in multi-point binding interactions between brazzein, a sweet protein, and the T1R2-T1R3 human sweet receptor. *J Mol Biol* 398: 584-99

Aungst JL, Heyward PM, Puche AC, Karnup SV, Hayar A, et al. 2003. Centre-Surround Inhibition Among Olfactory Bulb Glomeruli *Nature* 426: 623-29

Bargmann CI, Hartwieg E, Horvitz HR. 1993. Odorant-Selective Genes and Neurons Mediate Olfaction in C. elegans. *Cell* 74: 515-27

Bargmann CI, Horvitz HR. 1991. Chemosensory Neurons with Overlapping Functions Direct Chemotaxis to Multiple Chemicals in C. elegans. *Neuron* 7: 729-42

Barrios AW, Nunez G, Sanchez Quinteiro P, Salazar I. 2014. Anatomy, histochemistry, and immunohistochemistry of the olfactory subsystems in mice. *Front Neuroanat* 8: 63

Bates AS, Schlegel P, Roberts RJV, Drummond N, Tamimi IFM, et al. 2020. Complete Connectomic Reconstruction of Olfactory Projection Neurons in the Fly Brain. *Curr Biol* 30: 3183-99 e6

Behrens M, Brockhoff A, Batram C, Kuhn C, Appendino G, Meyerhof W. 2009. The human bitter taste receptor hTAS2R50 is activated by the two natural bitter terpenoids andrographolide and amarogentin. *J Agric Food Chem* 57: 9860-6

Belluscio L, Koentges G, Axel R, Dulac C. 1999. A Map of Pheromone Receptor Activity in the Mammalian Brain. *Cell* 97: 209-20

Benton R, Sachse S, Michnick SW, Vosshall LB. 2006. Atypical membrane topology and heteromeric function of Drosophila odorant receptors in vivo. *PLoS Biol* 4: e20

Benton R, Vannice KS, Gomez-Diaz C, Vosshall LB. 2009. Variant ionotropic glutamate receptors as chemosensory receptors in Drosophila. *Cell* 136: 149-62

Berg HC, Brown DA. 1972. Chemotaxis in Escherichia coli Analysed by Three-Dimensional Tracking *Nature* 239: 500-04

Bhandawat V, Olsen SR, Gouwens NW, Schlief ML, Wilson RI. 2007. Sensory processing in the Drosophila antennal lobe increases reliability and separability of ensemble odor representations. *Nat Neurosci* 10: 1474-82

Bo X, Alavi A, Xiang Z, Oglesby I, Ford A, Burnstock G. 1999. Localization of ATP-Gated P2X2 and P2X3 Receptor Immunoreactive Nerves in Rat Taste Buds. *NeuroReport* 10: 1107-11

Brechbuhl J, Klaey M, Broillet MC. 2008. Grueneberg Ganglion Cells Mediate Alarm Pheromone Detection in Mice. *Science* 321: 1092-95

Brechbuhl J, Klaey M, Moine F, Bovay E, Hurni N, et al. 2014. Morphological and physiological species-dependent characteristics of the rodent Grueneberg ganglion. *Front Neuroanat* 8: 87

Bressel OC, Khan M, Mombaerts P. 2016. Linear correlation between the number of olfactory sensory neurons expressing a given mouse odorant receptor gene and the total volume of the corresponding glomeruli in the olfactory bulb. *J Comp Neurol* 524: 199-209

Brockhoff A, Behrens M, Massarotti A, Appendino G, Meyerhof W. 2007. Broad Tuning of the Human Bitter Taste Receptor hTAS2R46 to Various Sesquiterpene Lactones, Clerodane and Labdane Diterpenoids, Strychnine, adn Denatonium. *J Agric Food Chem* 55: 6236-43

Buck LB, Axel R. 1991. A Novel Multigene Family May Encode Odorant Receptors: A Molecular Basis for Odor Recognition. *Cell* 65: 175-87

Butterwick JA, Del Marmol J, Kim KH, Kahlson MA, Rogow JA, et al. 2018. Cryo-EM structure of the insect olfactory receptor Orco. *Nature* 560: 447-52

Caicedo A, Roper SD. 2001. Taste Receptor Cells that Discriminate between Bitter Stimuli. *Science* 291: 1557-60

Cameron P, Hiroi M, Ngai J, Scott K. 2010. The molecular basis for water taste in Drosophila. *Nature* 465: 91-5

Cao Y, Zhao FL, Kolli T, Hivley R, Herness S. 2009. GABA expression in the mammalian taste bud functions as a route of inhibitory cell-to-cell communication. *Proc Natl Acad Sci U S A* 106: 4006-11

Challis RC, Tian H, Wang J, He J, Jiang J, et al. 2015. An Olfactory Cilia Pattern in the Mammalian Nose Ensures High Sensitivity to Odors. *Curr Biol* 25: 2503-12

Chandrashekar J, Kuhn C, Oka Y, Yarmolinsky DA, Hummler E, et al. 2010. The cells and peripheral representation of sodium taste in mice. *Nature* 464: 297-301

Chandrashekar J, Mueller KL, Hoon MA, Adler E, Feng L, et al. 2000. T2Rs Function as Bitter Taste Receptors. *Cell* 100: 703-11

Chang RB, Waters H, Liman ER. 2010. A proton current drives action potentials in genetically identified sour taste cells. *Proc Natl Acad Sci U S A* 107: 22320-5

Chen N, Pai S, Zhao Z, Mah A, Newbury R, et al. 2005. Identification of a nematode chemosensory gene family. *Proc Natl Acad Sci U S A* 102: 146-51

Chen X, Gabitto M, Peng Y, Ryba NJ, Zuker CS. 2011. A Gustotopic Map of Taste Qualities in the Mammalian Brain. *Science* 333: 1262-66

Chen Y, Amrein H. 2017. Ionotropic Receptors Mediate Drosophila Oviposition Preference through Sour Gustatory Receptor Neurons. *Curr Biol* 27: 2741-50 e4

Chess A, Simon I, Cedar H, Axel R. 1994. Allelic Inactivation Regulates Olfactory Receptor Gene Expression. *Cell* 78: 823-34

Clyne PJ, Warr CG, Carlson JR. 2000. Candidate Taste Receptors in Drosophila *Science* 287: 1830-34

Colosimo ME, Brown A, Mukhopadhyay S, Gabel C, Lanjuin AE, et al. 2004. Identification of thermosensory and olfactory neuron-specific genes via expression profiling of single neuron types. *Curr Biol* 14: 2245-51

Cook SJ, Jarrell TA, Brittin CA, Wang Y, Bloniarz AE, et al. 2019. Whole-animal connectomes of both Caenorhabditis elegans sexes. *Nature* 571: 63-71

Couto A, Alenius M, Dickson BJ. 2005. Molecular, anatomical, and functional organization of the Drosophila olfactory system. *Curr Biol* 15: 1535-47

Croset V, Rytz R, Cummins SF, Budd A, Brawand D, et al. 2010. Ancient protostome origin of chemosensory ionotropic glutamate receptors and the evolution of insect taste and olfaction. *PLoS Genet* 6: e1001064

Croset V, Schleyer M, Arguello JR, Gerber B, Benton R. 2016. A molecular and neuronal basis for amino acid sensing in the Drosophila larva. *Sci Rep* 6: 34871

Culotti JG, Russel RL. 1978. Osmotic Avoidance Defective Mutants of the Nematode Caenorhabditis elegans. *Genetics* 90: 243-56

D'Aniello B, Semin GR, Scandurra A, Pinelli C. 2017. The Vomeronasal Organ: A Neglected Organ. *Front Neuroanat* 11: 70

Dahanukar A, Foster K, van der Goes van Naters WM, Carlson JR. 2001. A Gr receptor is required for response to the sugar trehalose in taste neurons of Drosophila. *Nat Neurosci* 4: 1182-6

Dahanukar A, Lei YT, Kwon JY, Carlson JR. 2007. Two Gr genes underlie sugar reception in Drosophila. *Neuron* 56: 503-16

de Bruyne M, Foster K, Carlson JR. 2001. Odor Coding in the Drosophila Antenna. *Neuron* 30: 537-52

DeFazio RA, Dvoryanchikov G, Maruyama Y, Kim JW, Pereira E, et al. 2006. Separate populations of receptor cells and presynaptic cells in mouse taste buds. *J Neurosci* 26: 3971-80

Del Punta K, Leinders-Zufall T, Rodriguez I, Jukam D, Wysocki CJ, et al. 2002. Deficient Pheromone Responses in Mice Lacking a Cluster of Vomeronasal Receptor Genes. 419: 70-74

Delay RJ, Kinnamon JC, Roper SD. 1986. Ultrastructure of Mouse Vallate Taste Buds: II. Cell Types and Cell Lineage *J Comp Neurol* 253: 242-52

Dobritsa A, van der Goes van Naters WM, Warr CG, Steinbrecht RA, Carlson JR. 2003. Intergrating the Molecular and Cellular Basis of Odor Coding in the Drosophila Antenna. *Neuron* 37: 827-41

Dulac C, Axel R. 1995. A Novel Family of Genes Encoding Putative Receptors in Mammals. *Cell* 83: 195-206

Dunipace L, Meister S, McNealy C, Amrein H. 2001. Spatially Restricted Expression of Candidate Taste Receptors in the Drosophila Gustatory System. *Curr Biol* 11: 822-35

Falk R, Bleiser-Avivi N, Atidia J. 1976. Labellar Taste Organs of Drosophila melanogaster *J Morph* 150: 327-42

Feinstein P, Bozza T, Rodriguez I, Vassalli A, Mombaerts P. 2004. Axon guidance of mouse olfactory sensory neurons by odorant receptors and the beta2 adrenergic receptor. *Cell* 117: 833-46

Fischler W, Kong P, Marella S, Scott K. 2007. The detection of carbonation by the Drosophila gustatory system. *Nature* 448: 1054-7

Fishilevich E, Vosshall LB. 2005. Genetic and functional subdivision of the Drosophila antennal lobe. *Curr Biol* 15: 1548-53
Fleischer J, Schwarzenbacher K, Besser S, Hass N, Breer H. 2006. Olfactory receptors and signalling elements in the Grueneberg ganglion. *J Neurochem* 98: 543-54
Fleischer J, Schwarzenbacher K, Breer H. 2007. Expression of trace amine-associated receptors in the Grueneberg ganglion. *Chem Senses* 32: 623-31
Flood TF, Iguchi S, Gorczyca M, White B, Ito K, Yoshihara M. 2013. A single pair of interneurons commands the Drosophila feeding motor program. *Nature* 499: 83-7
French A, Ali Agha M, Mitra A, Yanagawa A, Sellier MJ, Marion-Poll F. 2015a. Drosophila Bitter Taste(s). *Front Integr Neurosci* 9: 58
French AS, Sellier MJ, Ali Agha M, Guigue A, Chabaud MA, et al. 2015b. Dual mechanism for bitter avoidance in Drosophila. *J Neurosci* 35: 3990-4004
Frisch D. 1967. Ultrastructure of Mouse Olfactory Mucosa. *Am J Anat* 121: 87-120
Fujii S, Yavuz A, Slone J, Jagge C, Song X, Amrein H. 2015. Drosophila sugar receptors in sweet taste perception, olfaction, and internal nutrient sensing. *Curr Biol* 25: 621-27
Fuss SH, Omura M, Mombaerts P. 2005. The Grueneberg ganglion of the mouse projects axons to glomeruli in the olfactory bulb. *Eur J Neurosci* 22: 2649-54
Gabel CV, Gabel H, Pavlichin D, Kao A, Clark DA, Samuel AD. 2007. Neural circuits mediate electrosensory behavior in Caenorhabditis elegans. *J Neurosci* 27: 7586-96
Gao Q, Yuan B, Chess A. 2000. Convergent Projections of Drosophila Olfactory Neurons to Specific Glomeruli in the Antennal Lobe. *Nat Neurosci* 3: 780-85
Gendre N, Luer K, Friche S, Grillenzoni N, Ramaekers A, et al. 2004. Integration of complex larval chemosensory organs into the adult nervous system of Drosophila. *Development* 131: 83-92
Goldman AL, Van der Goes van Naters W, Lessing D, Warr CG, Carlson JR. 2005. Coexpression of two functional odor receptors in one neuron. *Neuron* 45: 661-6
Gordon MD, Scott K. 2009. Motor control in a Drosophila taste circuit. *Neuron* 61: 373-84
Grosjean Y, Rytz R, Farine JP, Abuin L, Cortot J, et al. 2011. An olfactory receptor for food-derived odours promotes male courtship in Drosophila. *Nature* 478: 236-40
Grueneberg H. 1973. A Ganglion Probably Belonging to the N. terminalis System in the Nasal Mucosa of the Mouse. *Z Anat Entwickl Gesch* 140: 39-52
Grutsch JF, Robertson A. 1978. The cAMP Sidnal from Dictyostelium discoideum Amoebae. *Dev Biol* 66: 285-93
Hall DH, Russel RL. 1991. The Posterior Nervous System of the Nematode Caenorhabditis elegans: Serial Reconstruction of Identified Neurons and Complete Pattern of Synaptic Interactions. *J Neurosci* 11: 1-22
Hallem EA, Carlson JR. 2006. Coding of odors by a receptor repertoire. *Cell* 125: 143-60
Hallem EA, Ho MG, Carlson JR. 2004. The molecular basis of odor coding in the Drosophila antenna. *Cell* 117: 965-79
Hart AC, Sims S, Kaplan JM. 1995. Synaptic Code for Sensory Modalities Revealed by C. elegans GLR-1 Glutamate Receptor. *Nature* 378

He J, Ma L, Kim S, Nakai J, Yu CR. 2008. Encoding Gender and Individual Information in the Mouse Vomeronasal Organ *Science* 320: 535-38

Heck GL, Mierson S, DeSimone JA. 1984. Salt Taste Transduction Occurs through an Amiloride-Sensitive Sodium Transport Pathway. *Science* 223: 403-05

Heimbeck G, Bugnon V, Gendre N, Keller A, Stocker RF. 2001. A central neural circuit for experience-independent olfactory and courtship behavior in Drosophila melanogaster. *Proc Natl Acad Sci U S A* 98: 15336-41

Herrada G, Dulac C. 1997. A Novel Family of Putative Pheromone Receptors in Mammals with a Topographically Organized and Sexually Dimorphic Distribution *Cell* 90: 763-73

Hilliard MA, Bargmann CI, Bazzicalupo P. 2002. C. elegans Responds to Chemical Repellents by Integrating Sensory Inputs from the Head and the Tail. *Curr Biol* 12: 730-34

Hilliard MA, Bergamasco C, Arbucci S, Plasterk RH, Bazzicalupo P. 2004. Worms taste bitter: ASH neurons, QUI-1, GPA-3 and ODR-3 mediate quinine avoidance in Caenorhabditis elegans. *EMBO J* 23: 1101-11

Horio N, Yoshida R, Yasumatsu K, Yanagawa Y, Ishimaru Y, et al. 2011. Sour taste responses in mice lacking PKD channels. *PLoS One* 6: e20007

Huang AL, Chen X, Hoon MA, Chandrashekar J, Guo W, et al. 2006. The cells and logic for mammalian sour taste detection. *Nature* 442: 934-8

Huang YJ, Maruyama Y, Dvoryanchikov G, Pereira E, Chaudhari N, Roper SD. 2007. The role of pannexin 1 hemichannels in ATP release and cell-cell communication in mouse taste buds. *Proc Natl Acad Sci U S A* 104: 6436-41

Huang YJ, Maruyama Y, Lu KS, Pereira E, Plonsky I, et al. 2005. Mouse taste buds use serotonin as a neurotransmitter. *J Neurosci* 25: 843-7

Iino Y, Yoshida K. 2009. Parallel use of two behavioral mechanisms for chemotaxis in Caenorhabditis elegans. *J Neurosci* 29: 5370-80

Imai T, Suzuki M, Sakano H. 2006. Odorant Receptor-Derived cAMP Signals Direct Axonal Targeting. *Science* 314: 657-61

Inada H, Kawabata F, Ishimaru Y, Fushiki T, Matsunami H, Tominaga M. 2008. Off-response property of an acid-activated cation channel complex PKD1L3-PKD2L1. *EMBO Rep* 9: 690-7

Inglis PN, Ou G, Leroux MR, Scholey JM. 2007. The sensory cilia of Caenorhabditis elegans. *WormBook*: 1-22

Inoshita T, Tanimura T. 2006. Cellular identification of water gustatory receptor neurons and their central projection pattern in Drosophila. *Proc Natl Acad Sci U S A* 103: 1094-9

Ishii T, Mombaerts P. 2011. Coordinated coexpression of two vomeronasal receptor V2R genes per neuron in the mouse. *Mol Cell Neurosci* 46: 397-408

Ishimaru Y, Inada H, Kubota M, Zhuang H, Tominaga M, Matsunami H. 2006. Transient receptor potential family members PKD1L3 and PKD2L1 form a candidate sour taste receptor. *Proc Natl Acad Sci U S A* 103: 12569-74

Izquierdo EJ, Lockery SR. 2010. Evolution and analysis of minimal neural circuits for klinotaxis in Caenorhabditis elegans. *J Neurosci* 30: 12908-17

Jaeger AH, Stanley M, Weiss ZF, Musso PY, Chan RC, et al. 2018. A complex peripheral code for salt taste in Drosophila. *Elife* 7

Jafari S, Alkhori L, Schleiffer A, Brochtrup A, Hummel T, Alenius M. 2012. Combinatorial activation and repression by seven transcription factors specify Drosophila odorant receptor expression. *PLoS Biol* 10: e1001280

Jefferis GS, Potter CJ, Chan AM, Marin EC, Rohlfing T, et al. 2007. Comprehensive maps of Drosophila higher olfactory centers: spatially segregated fruit and pheromone representation. *Cell* 128: 1187-203

Jiang P, Ji Q, Liu Z, Snyder LA, Benard LM, et al. 2004. The cysteine-rich region of T1R3 determines responses to intensely sweet proteins. *J Biol Chem* 279: 45068-75

Jiao Y, Moon SJ, Wang X, Ren Q, Montell C. 2008. Gr64f is required in combination with other gustatory receptors for sugar detection in Drosophila. *Curr Biol* 18: 1797-801

Jin H, Fishman ZH, Ye M, Wang L, Zuker CS. 2021. Top-Down Control of Sweet and Bitter Taste in the Mammalian Brain. *Cell* 184: 257-71 e16

Johnson JR, Edwards MR, Davies H, Newman D, Holden W, et al. 2017. Ethanol Stimulates Locomotion via a Galphas-Signaling Pathway in IL2 Neurons in Caenorhabditis elegans. *Genetics* 207: 1023-39

Jones WD, Cayirlioglu P, Kadow IG, Vosshall LB. 2007. Two chemosensory receptors together mediate carbon dioxide detection in Drosophila. *Nature* 445: 86-90

Kaluza JF, Gussing F, Bohm S, Breer H, Strotmann J. 2004. Olfactory receptors in the mouse septal organ. *J Neurosci Res* 76: 442-52

Kaplan JM, Horvitz HR. 1993. A Dual Mechanosensory and Chemosensory Neuron in Caenorhabditis elegans. *Proc Natl Acad Sci U S A* 90: 2227-31

Karunadasa DK, Chapman C, Bicknell RJ. 2006. Expression of pheromone receptor gene families during olfactory development in the mouse: expression of a V1 receptor in the main olfactory epithelium. *Eur J Neurosci* 23: 2563-72

Kataoka S, Yang R, Ishimaru Y, Matsunami H, Sevigny J, et al. 2008. The candidate sour taste receptor, PKD2L1, is expressed by type III taste cells in the mouse. *Chem Senses* 33: 243-54

Kato S, Xu Y, Cho CE, Abbott LF, Bargmann CI. 2014. Temporal responses of C. elegans chemosensory neurons are preserved in behavioral dynamics. *Neuron* 81: 616-28

Kawagishi K, Ando M, Yokouchi K, Sumitomo N, Karasawa M, et al. 2014. Stereological quantification of olfactory receptor neurons in mice. *Neuroscience* 272: 29-33

Kendroud S, Bohra AA, Kuert PA, Nguyen B, Guillermin O, et al. 2018. Structure and development of the subesophageal zone of the Drosophila brain. II. Sensory compartments. *J Comp Neurol* 526: 33-58

Kimoto H, Haga S, Sato K, Touhara K. 2005. Sex-specific peptides from exocrine glands stimulate mouse vomeronasal sensory neurons. *Nature* 437: 898-901

Kinnamon JC, Henzler DM, Royer SM. 1993. HVEM Ultrastructural Analysis of Mouse Fungiform Taste Buds, Cell Types, and Associated Synapses. *Microsc Res Techniq* 26: 142-56

Kishi K, Mori K, Tazawa Y. 1982. Three-Dimensional Analysis of Dendritic Trees of Mitral Cells in the Rabbit Olfactory Bulb. *Neurosci Lett* 28: 127-32

Kobayakawa K, Kobayakawa R, Matsumoto H, Oka Y, Imai T, et al. 2007. Innate versus learned odour processing in the mouse olfactory bulb. *Nature* 450: 503-8

Kobayashi K. 1989. Three-Dimensional Architecture of the Connective Tissue Papillae of the Mouse Tongue as Viewed by Scanning Electron Microscopy. *Acta Anat Nippon* 64: 523-38
Kobayashi K. 1994. Three-Dimensional Fine Structure of the Lingual Papillae and their Connective Tissue Cores in the Human Tongue. *Acta Anat Nippon* 69: 624-35
Koh TW, He Z, Gorur-Shandilya S, Menuz K, Larter NK, et al. 2014. The Drosophila IR20a clade of ionotropic receptors are candidate taste and pheromone receptors. *Neuron* 83: 850-65
Kojima I, Nakagawa T, Hamano K, Medina J, Li L, Nagasawa M. 2015. Glucose-Sensing Receptor T1R3: A New Signaling Receptor Activated by Glucose in Pancreatic b-Cells. *Biol Pharm Bull* 38: 674-79
Komiyama T, Luo L. 2006. Development of wiring specificity in the olfactory system. *Curr Opin Neurobiol* 16: 67-73
Krautwurst D, Yau K, Reed RR. 1998. Identification of Ligands for Olfactory Receptors by Functional Expression of a Receptor Library *Cell* 95: 917-26
Kuhn C, Bufe B, Winnig M, Hofmann T, Frank O, et al. 2004. Bitter taste receptors for saccharin and acesulfame K. *J Neurosci* 24: 10260-5
Kwon JY, Dahanukar A, Weiss LA, Carlson JR. 2007. The molecular basis of CO2 reception in Drosophila. *Proc Natl Acad Sci U S A* 104: 3574-8
Laissue PP, Reiter C, Hiesinger PR, Halter S, Fischbach KF, Stocker RF. 1999. Three-Dimensional Reconstruction of the Antennal Lobe in Drosophila melanogaster. *J Comp Neurol* 405: 543-52
Lambert A, Takahashi N, Charon NW, Picardeau M. 2012. Chemotactic behavior of pathogenic and nonpathogenic Leptospira species. *Appl Environ Microbiol* 78: 8467-9
Larsson MC, Domingos AI, Jones WD, Chiappe ME, Amrein H, Vosshall LB. 2004. Or83b encodes a broadly expressed odorant receptor essential for Drosophila olfaction. *Neuron* 43: 703-14
Lee H, Choi MK, Lee D, Kim HS, Hwang H, et al. 2011. Nictation, a dispersal behavior of the nematode Caenorhabditis elegans, is regulated by IL2 neurons. *Nat Neurosci* 15: 107-12
Lee MJ, Sung HY, Jo H, Kim HW, Choi MS, et al. 2017. Ionotropic Receptor 76b Is Required for Gustatory Aversion to Excessive Na+ in Drosophila. *Mol Cells* 40: 787-95
Lee Y, Poudel S, Kim Y, Thakur D, Montell C. 2018. Calcium Taste Avoidance in Drosophila. *Neuron* 97: 67-74 e4
Leinders-Zufall T, Lane AP, Puche AC, Ma W, Novotny MV, et al. 2000. Ultrasensitive Pheromone Detection by Mammalian Vomeronasal Neurons. *Nature* 405: 792-96
Li X, Staszewski L, Xu H, Durick K, Zoller M, Adler E. 2002. Human receptors for sweet and umami taste. *Proc Natl Acad Sci U S A* 99: 4692-6
Lindemann B. 2001. Receptors and Transduction in Taste. *Nature* 413: 219-25
Liu HC, Lee JC. 1982. Scanning Electron Microscopic and Histochemical Studies of Foliate Papillae in the Rabbit, Rat and Mouse. *Acta Anat* 112: 310-20
Lomvardas S, Barnea G, Pisapia DJ, Mendelsohn M, Kirkland J, Axel R. 2006. Interchromosomal interactions and olfactory receptor choice. *Cell* 126: 403-13

Loomis WF. 2014. Cell signaling during development of Dictyostelium. *Dev Biol* 391: 1-16

Lu T, Qiu YT, Wang G, Kwon JY, Rutzler M, et al. 2007. Odor coding in the maxillary palp of the malaria vector mosquito Anopheles gambiae. *Curr Biol* 17: 1533-44

Ma M, Grosmaitre X, Iwema CL, Baker H, Greer CA, Shepherd GM. 2003. Olfactory Signal Transduction in the Mouse Septal Organ *J Neurosci* 23: 317-24

Ma M, Shepherd GM. 2000. Functional mosaic organization of mouse olfactory receptor neurons. *Proc Natl Acad Sci U S A* 97: 12869-74

Malnic B, Hirono J, Sato T, Buck LB. 1999. Combinatorial Receptor Codes for Odors. *Cell* 96: 713-23

Marella S, Fischler W, Kong P, Asgarian S, Rueckert E, Scott K. 2006. Imaging taste responses in the fly brain reveals a functional map of taste category and behavior. *Neuron* 49: 285-95

Marin EC, Jefferis GSXE, Komiyama T, Zhu H, Luo L. 2002. Representation of the Glomerular Olfactory Map in the Drosophila Brain. *Cell* 109: 243-55

Marshall DA, Maruniak JA. 1986. Masera's Organ Responds to Odorants. *Brain Res* 366: 329-32

Martini S, Silvotti L, Shirazi A, Ryba NJ, Tirindelli R. 2001. Co-Expression of Putative Pheromone Receptors in the Sensory Neurons of the Vomeronasal Organ. *J Neurosci* 21: 843-48

Maruyama IN. 2016. Receptor Guanylyl Cyclases in Sensory Processing. *Front Endocrinol (Lausanne)* 7: 173

Masuda K, Koizumi A, Nakajima K, Tanaka T, Abe K, et al. 2012. Characterization of the modes of binding between human sweet taste receptor and low-molecular-weight sweet compounds. *PLoS One* 7: e35380

Matsunami H, Buck LB. 1997. A Multigene Family Encoding a Diverse Array of Putative Pheromone Receptors in Mammals. *Cell* 90: 775-84

Matsunami H, Montmayeur J, Buck LB. 2000. A Family of Candidate Taste Receptors in Human and Mouse. *Nature* 404: 601-04

McKellar CE, Siwanowicz I, Dickson BJ, Simpson JH. 2020. Controlling motor neurons of every muscle for fly proboscis reaching. *Elife* 9

Mellem JE, Brockie PJ, Zheng Y, Madsen DM, Maricq AV. 2002. Decoding of Polymodal Sensory Stimuli by Postsynaptic Glutamate Receptors in C. elegans. *Neuron* 36: 933-44

Melton T, Hartman PE, Stratis JP, Lee TL, Davis AT. 1978. Chemotaxis of Salmonella typhimurium to Amino Acids and Some Sugars. *J Bacteriol* 133: 708-16

Metaxakis A, Petratou D, Tavernarakis N. 2018. Multimodal sensory processing in Caenorhabditis elegans. *Open Biol* 8

Meunier N, Marion-Poll F, Rospars JP, Tanimura T. 2003. Peripheral coding of bitter taste in Drosophila. *J Neurobiol* 56: 139-52

Meyerhof W, Batram C, Kuhn C, Brockhoff A, Chudoba E, et al. 2010. The molecular receptive ranges of human TAS2R bitter taste receptors. *Chem Senses* 35: 157-70

Mistretta C, Baum BJ. 1984. Quantitative Study of Taste Buds in Fungiform and Circumvallate Papillae of Young and Aged Rats *J Anat* 138: 323-32

Mistretta C, Goosens KA, Farinas I, Reichardt LF. 1999. Alterations in Size, Number, and Morphology of Gustatory Papillae and Taste Buds in BDNF Null Mutant Mice Demonstrate Neural Dependence of Developing Taste Organs. *J Comp Neurol* 409: 13-24

Miyamoto T, Chen Y, Slone J, Amrein H. 2013. Identification of a Drosophila glucose receptor using Ca2+ imaging of single chemosensory neurons. *PLoS One* 8: e56304

Miyazaki T, Lin TY, Ito K, Lee CH, Stopfer M. 2015. A gustatory second-order neuron that connects sucrose-sensitive primary neurons and a distinct region of the gnathal ganglion in the Drosophila brain. *J Neurogenet* 29: 144-55

Mombaerts P, Wang F, Dulac C, Chao SK, Nemes A, et al. 1996. Visualizing an Olfactory Sensory Map. *Cell* 87: 675-86

Moon SJ, Kottgen M, Jiao Y, Xu H, Montell C. 2006. A taste receptor required for the caffeine response in vivo. *Curr Biol* 16: 1812-7

Mori I, Ohshima Y. 1995. Neural Regulation of Thermotaxis in Caenorhabditis elegans. *Nature* 376: 344-48

Moulton RC, Montie TC. 1979. Chemotaxis by Pseudomonas aeruginosa. *J Bacteriol* 137: 274-80

Mueller KL, Hoon MA, Erlenbach I, Chandrashekar J, Zuker CS, Ryba NJ. 2005. The Receptors and Coding Logic for Bitter Taste. *Nature* 434: 225-9

Munger SD, Leinders-Zufall T, Zufall F. 2009. Subsystem organization of the mammalian sense of smell. *Annu Rev Physiol* 71: 115-40

Nayak S, Singh R. 1983. Sensilla on the tarsal segments and mouthparts of adult Drosophila melanogaster meigen *Int J Insect Morphol & Embryol* 12: 273-91

Nelson G, Chandrashekar J, Hoon MA, Feng L, Zhao G, et al. 2002. An Amino-Acid Taste Receptor. *Nature* 416: 199-202

Nelson G, Hoon MA, Chandrashekar J, Zhang Y, Ryba NJ, Zuker CS. 2001. Mammalian Sweet Taste Receptors. *Cell* 106: 381-90

Neuhaus EM, Gisselmann G, Zhang W, Dooley R, Stortkuhl K, Hatt H. 2005. Odorant receptor heterodimerization in the olfactory system of Drosophila melanogaster. *Nat Neurosci* 8: 15-7

Ninomiya Y. 1998. Reinnervation of Cross-Regerated Gustatory Nerve Fibers into Amiloride-Sensitive and Amiloride-Insensitive Taste Receptor Cells. *Proc Natl Acad Sci U S A* 95: 5347-50

Ninomiya Y, Sako N, Funakoshi M. 1989. Strain Differences in Amiloride Inhibition of NaCl Responses in Mice, Mus musculus. *J Comp Physiol A* 166: 1-5

Nuemket N, Yasui N, Kusakabe Y, Nomura Y, Atsumi N, et al. 2017. Structural basis for perception of diverse chemical substances by T1r taste receptors. *Nat Commun* 8: 15530

Ogata T, Ohtubo Y. 2020. Quantitative Analysis of Taste Bud Cell Numbers in the Circumvallate and Foliate Taste Buds of Mice. *Chem Senses* 45: 261-73

Ohtubo Y, Yoshii K. 2011. Quantitative analysis of taste bud cell numbers in fungiform and soft palate taste buds of mice. *Brain Res* 1367: 13-21

Oka Y, Butnaru M, von Buchholtz L, Ryba NJ, Zuker CS. 2013. High salt recruits aversive taste pathways. *Nature* 494: 472-5

Oliveira-Maia AJ, Stapleton-Kotloski JR, Lyall V, Phan TH, Mummalaneni S, et al. 2009. Nicotine activates TRPM5-dependent and independent taste pathways. *Proc Natl Acad Sci U S A* 106: 1596-601

Ordal GW, Gibson KJ. 1977. Chemotaxis Toward Amino Acids by Bacillus subtilis. *J Bacteriol* 129: 151-55

Ordal GW, Villani DP, Rosendahl MS. 1979. Chemotaxis Towards Sugars by Bacillus subtilis. *J Gen Microbiol* 115: 167-72

Pedersen PE, Benson TE. 1986. Projection of Septal Organ Receptor Neurons to the Main Olfactory Bulb in Rats. *J Comp Neurol* 252: 555-62

Perkins LA, Hedgecock EM, Thomson JN, Culotti JG. 1986. Mutant Sensory Cilia in the Nematode Caenorhabditis elegans. *Dev Biol* 117

Pierce-Shimomura JT, Dores M, Lockery SR. 2005. Analysis of the effects of turning bias on chemotaxis in C. elegans. *J Exp Biol* 208: 4727-33

Pierce-Shimomura JT, Faumont S, Gaston MR, Pearson BJ, Lockery SR. 2001. The Homeobox Gene lim-6 is Required for Distinct Chemosensory Representations in C. elegans. *Nature* 410: 694-98

Pierce-Shimomura JT, Morse TM, Lockery SR. 1999. The Fundamental Role of Pirouettes in Caenorhabditis elegans Chemotaxis. *J Neurosci* 19: 9557-69

Pronin AN, Tang H, Connor J, Keung W. 2004. Identification of ligands for two human bitter T2R receptors. *Chem Senses* 29: 583-93

Ray K, Hartenstein V, Rodrigues V. 1993. Development of the Taste Bristles on the Labellum of Drosophila melanogaster. *Dev Biol* 155: 26-37

Ressler KJ, Sullivan SL, Buck LB. 1993. A Zonal Organization of Odorant Receptor Gene Expression in the Olfactory Epithelium. *Cell* 73: 597-609

Ressler KJ, Sullivan SL, Buck LB. 1994. Information Coding in the Olfactory System: Evidence for a Stereotyped and Highly Organized Epitope Map in the Olfactory Bulb. *Cell* 79: 1245-55

Riesgo-Escovar JR, Piekos WB, Carlson JR. 1997a. The Drosophila Antenna: Ultrastructural and Physiological Studies in Wild-Type and lozenge Mutants. *J Comp Physiol A* 180: 151-60

Riesgo-Escovar JR, Piekos WB, Carlson JR. 1997b. The Maxillary Palp of Drosophila: Ultrastructure and Physiology depends on the lozenge Gene.

Robertson HM, Kent LB. 2009. Evolution of the Gene Lineage Encoding the Carbon Dioxide Receptor in Insects *J Insect Sci* 9: 14pp

Robertson HM, Warr CG, Carlson JR. 2003. Molecular evolution of the insect chemoreceptor gene superfamily in Drosophila melanogaster. *Proc Natl Acad Sci U S A* 100 Suppl 2: 14537-42

Rodriguez I, Del Punta K, Rothman A, Ishii T, Mombaerts P. 2002. Multiple new and isolated families within the mouse superfamily of V1r vomeronasal receptors. *Nat Neurosci* 5: 134-40

Rodriguez I, Feinstein P, Mombaerts P. 1999. Variable Patterns of Axonal Projections of Sensory Neurons in the Mouse Vomeronasal System. *Cell* 97: 199-208

Romanov RA, Rogachevskaja OA, Bystrova MF, Jiang P, Margolskee RF, Kolesnikov SS. 2007. Afferent neurotransmission mediated by hemichannels in mammalian taste cells. *EMBO J* 26: 657-67

Roppolo D, Ribaud V, Jungo VP, Luscher C, Rodriguez I. 2006. Projection of the Gruneberg ganglion to the mouse olfactory bulb. *Eur J Neurosci* 23: 2887-94
Sato K, Pellegrino M, Nakagawa T, Nakagawa T, Vosshall LB, Touhara K. 2008. Insect olfactory receptors are heteromeric ligand-gated ion channels. *Nature* 452: 1002-6
Schaap P, Konijn TM, van Haastert PJM. 1984. cAMP Pulses Coordinate Morphogenetic Movement During Fruiting Body Formation of Dictyostelium minutum. *Proc Natl Acad Sci U S A* 81: 2122-26
Schmid A, Pyrski M, Biel M, Leinders-Zufall T, Zufall F. 2010. Grueneberg ganglion neurons are finely tuned cold sensors. *J Neurosci* 30: 7563-8
Schwarz O, Bohra AA, Liu X, Reichert H, VijayRaghavan K, Pielage J. 2017. Motor control of Drosophila feeding behavior. *Elife* 6
Scott K, Brady R, Cravchik A, Morozov P, Rzhetsky A, et al. 2001. A Chemosensory Gene Family Encoding Candidate Gustatory and Olfactory Receptors in Drosophila *Cell* 104: 661-73
Seymour FWK, Doetsch RN. 1973. Chemotactic Responses by Motile Bacteria. *J Gen Microbiol* 78: 287-96
Shanbhag SR, Mueller B, Steinbrecht RA. 1999a. Atlas of Olfactory Organs of Drosophila melanogaster: 1. Types, External Organization, Innervation and Distribution of Olfactory Sensilla. *Int J Insect Morphol & Embryol* 28: 377-97
Shanbhag SR, Muller B, Steinbrecht RA. 1999b. Atlas of Olfactory Organs of Drosophila melanogaster: 1. Types, External Organization, Innervation and Distribution of Olfactory Sensilla 28: 377-97
Shanbhag SR, Park SK, Pikielny CW, Steinbrecht RA. 2001. Gustatory organs of Drosophila melanogaster: fine structure and expression of the putative odorant-binding protein PBPRP2. *Cell Tissue Res* 304: 423-37
Silbering AF, Galizia CG. 2007. Processing of odor mixtures in the Drosophila antennal lobe reveals both global inhibition and glomerulus-specific interactions. *J Neurosci* 27: 11966-77
Silbering AF, Rytz R, Grosjean Y, Abuin L, Ramdya P, et al. 2011. Complementary function and integrated wiring of the evolutionarily distinct Drosophila olfactory subsystems. *J Neurosci* 31: 13357-75
Slone J, Daniels J, Amrein H. 2007. Sugar receptors in Drosophila. *Curr Biol* 17: 1809-16
Smith JL, Doetsch RN. 1969. Studies on Negative Chemotaxis and the Survival Value of Motility in Pseudomonas fluorescens. *J Gen Microbiol* 55: 379-91
Sourjik V, Wingreen NS. 2012. Responding to chemical gradients: bacterial chemotaxis. *Curr Opin Cell Biol* 24: 262-8
Stocker RF. 1994. The Organization of the Chemosensory System in Drosophila melanogaster: a Review *Cell Tissue Res* 275: 3-26
Stocker RF, Lienhard MC, Borst A, Fischbach KF. 1990. Neuronal Architecture of the Antennal Lobe in Drosophila melanogaster. *Cell Tissue Res* 262: 9-34
Stocker RF, Schorderet M. 1981. Cobalt Filling of Sensory Projections from Internal and External Mouthparts in Drosophila. *Cell Tissue Res* 216: 513-23
Stone LM, Finger TE, Tam PPL, Tan S. 1995. Taste Receptor Cells Arise from Local Epithelium, not Neurogenic Ectoderm. *Proc Natl Acad Sci U S A* 92: 1916-20

Strotmann J, Wanner I, Helfrich T, Beck A, Meinken C, et al. 1994. Olfactory Neurones Expressing Distinct Odorant Receptor Subtypes are Spatially Segregated in the Nasal Neuroepithelium *Cell Tissue Res* 276: 429-38

Su CY, Menuz K, Carlson JR. 2009. Olfactory perception: receptors, cells, and circuits. *Cell* 139: 45-59

Sung HY, Jeong YT, Lim JY, Kim H, Oh SM, et al. 2017. Heterogeneity in the Drosophila gustatory receptor complexes that detect aversive compounds. *Nat Commun* 8: 1484

Suzuki H, Thiele TR, Faumont S, Ezcurra M, Lockery SR, Schafer WR. 2008. Functional asymmetry in Caenorhabditis elegans taste neurons and its computational role in chemotaxis. *Nature* 454: 114-7

Tanimura T, Isono K, Takamura T, Shimada I. 1982. Genetic Dimorphism in the Taste Sensitivity to Trehalose in Drosophila melanogaster. *J Comp Physiol A* 147: 433-37

Tanimura T, Isono K, Yamamoto K. 1988. Taste Sensitivity to Trehalose and Its Alteration by Gene Dosage in Drosophila melanogaster. *Genetics* 119: 399-406

Thiele TR, Faumont S, Lockery SR. 2009. The neural network for chemotaxis to tastants in Caenorhabditis elegans is specialized for temporal differentiation. *J Neurosci* 29: 11904-11

Thomas JH, Robertson HM. 2008. The Caenorhabditis chemoreceptor gene families. *BMC Biol* 6: 42

Thorne N, Amrein H. 2008. Atypical expression of Drosophila gustatory receptor genes in sensory and central neurons. *J Comp Neurol* 506: 548-68

Thorne N, Chromey C, Bray S, Amrein H. 2004. Taste perception and coding in Drosophila. *Curr Biol* 14: 1065-79

Tian H, Ma M. 2004. Molecular organization of the olfactory septal organ. *J Neurosci* 24: 8383-90

Tordoff MG, Alarcon LK, Valmeki S, Jiang P. 2012. T1R3: a human calcium taste receptor. *Sci Rep* 2: 496

Trinh K, Storm DR. 2003. Vomeronasal organ detects odorants in absence of signaling through main olfactory epithelium. *Nat Neurosci* 6: 519-25

Troemel ER, Chou JH, Dwyer ND, Colbert HA, Bargmann CI. 1995. Divergent Seven Transmembrane Receptors are Candidate Chemosensory Receptors in C. elegans. *Cell* 83: 207-18

Troemel ER, Kimmel BE, Bargmann CI. 1997. Reprogramming Chemotaxis Responses: Sensory Neurons Define Olfactory Preferences in C. elegans. *Cell* 91: 161-69

Tso W, Adler J. 1974. Negative Chemotaxis in Escherichia coli. *J Bacteriol* 118: 560-76

Tu Y, Cooper AJ, Teng B, Chang RB, Artiga DJ, et al. 2018. An Evolutionary Conserved Gene Family Encodes Proton-Selective Ion Channels. *Science* 359: 1047-50

Ueno K, Ohta M, Morita H, Mikuni Y, Nakajima S, et al. 2001. Trehalose Sensitivity in Drosophila correlates with Mutations in and Expression of the Gustatory Receptor Gene Gr5a. *Curr Biol* 11: 1451-55

Vaccarezza OL, Sepich LN, Tramezzani JH. 1981. The Vomeronasal Organ of the Rat. *J Anat* 132: 167-85

Vassar R, Chao SK, Sitcheran R, Nunez JM, Vosshall LB, Axel R. 1994. Topographic Organization of Sensory Projections to the Olfactory Bulb. *Cell* 79: 981-91

Vassar R, Ngai J, Axel R. 1993. Spatial Segregation of Odorant Receptor Expression in the Mammalian Olfactory Epithelium. *Cell* 74: 309-18

Venkatesh S, Singh RN. 1984. Sensilla on the Third Antennal Segment of Drosophila melanogaster meigen (Diptera: Drosophilidae). *Int J Insect Morphol & Embryol* 13: 51-63

Vidal B, Aghayeva U, Sun H, Wang C, Glenwinkel L, et al. 2018. An atlas of Caenorhabditis elegans chemoreceptor expression. *PLoS Biol* 16: e2004218

Vosshall LB, Amrein H, Morozov PS, Rzhetsky A, Axel R. 1999. A Spatial Map of Olfactory Receptor Expression in the Drosophila Antenna *Cell* 96: 725-36

Vosshall LB, Wong AM, Axel R. 2000. An Olfactory Sensory Map in the Fly Brain. *Cell* 102: 147-59

Wachowiak M, Cohen LB. 2001. Representation of Odorants by Receptor Neuron Input in the Mouse Olfactory Bulb. *Neuron* 32

Wang Z, Balet Sindreu C, Li V, Nudelman A, Chan GC, Storm DR. 2006. Pheromone detection in male mice depends on signaling through the type 3 adenylyl cyclase in the main olfactory epithelium. *J Neurosci* 26: 7375-9

Wang Z, Singhvi A, Kong P, Scott K. 2004. Taste representations in the Drosophila brain. *Cell* 117: 981-91

Ward A, Liu J, Feng Z, Xu XZ. 2008. Light-sensitive neurons and channels mediate phototaxis in C. elegans. *Nat Neurosci* 11: 916-22

Ward S. 1973. Chemotaxis by the Nematode Caenorhabditis elegans: Identification of Attractants and Analysis of the Response by the Use of Mutants. *Proc Natl Acad Sci U S A* 70: 817-21

Ward S, Thomson N, White JG, Brenner S. 1975. Electron Microscopical Reconstructionof the Anterior Sensory Anatomy of the Nematode Caenorhabditis elegans. *J Comp Neurol* 160: 313-38

Ware RW, Clark D, Crossland K, Russel RL. 1975. The Nerve Ring of the Nematode Caenorhabditis elegans: Sensory Input and Motor Output. *J Comp Neurol* 162: 71-110

Weiler E, Farbman AI. 2003. The septal organ of the rat during postnatal development. *Chem Senses* 28: 581-93

Weiss LA, Dahanukar A, Kwon JY, Banerjee D, Carlson JR. 2011. The molecular and cellular basis of bitter taste in Drosophila. *Neuron* 69: 258-72

Wes PD, Bargmann CI. 2001. C. elegans Odour Discrimination requires Asymmetric Diversity in Olfactory Neurons. *Nature* 410: 698-701

White JG, Southgate E, Thomson JN, Brenner S. 1986. The Structure of the Nervous System of the Nematode Caenorhabditis elegans. *Philos Trans R Soc Lond B Biol Sci* 314: 1-340

Wicher D, Schafer R, Bauernfeind R, Stensmyr MC, Heller R, et al. 2008. Drosophila odorant receptors are both ligand-gated and cyclic-nucleotide-activated cation channels. *Nature* 452: 1007-11

Wilson KCP, Raisman G. 1980. Age-Related Changes in the Neurosensory Epithelium of the Mouse Vomeronasal Organ: Extended Period of Post-Natal Growth in Size and Evidence for Rapid Cell Turnover in the Adult *Brain Res* 185: 103-13

Wilson RI, Turner GC, Laurent G. 2004. Transformation of Olfactory Representations in the Drosophila Antennal Lobe *Science* 303

Wong AM, Wang JW, Axel R. 2002. Spatial Representation of the Glomerular Map in the Drosophila Protocerebrum. *Cell* 109: 229-41

Xu H, Staszewski L, Tang H, Adler E, Zoller M, Li X. 2004. Different functional roles of T1R subunits in the heteromeric taste receptors. *Proc Natl Acad Sci U S A* 101: 14258-63

Yang H, Shi P, Zhang YP, Zhang J. 2005. Composition and evolution of the V2r vomeronasal receptor gene repertoire in mice and rats. *Genomics* 86: 306-15

Yang R, Crowley HH, Rock ME, Kinnamon JC. 2000. Taste Cell with Synapses in Rat Circumvallate Papillae Display SNAP-25-Like Immunoreactivity *J Comp Neurol* 424: 205-15

Yarmolinsky DA, Zuker CS, Ryba NJ. 2009. Common sense about taste: from mammals to insects. *Cell* 139: 234-44

Yoshida K, Hirotsu T, Tagawa T, Oda S, Wakabayashi T, et al. 2012. Odour concentration-dependent olfactory preference change in C. elegans. *Nat Commun* 3: 739

Yoshida R, Horio N, Murata Y, Yasumatsu K, Shigemura N, Ninomiya Y. 2009. NaCl responsive taste cells in the mouse fungiform taste buds. *Neuroscience* 159: 795-803

Young LY, Mitchell R. 1973. Negative Chemotaxis of Marine Bacteria to Toxic Chemicals. *Appl Microbiol* 25: 972-75

Yu S, Avery L, Baude E, Garbers DL. 1997. Guanylyl Cyclase Expression in Specific Sensory Neurons: A New Family of Chemosensory Receptors *Proc Natl Acad Sci U S A* 94: 3384-87

Zapiec B, Mombaerts P. 2020. The Zonal Organization of Odorant Receptor Gene Choice in the Main Olfactory Epithelium of the Mouse. *Cell Rep* 30: 4220-34 e5

Zhang J, Jin H, Zhang W, Ding C, O'Keeffe S, et al. 2019. Sour Sensing from the Tongue to the Brain. *Cell* 179: 392-402 e15

Zhang X, Zhang X, Firestein S. 2007. Comparative genomics of odorant and pheromone receptor genes in rodents. *Genomics* 89: 441-50

Zhang YV, Ni J, Montell C. 2013. The Molecular Basis for Attractive Salt-Taste Coding in Drosophila. *Science* 340: 1334-38

Zhao GQ, Zhang Y, Hoon MA, Chandrashekar J, Erlenbach I, et al. 2003. The Receptors for Mammalian Sweet and Umami Taste. *Cell* 115: 255-66

Chapter 2: Drosophila gustatory projections are segregated by taste modality and connectivity

Parts of this work were completed in collaboration with David Harris and Gabriella Sterne

Abstract

Gustatory sensory neurons detect caloric and harmful compounds in potential food and convey this information to the brain to inform feeding decisions. To examine the signals that gustatory neurons transmit and receive, we reconstructed gustatory axons and their synaptic sites in the adult *Drosophila melanogaster* brain, utilizing a whole-brain electron microscopy volume. We reconstructed 87 gustatory projections from the proboscis labellum in the right hemisphere and 57 in the left, representing the majority of labellar gustatory axons. Morphology- and connectivity-based clustering revealed six distinct clusters representing neurons recognizing different taste modalities. Gustatory neurons contain a nearly equal number of interspersed pre-and post-synaptic sites, with extensive synaptic connectivity among gustatory axons. The vast majority of synaptic connections are between neurons recognizing the same taste modality, although connections also exist between neurons of different taste modalities. This study resolves the anatomy of labellar gustatory projections, reveals that gustatory projections are segregated based on taste modality, and uncovers synaptic connections that may alter the transmission of gustatory signals.

Introduction

All animals have specialized sensory neurons dedicated to the detection of the rich variety of chemicals in the environment that indicate the presence of food sources, predators and conspecifics. Gustatory sensory neurons have evolved to specialize in detecting food-associated chemicals and report the presence of caloric or potentially harmful compounds. Examining the activation and modulation of gustatory sensory neurons is essential as it places fundamental limits on the taste information that is funneled to the brain and integrated to form feeding decisions.

The *Drosophila melanogaster* gustatory system is an attractive model to examine the signals that gustatory neurons transmit and receive. Molecular genetic approaches coupled with physiology and behavior have established five different classes of gustatory receptor neurons (GRNs) in adult *Drosophila* that detect different taste modalities. One class, expressing members of the Gustatory Receptor (GR) family including Gr5a and Gr64f, detects sugars and elicits acceptance behavior (Dahanukar et al 2001, Dahanukar et al 2007, Thorne et al 2004, Wang et al 2004). A second class expressing different GRs including Gr66a detects bitter compounds and mediates rejection behavior (Thorne et al 2004, Wang et al 2004). A third class contains an ion channel PPK28 and detects water (Cameron et al 2010, Chen et al 2010). The fourth expresses the PPK23 ion channel and mediates detection of high salt concentrations, whereas the fifth expresses the Ir94e ionotropic receptor and detects low salt concentrations (Jaeger et al 2018). In addition to well-characterized gustatory neurons and a peripheral strategy for taste detection akin to mammals with its classification of tastants into few distinct modalities, the reduced number neurons throughout the *Drosophila* nervous system offers the opportunity to examine gustatory transmission with high resolution.

The cell bodies of gustatory neurons are housed in chemosensory bristles in peripheral tissues including the proboscis labellum, which is an external mouthparts organ that detects taste compounds prior to ingestion (Stocker 1994). Gustatory neurons from each labellum half send bilaterally symmetric axonal projections to the subesophageal zone (SEZ) of the fly brain via the labial nerves. Gustatory axons terminate in the medial SEZ in a region called the anterior central sensory center (ACSC) (Hartenstein et al 2018, Miyazaki & Ito 2010, Thorne et al 2004, Wang et al 2004). Axons from bitter gustatory neurons send branches to the midline and form an interconnected medial ring whereas other gustatory axons remain ipsilateral and anterolateral to bitter projections. Although projections of different gustatory classes have been mapped using light level microscopy, the synaptic connectivity of gustatory axons in adult *Drosophila* is largely unexamined.

To explore the connectivity of GRNs and to lay the groundwork to study gustatory circuits, we used the recently available Full Adult Fly Brain Electron Microscopy dataset to fully reconstruct gustatory axons and their synaptic sites (Zheng et al 2018). We reconstructed 87 GRN axonal projections in the right hemisphere and 57 in the left, representing between 83-96% and 54-63% of the total expected, respectively. We used morphology- and connectivity-based clustering to identify six distinct clusters, likely representing neurons recognizing different taste modalities. By annotating chemical synapses, we observed that GRNs contain a nearly equal number of interspersed pre- and post-synaptic sites. Interestingly, many synaptic connections are among GRNs, with GRN-GRN connections yielding four distinct groups of connected neurons. Three of these groups segregate neurons based on taste modality, whereas one group contains neurons

representing two modalities. We used calcium imaging approaches to test the function of GRN-GRN connectivity, both of neurons of the same taste modality as well as connectivity between taste modalities. Additionally, we characterized the taste response profile of a second order neuron downstream of likely sugar projections in the EM and found it to respond selectively to sucrose. Our study reveals extensive anatomical connectivity between gustatory sensory neurons, arguing for pre-synaptic processing of taste information prior to transmission to downstream circuits.

Results

GRN axons contain pre-synaptic and post-synaptic sites

To systematically characterize gustatory inputs and outputs, we manually traced gustatory axons in the Full Adult Fly Brain (FAFB) Electron Microscopy dataset, using the annotation platform CATMAID (Saalfeld et al 2009, Zheng et al 2018). GRNs from the proboscis labellum send axons through the labial nerve to the SEZ (**Figure 2-1 A**). The labial nerve is a compound nerve, carrying sensory axons from the labellum, maxillary palp, and eye, as well as motor axons innervating proboscis musculature (Hampel et al 2020, Hartenstein et al 2018, Miyazaki & Ito 2010, Nayak & Singh 1983, Rajashekhar & Singh 1994). Different sensory afferents occupy different domains in the SEZ, with labellar gustatory axons terminating in the anterior central sensory center (ACSC) (Hartenstein et al 2018, Miyazaki & Ito 2010, Thorne et al 2004, Wang et al 2004). Therefore, to trace gustatory axons, we began by tracing neurites in the right labial nerve, readily identifiable in the EM dataset (**Figure 2-1 B, C**), and selected fibers that terminated in the anterior central SEZ to trace to completion.

In tracing axons, we found that neurites with small to medium sized diameters in the dorsomedial labial nerve (**Figure 2-1 C**) projected along a single neural tract (**Figure 2-1 D**) to the anterior central region of the SEZ. This neural tract served as an additional site to select arbors for reconstruction. Individual fibers followed along the same tract and showed variation in terminal branching (**Figure 2-1 E**). In total, we identified 87 axonal projections in the right hemisphere. Tracing from the left labial nerve and neural tract in the left hemisphere, we identified an additional 57 projections. There are 90-104 GRNs per labellum half (Jaeger et al 2018, Stocker 1994), arguing that we have identified 83-96% of the GRN fibers from the right labellum and 54-63% from the left. The projections from the left and right labial nerves are symmetric and converge in a dense web in the anterior central SEZ (**Figure 2-1 F**). This arborization pattern recapitulates the labellar sensory projections of the ACSC (Hartenstein et al 2018).

In addition to the skeleton reconstructions, we manually annotated pre- and postsynaptic sites. The presence of t-shaped structures characteristic of presynaptic release sites ('T bars'), synaptic vesicles, and a synaptic cleft were used to identify a synapse, consistent with previous studies (Zheng et al 2018). We found that synapses are sparse along the main neuronal tract and abundant at the terminal arborizations (**Figure 2-1 E**). Interestingly, each GRN has a large number of pre- and post-synaptic sites intermixed along the arbors (**Figure 2-1 E, G-I**). On average, a GRN contains 175 presynaptic sites and 168 postsynaptic sites, with individual GRNs showing wide variation in pre- and post- synapse number (**Supplemental Figure 2-1.1**). Our EM reconstructions reveal that GRNs represent a morphologically diverse population that not only relays taste information to the brain but also receives extensive synaptic inputs.

Different GRN classes can be identified by morphology and connectivity

Drosophila GRNs comprise genetically defined, discrete populations that are specialized for the detection of specific taste modalities (Wang et al 2004, Cameron et al 2010, Jaeger et al 2018). As the EM dataset does not contain markers to distinguish between GRNs recognizing different taste modalities, we set out to identify subpopulations of reconstructed GRNs based on their anatomy and connectivity.

We used the NBLAST algorithm to perform automated clustering of GRN axons to define different subpopulations (Costa et al 2016). Each traced skeleton on the right was registered to a standard template brain (Jennet et al 2012). We confined the analysis to GRNs in the right hemisphere because tracing is near completion and because the left and right hemispheres in the SEZ standard brain do not align. The 87 GRNs were compared pairwise in an all-by-all matrix. For each pair, an NBLAST neuronal similarity score was computed based on the position and geometry of the query and target GRN. Additionally, connectivity data comprised of all synapses between each pair of neurons was included in our analysis (**Supplemental Figure 2-2.1**). We then used Ward's method to hierarchically cluster GRNs into groups (Costa et al 2016). We chose six groups as the number that minimizes within-cluster variance (**Figure 2-2 A**) (Braun et al 2010).

The six GRN groups are morphologically distinct, occupying discrete zones in the SEZ and sharing anatomically similar terminal branches. To evaluate whether the different groups represent GRNs detecting different taste modalities, we examined the number of GRNs in each group and their anatomy. Based on previous studies (Jaeger et al 2018), there are 20 bitter-sensing GRNs, 9 low salt GRNs, 15 high salt GRNs, 31 sugar GRNs, and 15 water GRNs per labellum half. In addition, bitter GRN axons cross the midline whereas other GRN axons do not. Group 1 and 2 cluster together, cross the midline and comprise 18 GRNs, suggesting that they represent bitter GRNs (**Figure 2-2 B, C**) (Wang et al 2004, Thorne et al 2004). Group 3 contains 12 GRNs, with projections that resemble low salt GRNs (**Figure 2-2 D**) (Jaeger et al 2018). Group 4 contains 17 GRNs that we hypothesize are water GRNs based on anatomy (**Figure 2-2 E**) (Cameron et al 2010, Chen et al 2010). Group 5 has 18 GRNs and most resembles the projection patterns of high salt-sensing neurons (**Figure 2-2 F**) (Jaeger et al 2018). Group 6 contains 21 GRNs and may correspond to sugar GRNs (**Figure 2-2 G**) (Wang et al 2004, Thorne et al 2004). We emphasize that the assignment of different groups to different taste modalities remains tentative until additional experimentation.

GRNs are highly interconnected via chemical synapses

During our reconstruction of GRNs in the EM dataset, we noticed that GRNs are both pre- and post-synaptic to other GRNs. To gain insight into GRN-GRN communication, we focused on connections comprised of five or more synapses, consistent with previous studies (Buhmann et al 2021, Li et al 2020a, Takemura et al 2013, Takemura et al 2015). We determined that each GRN receives between 0% and 52% (average = 25%) of its synaptic input from other GRNs (**Figure 2-3 A**). The number of synapses between GRNs suggests that communication between sensory neurons may directly regulate sensory output.

To examine whether connections exist exclusively between neurons of the same anatomy- and connectivity- based cluster, potentially representing the same taste

modality, or between multiple clusters, we plotted the connections between all GRNs in a matrix (**Figure 2-3 B**). We found that GRNs are connected in four distinct groups, with extensive synapses between individual GRNs. One group of interconnected neurons contains all neurons of clusters 1 and 2, likely representing bitter GRNs. A second group contains neurons of cluster 3, likely representing low-salt GRNs. A third connectivity group is comprised of cluster 5, likely representing high-salt GRNs. The fourth connectivity group contains mostly neurons of clusters 4 and 6, which we postulate are water and sugar GRNs. At 41 neurons, this anatomically mixed connectivity group is too large to correspond to neurons of a single taste modality. Thus, while three groups of synaptically connected clusters correspond to anatomical classes, one group contains neurons of multiple anatomical classes, suggesting pre-synaptic communication both within neurons representing a single taste modality and between neurons of different modalities.

Comparing the synaptic connectivity within and between anatomy- and connectivity-based clusters reveals that the vast majority of synapses are between neurons of the same cluster (**Figure 2-3 C**). For example, cluster 4 neurons receive 1212 synapses from other cluster 4 neurons and 85 from other neurons. The large number of synapses between neurons belonging to the same anatomical class suggests that communication between GRNs of the same taste modality is predominant. However, there are also a small number of synapses between GRNs detecting different modalities.

Overall, we found large numbers of chemical synapses between GRNs. Connectivity between GRNs of the same anatomical cluster could provide a mechanism to amplify signals of the same taste modality. In addition, the connectivity between GRNs of different anatomical clusters could serve to integrate taste information from different modalities before transmission to downstream circuitry.

Interactions between sugar and water GRNs are not observed by calcium or voltage imaging

To examine whether the small number of connections between GRNs of different taste modalities results in cross-activation of GRNs detecting different primary tastant classes, we explored if activation of one GRN class results in propagation of activity to other GRN classes. As the connectivity data suggests that sugar and water GRNs are weakly connected, we wondered if appetitive GRNs might be interconnected to amplify appetitive signals to downstream feeding circuits. To test for interactions between appetitive GRNs, we undertook calcium and voltage imaging studies in which we monitored the response of a GRN class upon activation of other GRN classes.

We expressed the calcium indicator GCaMP6s in genetically defined sugar, water, bitter or high salt sensitive GRNs to monitor excitatory responses upon artificial activation of different GRN classes. To ensure robust and specific activation of GRNs, we expressed the mammalian ATP receptor P2X2 in sugar, water, bitter or high salt GRNs, and activated the GRNs with an ATP solution presented to the fly proboscis while imaging gustatory projections in the brain (Yao et al 2012, Harris et al 2015). Expressing both P2X2 and GCaMP6s in sugar, water or bitter GRNs elicited strong excitation upon ATP presentation irrespective of the feeding state of the fly. The response to ATP in flies expressing P2X2 and GCaMP6s in high salt GRNs was less pronounced, indicating potential technical problems (**Figure 2-4 A, B, G, H; Supplemental Figures 2-4.1-10 C,**

D). As bitter cells are synaptically connected to each other but not to sugar or water cells, we hypothesized that they would not be activated by sugar or water GRN activation. Consistent with the EM connectivity, activation of sugar or water GRNs did not activate bitter cells, nor did bitter cell activation elicit responses in sugar or water axons (**Supplemental Figure 2-4.1 E, F, I, J; Supplemental Figure 2-4.2 E, F; Supplemental Figure 2-4.3 G, H**). Previous studies indicate overlapping cell populations between bitter and high salt GRNs (Jaeger et al 2018). Consistent with these findings, we observed a response in bitter GRNs to high salt GRN activation (**Supplemental Figure 2-4.1 G, H**). It is not possible to discern whether this interaction is reciprocal as high salt neurons showed slight responses to the ATP tastant solution, possibly reacting to the presence of the sodium counter ions (**Supplemental Figure 2-4.4 A, B**). In contrast, the EM connectivity indicates interactions between sugar and water GRNs. However, we did not observe responses in sugar GRNs upon water GRN activation (**Figure 2-4 C, D; Supplemental Figure 2-4.2 K, L**) or responses in water GRNs upon sugar GRN activation (**Figure 2-4 I, J; Supplemental Figure 2-4.3 E, F**). To examine whether interactions between sugar and water GRNs specifically or low level connections between modalities generally are modulated by the feeding state of the fly, we performed the activation and imaging experiments in fed and starved flies (**Supplemental Figure 2-4.1-8**). These experiments did not reveal feeding state dependent interactions between GRN populations. We further attempted to recreate the internal state of a thirsty fly by increasing the osmolality of the artificial hemolymph used during dissection and imaging, creating a pseudo-desiccated state. This allowed us to side-step the poor health of flies undergoing desiccation. We examined potential interactions between sugar and water GRNs and other taste modalities in pseudo-desiccated flies and did not find cross-activation (**Supplemental Figure 2-4.9-10**).

We hypothesized that interactions between sugar and water GRNs might be inhibitory, providing a mechanism to weight different appetitive taste inputs. To examine this, we expressed the voltage indicator ArcLight, which preferentially reports hyperpolarization, in sugar GRNs while activating water GRNs via P2X2 and vice versa. These experiments revealed no change in voltage in one appetitive gustatory class upon activation of the other (**Figure 2-4 E, F, K, L: Supplemental Figure 2-4.11**). Overall, our imaging studies show that, despite the potential for crosstalk between different modalities revealed by EM, communication between appetitive GRNs was not observed by calcium or voltage imaging of gustatory axons.

Activation of a few bitter GRNs elicits activity in additional bitter GRNs

As neurons of the same taste category are strongly interconnected, we hypothesized that activation of a subset of GRNs of one taste modality might result in the activation of additional GRNs of the same modality. Because bitter GRNs are readily distinguished based on anatomy and connectivity, we examined whether activating a bitter GRN subset would excite other bitter GRNs. Members of the GR gene family are expressed in distinct subsets of bitter GRNs. Gr47a is expressed in 3-4 GRNs per labellum half whereas Gr66a is expressed in all 19 bitter GRNs (Weiss et al 2011). We therefore expressed P2X2 in Gr47a neurons for activation of a sparse bitter GRN subset and GCaMP6s in Gr66a neurons for simultaneous monitoring of responses in all bitter GRNs. As the projection patterns of Gr47a and Gr66a overlap, we co-expressed the red

marker tdTomato in Gr47a neurons to evaluate the response in Gr47a cells and in non-overlapping bitter projections (**Figure 2-5 A, C**). We generated masks to distinguish activity overlapping with the tdTomato signal and activity in the rest of the bitter projection (**Figure 2-5 B, D**). When examining the GCaMP6s signal that overlaps with tdTomato as well as parts of the bitter projection not overlapping with tdTomato and the entire taste projection as a whole, we observed no response to the negative control tastant PEG and a robust response to the positive control tastant mixture of bitters across the board (**Figure 2-5 E, F I, J; Supplemental Figure 2-5.1 A, B, E, F**). Additionally, we saw a strong response in Gr47a projections upon P2X2 activation with ATP, as expected (**Figure 2-5 G, H; Supplemental Figure 2-5.1 C, D**). However, we also observed activity in additional Gr66a fibers outside of the Gr47a projection pattern upon activation of Gr47a axons, with activity patterns in both subpopulations comparable to the activity of the entire taste projection (**Figure 2-5 G, H; Supplemental Figure 2-5.1 C, D**). While this suggests that activation of a subset of bitter neurons excites additional bitter projections, additional study is required to ensure that the GCaMP6s signal observed beyond Gr47a axons is not due to light scatter of the GCaMP6s signal in Gr47a axons. Nevertheless, this preliminary data suggests that the connectivity between bitter GRNs serves to amplify bitter sensory responses.

A second-order taste neuron responds selectively to sucrose and causes proboscis extension

To further test the potential interaction between sugar and water sensory neurons and to validate the identification of GRN subtypes in the EM dataset, we sought to trace a second-order gustatory neuron downstream of sugar GRNs and test if it responds to both sugar and water taste detection. By tracing from a putative sugar-sensing GRN (Skeleton ID 7349219), we identified a second-order neuron predominantly connected to cluster 6 GRNs with comparatively few inputs from clusters 4 and 5 (**Figure 2-6 A, E, F**). We identified a Gal4 line containing this second order neuron (**Figure 2-6 C, Supplemental Figure 2-6.1**), which we named Famine (FMIn). FMIn extensively overlaps with sugar sensing GRNs in the EM dataset (Figure 2-6 B), forming 349 synapses (**Figure 2-6 E, F**). This anatomical overlap is also observable by colabeling studies of sugar GRNs and FMIn single-cell mosaics (**Figure 2-6 D**)(Gordon & Scott 2009).

We tested the function of FMIn using calcium imaging and behavioral approaches. Monitoring the response of FMIn to taste compounds delivered to the fly proboscis revealed that FMIn responded selectively to sucrose but not to water or bitter compounds in food-deprived flies, demonstrating that FMIN is a second-order sugar-sensing gustatory neuron (**Figure 2-6 G, H**). The calcium imaging studies also argue that excitatory interactions between sugar and water GRNs are not readily apparent in second-order neuron activity. To test the behavioral function of FMIn, we activated it using specific expression of a red shifted light-gated cation channel, ReaChR, and found that this elicited proboscis extension, a behavior produced by activation of appetitive GRNs (**Figure 2-6 I**). We used mosaic approaches to restrict expression of ReaChR and further found that the strength of the response was dependent on whether ReaChR was expressed in only one or both FMINs. These studies demonstrate the sugar selectivity of

a second-order gustatory neuron and validate the EM classification of sugar-sensing GRNs.

Discussion

In this study, we characterized different classes of gustatory projections and their interconnectivity by high-resolution EM reconstruction. We identified different projection patterns corresponding to gustatory neurons recognizing different taste modalities. The extensive connections between GRNs of the same taste modality as well as the possible interactions between GRNs of two modalities provide anatomical evidence of pre-synaptic processing of gustatory information.

An emerging theme stemming from EM reconstructions of *Drosophila* sensory systems is that sensory neurons of the same subclass are synaptically connected. In general, different sensory neuron subclasses have spatially segregated axonal termini in the brain, thereby constraining the potential for connectivity. In the adult olfactory system, approximately 40% of the input onto olfactory receptor neurons (ORNs) comes from other ORNs projecting to the same olfactory glomerulus (Horne et al 2018, Schlegel et al 2021, Tobin et al 2017). Similarly, mechanosensory projections from the Johnston's Organ of the same submodality are anatomically segregated and synaptically connected (Hampel et al 2020). In *Drosophila* larvae, 25% of gustatory neuron inputs are from other GRNs, although functional classes were not resolved (Miroschnikow et al 2018). In the adult *Drosophila* gustatory system, we also find that GRNs are interconnected, with approximately 25% of GRN input coming from other GRNs. Consistent with other classes of sensory projections, we find that gustatory projections are segregated based on taste modality and form connected groups. A general function of sensory-sensory connections seen across sensory modalities may be to enhance weak signals or to increase dynamic range.

By clustering neurons based on anatomy and connectivity, we were able to resolve different GRN categories. The distinct morphologies of bitter neurons and low salt-sensing neurons, known from immunohistochemistry, are recapitulated in the projection patterns of clusters 1 and 2 and 3, enabling high-confidence identification. The projections of high salt, sugar and water-sensing neurons are ipsilateral, with similarities in their terminal arborizations (Jaeger et al 2018, Wang et al 2004). Nevertheless, comparisons between EM and light-level projections argue that these taste categories are also resolved into different, identifiable clusters. However, as these categories are based on anatomical comparisons alone, they remain tentative until further examination of taste response profiles of connected second-order neurons, now identifiable by EM.

Whereas clustering identified six different clusters, examining GRN-GRN connectivity revealed four synaptically connected groups. Three groups connect neurons of the same taste modality, whereas the fourth group likely contains both water and sugar neurons. While it is tempting to speculate that interactions between appetitive tastes may amplify or filter activation of feeding circuits, we were unable to identify cross-activation between sugar and water GRNs by calcium or voltage imaging. We also found no evidence for cross-activation of sugar and water sensory neurons when monitoring activity of a second-order gustatory neuron. It is possible that these interactions are dependent on the feeding state of the animal or act on a timeframe not examined in this study. Alternatively, activation may be highly localized to the synaptic terminal and not

resolved in these studies. Finally, the number of synapses is approximately 15-fold fewer between anatomical classes than within classes, suggesting that the small number of synapses may not be relevant for taste processing.

Overall, this study resolves the majority of labellar gustatory projections and their synaptic connections, revealing that gustatory projections are segregated based on taste modality and synaptically connected. The identification of GRNs detecting different taste modalities now provides an inroad to enable the examination of the downstream circuits that integrate taste information and guide feeding decisions.

Materials and Methods

Experimental Animals

Experimental animals were maintained on standard agar/molasses/cornmeal medium at 25°C. For imaging experiments requiring food-deprived animals, flies were placed in vials containing wet kimwipes for 23-26 hours immediately prior to the experiment. For behavior experiments, flies were placed on food supplemented with 400μM all trans retinal for 24 hours prior to the experiment.

Transgenic animals used were: *Gr64f-LexA* (Miyamoto et al 2012); *Gr64f-Gal4* (Dahanukar et al 2007); *Gr66a-LexA*; *ppk28-LexA*; *UAS-CD::tdTomato*; *LexAop-Gal80* (Thistle et al 2012); *Gr66a-Gal4* (Scott et al 2001); *ppk28-Gal4* (Cameron et al 2010); *LexAop-GCaMP6s,* UAS-GCaMP6s (Chen et al 2013); *UAS-ArcLight* (Cao et al 2013); *UAS-P2X2* (Lima & Miesenbock 2005); *GmR81E10-Gal4* (Jennet et al 2012); *Flippase 1026a* (Huang et al 2014); *Gr47a1-Gal4* (Kwon et al 2011); *UAS>mcherry::stop>ReaChR::Citrine* (Inagaki et al 2013); *UAS-CD8::GFP* (Lee & Luo, 1999); *Gr5a-LexA, tub>Gal80>* (Gordon & Scott 2009); *LexAop-myr::tdTomato* (Nern et al 2011).

EM reconstruction

Neuron skeletons were reconstructed in a serial sectioned transmission electron microscopy dataset of the whole fly brain (Zheng et al 2018) using the annotation software CATMAID (Saalfeld et al 2009). GRN projections were identified based on their extension into the labial nerve and localization to characteristic neural tracts in the SEZ. To identify second order neurons, random presynapses of skeleton 7349219 were chosen using the reconstruction sampler function of CATMAID and downstream partners were reconstructed. Skeletons were traced to completion either entirely manually or using a combination of an automated segmentation (Li et al 2020b) and manual tracing. Chemical synapses were annotated manually using criteria previously described (Zheng et al 2018). Skeletons were reviewed by a second specialist, so that the final reconstruction presents the consensus assessment of at least two specialists. Skeletons were exported from CATMAID using the natverse package (Bates et al 2020). FAFB neuronal reconstructions will be available from Virtual Fly Brain (https://fafb.catmaid.virtualflybrain.org/).

Clustering of GRNs

GRNs were hierarchically clustered based on morphology and connectivity using NBLAST and synapse counts. First, GRN skeletons traced in FAFB were registered to the JRC2010 template (Jennet et al. 2012) and compared in an all-by-all fashion with NBLAST (Costa et al. 2016). NBLAST analysis was carried out with the natverse toolkit in R (Bates et al. 2020; R Development Core Team, https://www.r-project.org/). The resulting matrix of NBLAST scores was merged with a second matrix containing all-by-all

synaptic connectivity counts for the same GRNs. The resulting merged matrix was absolute maximum scaled such that all values fall within the range of 0 and 1. The merged, scaled matrix was hierarchically clustered using Ward's method (Ward 1963) in Python (Python Software Foundation, https://www.python.org/) with SciPy (Virtanen et al 2020). Five groups were chosen based on prior knowledge of taste modalities, as GRNs for sugar, water, bitter, high salt, and low salt are known to be functionally, morphologically, and genetically distinct. One neuron was accidently not processed in this analysis. Its cluster identity was manually assigned based on its morphology and connectivity.

Connectivity of GRNs

Connectivity data of GRNs was exported from CATMAID and further analyzed using custom scripts in Python. Connectivity diagrams were generated using CytoScape (Shannon et al 2003).

Calcium and Voltage Imaging Preparation

For imaging studies of GRNs, mated females, 10 to 21 days post eclosion, were dissected as previously described (Harris et al 2015), so that the brain was submerged in artificial hemolymph (AHL) while the proboscis was kept dry and accessible for taste stimulation. To avoid occlusion of taste projections in the SEZ, the esophagus was cut. The front legs were removed for tastant delivery to the proboscis. AHL osmolality was assessed as previously described (Jourjine et al 2016) and adjusted according to the feeding status of the animal. In fed flies, AHL of ~250mOsmo was used (Wang et al 2003). The AHL used for starved flies was diluted until the osmolality was ~180mOsmo, consistent with measurements of the hemolymph osmolality in food deprived flies (Jourjine et al 2016). The AHL osmolality for experiments in pseudo-desiccated flies was adjusted to ~350 mOsmo by adding galactose, which is consistent with the hemolymph osmolality reported for thirst flies (Jourjine et al 2016). Due to low viability even after relatively short descation periods (~2 hours), flies were not desiccated but imaged after a 15 minute incubation in high osmolality AHL.

For imaging studies of FMIN, mated females, 3 to 10 days post eclosion, were deprived of food for 18 to 24 hours prior to imaging in an empty vial with a moist kimwipe. Flies were dissected as described above in ~250mOsmo AHL.

Calcium Imaging

Calcium transients reported by GCaMP6s were imaged on a 3i spinning disc confocal microscope with a piezo drive and a 20x water immersion objective (NA=1). For our studies of GRNs, stacks of 14 z sections, spaced 1.5 microns apart, were captured with a 488nm laser for 45 consecutive timepoints with an imaging speed of ~0.3 Hz and an optical zoom of 2.0. For better signal detection, signals were binned 8x8, except for Gr64f projections, which underwent 4x4 binning. For our studies of FMIn, stacks of 16 to 20 z sections spaced ~1.3 microns apart were captured with an 488nm laser for 20 consecutive timepoints with an imaging speed of ~0.5 Hz and an optical zoom of 1.6.

For our studies of Gr47a activation, we captured an z stack of the tdTomato expression pattern using a 568nm laser prior to and following calcium imaging experiments.

Voltage Imaging

Voltage responses reported by ArcLight were imaged similarly to the calcium imaging outlined above. To increase the imaging speed, the number of z planes was

reduced to 10, and the exposure time was decreased from 100ms to 75ms, resulting in an imaging speed of ~0.7Hz. To maintain a time course comparable to that of the calcium imaging experiments, the number of timepoints was increased to 90. Signals were binned 8x8 in each experiment.

Taste stimulations

Taste stimuli were delivered to the proboscis via a glass capillary as previously described (Harris et al 2015). For GRN studies, each fly was subjected to three consecutive imaging sessions, each consisting of a taste stimulation at time point 15, 25 and 35 (corresponding to 30, 50.5, 71.5 sec). During the first imaging session, the fly was presented with a 20% polyethylene glycol (PEG, average molecular weight 3350 g/mol) solution, acting as a negative control. PEG was used in all solutions except water solutions, as this PEG concentration inhibits activation of water GRNs (Cameron et al 2010). This was followed in the second session with stimulations with 100mM ATP in 20%PEG. In the last imaging session, each fly was presented with a tastant acting as a positive control in 20% PEG (Gr64f: 1M sucrose; Gr66a: 100mM caffeine, 10mM denatonium benzoate; ppk28: H2O; ppk23: 1M KCl in 20% PEG).

For FMIn studies, flies were imaged for two imaging sessions during which the tastant was delivered to the proboscis at time point 9. For one of these sessions, 1M Sucrose was the tastant and for the other either H2O or 100mM caffeine and 10mM denatonium benzoate in 20% PEG, so that each fly was exposed to two different tastant solutions.

Imaging Analysis

Image analysis was performed in FIJI (Schindelin et al 2012). Z stacks for each time point were converted into max z projections for further analysis. After combining these images into an image stack, they were aligned using the StackReg plugin in FIJI to correct for movement in the xy plane (Thevenaz et al 1998).

For our exploration of interactions between GRN subtypes, one ROI was selected encompassing the central arborization of the taste projection in the left or right hemisphere of the SEZ in each fly. Whether the projection in the left or right hemisphere was chosen depended on the strength of their visually gauged response to the positive control. The exception were Gr66a projections, in which the entire central projection served as ROI. If projections did not respond strongly to at least two of the three presentations of the positive control, the fly was excluded from further analysis. If projections responded to two or more presentations of the negative control, the fly was excluded from further analysis. A large ROI containing no GCaMP signal was chosen in the lateral SEZ to determine background fluorescence.

In calcium imaging experiments, the first five time points of each imaging session were discarded, leaving 40 time points for analysis with taste stimulations at time points 10, 20 and 30. The average fluorescence intensity of the background ROI was subtracted at each time point from that of the taste projection ROI. F0 was then defined as the average fluorescence intensity of the taste projection ROI post background subtraction of the first five time points. $\Delta F/F$ (%) was calculated as 100%* (F(t)-F0)/F0. Voltage imaging experiments were analyzed similarly, with ten initial time points discarded for a total of 80 time point in the analysis and tastant presentations at time points 20, 40 and 60.

To study whether a subset of bitter neurons can activate the rest of the bitter projections, we generated a max z projection of the expression pattern of Gr47a in FIJI.

This image was aligned to each movement-corrected image stack captured from the same fly (described above) using the Template Matching Plugin of FIJI (Tseng et al 2011). For the best result, we chose a rectangular ROI encompassing the entire bilateral central arborization of bitter GRNs as the alignment landmark. The aligned image of the Gr47a expression was converted into a Boolean mask using the Gaussian adaptive thresholding algorithm of the open cv package in python (Bradski 2000). This mask was used to split each image stack into two complementary image stacks, one containing only pixels within the masked area, one only containing those outside of it. These images were analyzed as described above, with blank pixels resulting from the masking process excluded from the calculation of average fluorescence intensity.

To study the taste responses in FMIn, an ROI encompassing the cell body of FMIn was selected. As the cell bodies of FMIn are commonly located extremely peripherally in the neuropil at or in the labial nerve, we chose to forgo background subtraction. We excluded the first three time points from further analysis, leaving 17 time points for analysis with tastant presentation at time point 6. F0 was calculated as the average of the first five remaining time points. dF/F(%) was calculated as 100%* (F(t)-F0)/F0. Graphs of traces were generated in GraphPad Prism.

Quantification of Calcium and Voltage Imaging

Graphs were generated in GraphPad Prism. To calculate the max ΔF/F (%) of GCaMP responses, the ΔF/F(%) of the three time points centered on the peak ΔF/F (%) after the first stimulus response were averaged. The average ΔF/F (%) of the three time points immediately preceding the stimulus onset were then subtracted to account for changing baselines during imaging. Arclight data was similarly analyzed, except that five timepoints centered on the peak ΔF/F (%) and five time points prior to stimulus onset were considered. Statistical tests were performed in Prism as indicated in figures.

Immunohistochemistry

To visualize the expression pattern of Gmr81E10-Gal4 and the overlap of FMIN and Gr5a, mated female flies, 10 to 14 days post eclosion, were dissected in PBS. Fixation in 4% paraformaldehyde and antibody staining was performed as previously described (Wang et al 2004). The primary antibodies used were mouse anti Brp (1:500), chicken anti GFP (Co-label only; 1:1000), rabbit anti GFP (Gal4 expression pattern only; 1:1000) and rabbit anti dsRed (Co-label only; 1:1000). The secondary antibodies used were goat anti rabbit AlexaFluor 488 (Gal4 Expression pattern only; 1:100), goat anti chicken AlexaFluor 488 (Co-label only; 1:1000), goat anti rabbit AlexaFluor 568 (Co-label only; 1:1000), and goat anti mouse AlexaFluor 647 (1:100). All images were acquired on a Zeiss upright confocal microscope, and their brightness and contrast were manually adjusted in FIJI.

PER Behavior

Mated female flies, 3 to 10 days post eclosion, were briefly anesthetized with CO2 and glued to a microscope slide with a small drop of nail polish. They were allowed to recover for ~2 hours in a dark empty pipette tip box with a moist kimwipe to prevent desiccation. Their light response was examined under a dissection microscope by observing their behavior for several seconds in ambient light before turning on the microscope's light source aimed directly at the fly. Only if the fly fully extended its proboscis was it classified as a 'responder'. Flies extending their proboscis in ambient light were excluded from the analysis. Behavior was recorded using a small digital

camera. Following the behavior experiments, flies were individually removed from the microscope slide and their brains dissected in PBS. For each fly, the expression pattern of UAS-ReaChR::Citrine was analyzed using a fluorescence microscope. Flies in which ReaChR was expressed in cells other than FMIn were excluded from analysis.

Acknowledgements

We thank Lori Horhor, Jolie Huang, Neil Ming, and Parisa Vaziri for EM tracing contributions. This work was supported by NIH R01DC013280 (K.S.) and NIH F32DK117671 (G.S.). FAFB was used for EM reconstructions (Zheng 2018). Neuronal reconstruction for this project took place in a collaborative CATMAID environment in which 27 labs are participating to build connectomes for specific circuits. Development and administration of the FAFB tracing environment and analysis tools were funded in part by National Institutes of Health BRAIN Initiative grant 1RF1MH120679-01 to Davi Bock and Greg Jefferis, with software development effort and administrative support provided by Tom Kazimiers (Kazmos GmbH) and Eric Perlman (Yikes LLC). We thank Peter Li for sharing his automatic segmentation (Li et al 2019).

Figures and Figure Legends

Figure 2-1

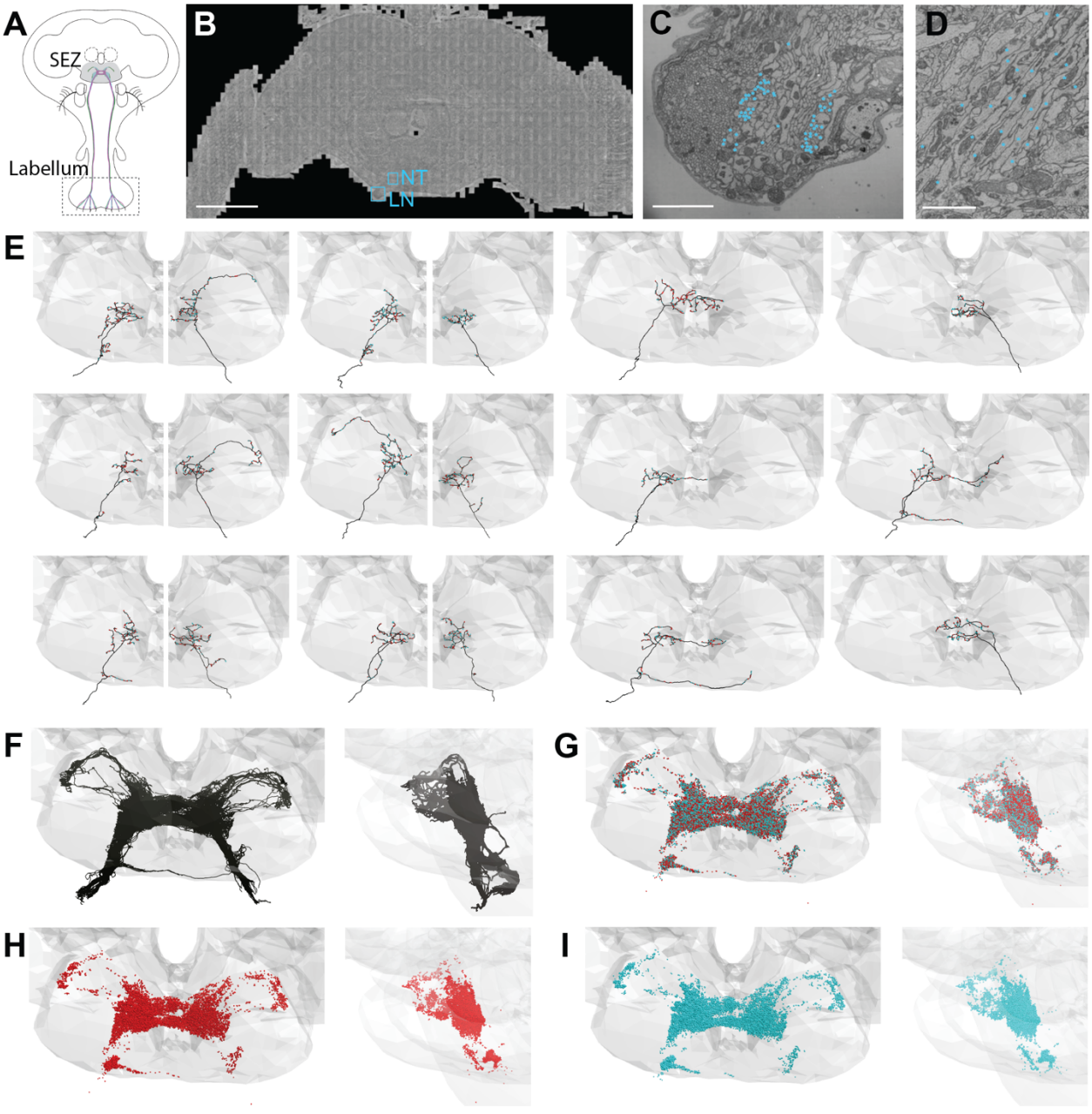

Figure 2-1. EM-based reconstructions of GRNs and synaptic sites.

(A) Schematic showing GRNs in the proboscis labellum and their projections in the SEZ. (B) Location of the labial nerve (LN) and neural tract (NT) containing GRNs of the right hemisphere in the FAFB dataset (Z slice 3320, scale bar = 100 μM). (C) Cross-section of the labial nerve with traced GRNs indicated by asterisks (Z slice 3320, scale bar = 5 μM). (D) Neural tract with traced GRNs indicated by asterisks (Z slice 2770, scale bar = 5 μM). (E) Examples of reconstructed GRNs with presynaptic (red) and postsynaptic (blue) sites. (F-I) Frontal and sagittal view of all reconstructed GRN axons (F), all presynaptic (red) and postsynaptic (blue) sites (G), presynaptic sites alone (H), and postsynaptic sites alone (I).

Supplemental Figure 2-1.1

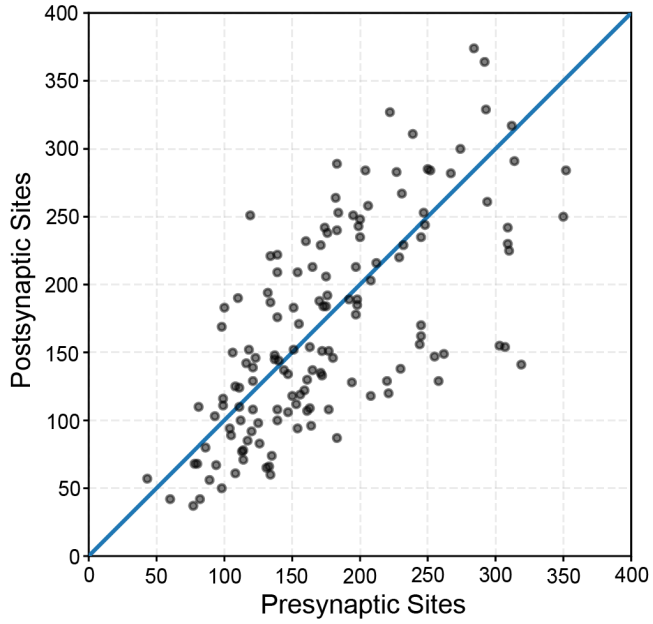

Supplemental Figure 2-1.1. GRNs contain similar numbers of pre- and postsynaptic sites.

Plot of pre- and post-synaptic sites for individual GRNs, denoted by grey circles. Diagonal line indicates one-to-one relationship of pre- and post-synaptic sites.

Figure 2-2

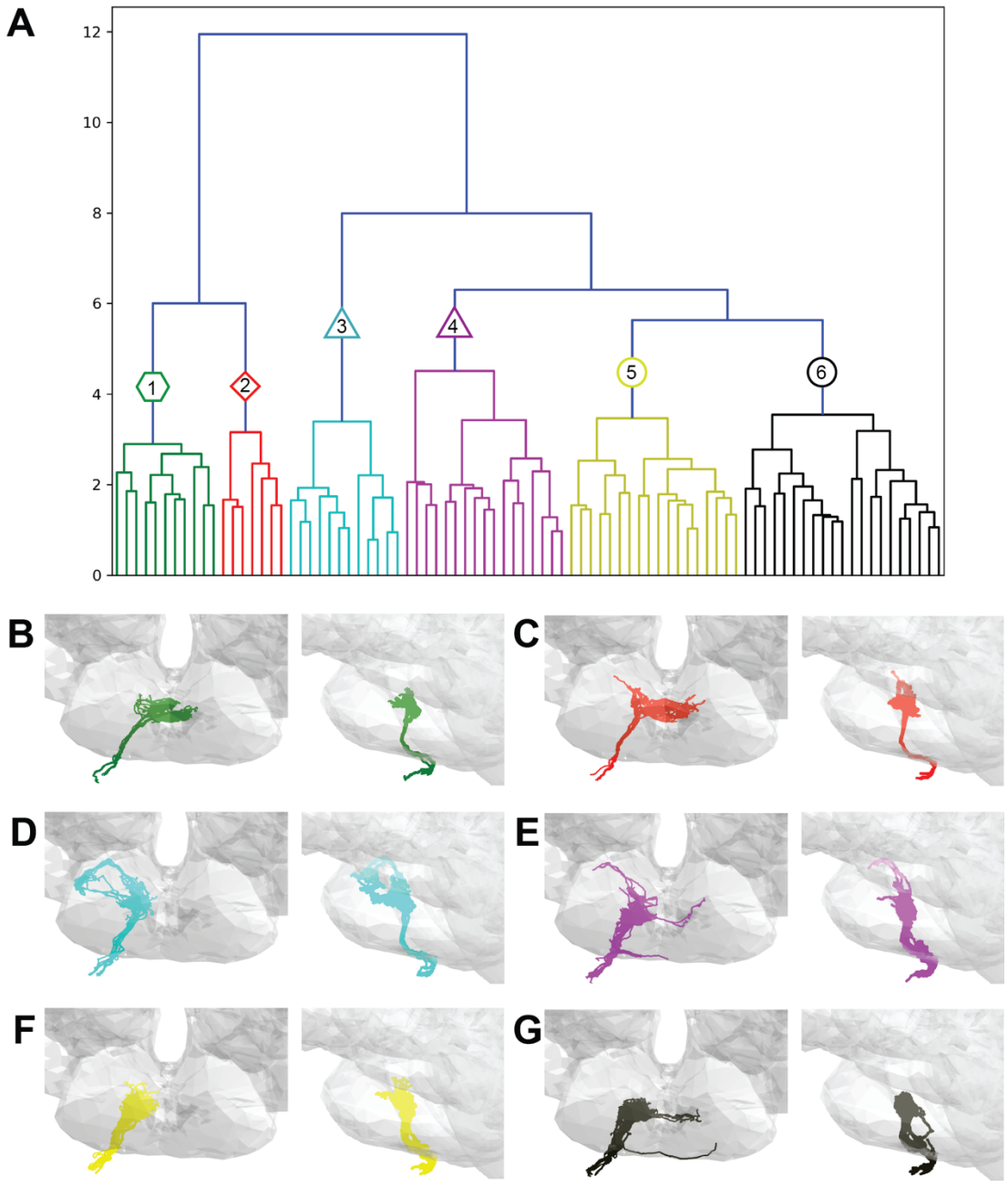

Figure 2-2. Morphology- and connectivity-based clustering generates groups of GRNs.

(A) Tree denoting relative similarity of GRNs based on morphology and connectivity. (B) Frontal and sagittal view of cluster 1 GRNs. (C) Frontal and sagittal view of cluster 2 GRNs. (D) Frontal and sagittal view of cluster 3 GRNs. (E) Frontal and sagittal view of cluster 4 GRNs. (F) Frontal and sagittal view of cluster 5 GRNs. (G) Frontal and sagittal view of cluster 6 GRNs.

Supplemental Figure 2-2.1

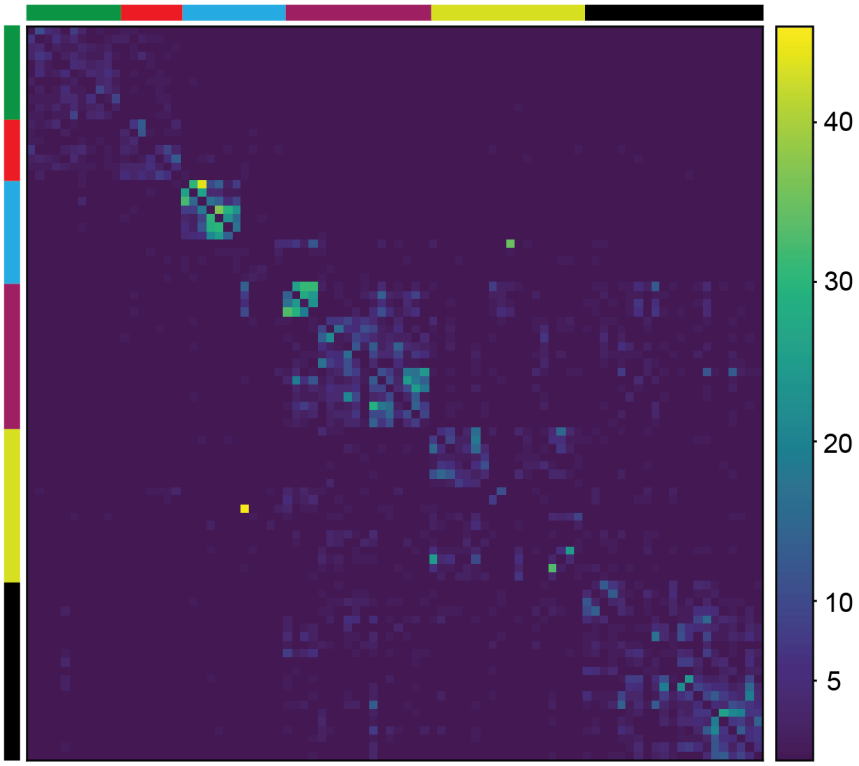

Supplemental Figure 2-2.1. Synaptic connections between GRNs.

Connectivity matrix of all GRNs of the right hemisphere. Presynaptic GRNs are arranged along the y axis, postsynaptic GRNs along the x axis. GRNs are ordered according to the combined morphological and connectivity clustering tree shown in Figure 2-2 A. Cluster identities of GRNs are indicated by colored bars. Color coding within the matrix indicates the number of synapses from the pre- to the post-synaptic neuron as indicated in the legend. All synapses are included in this analysis.

Figure 2-3

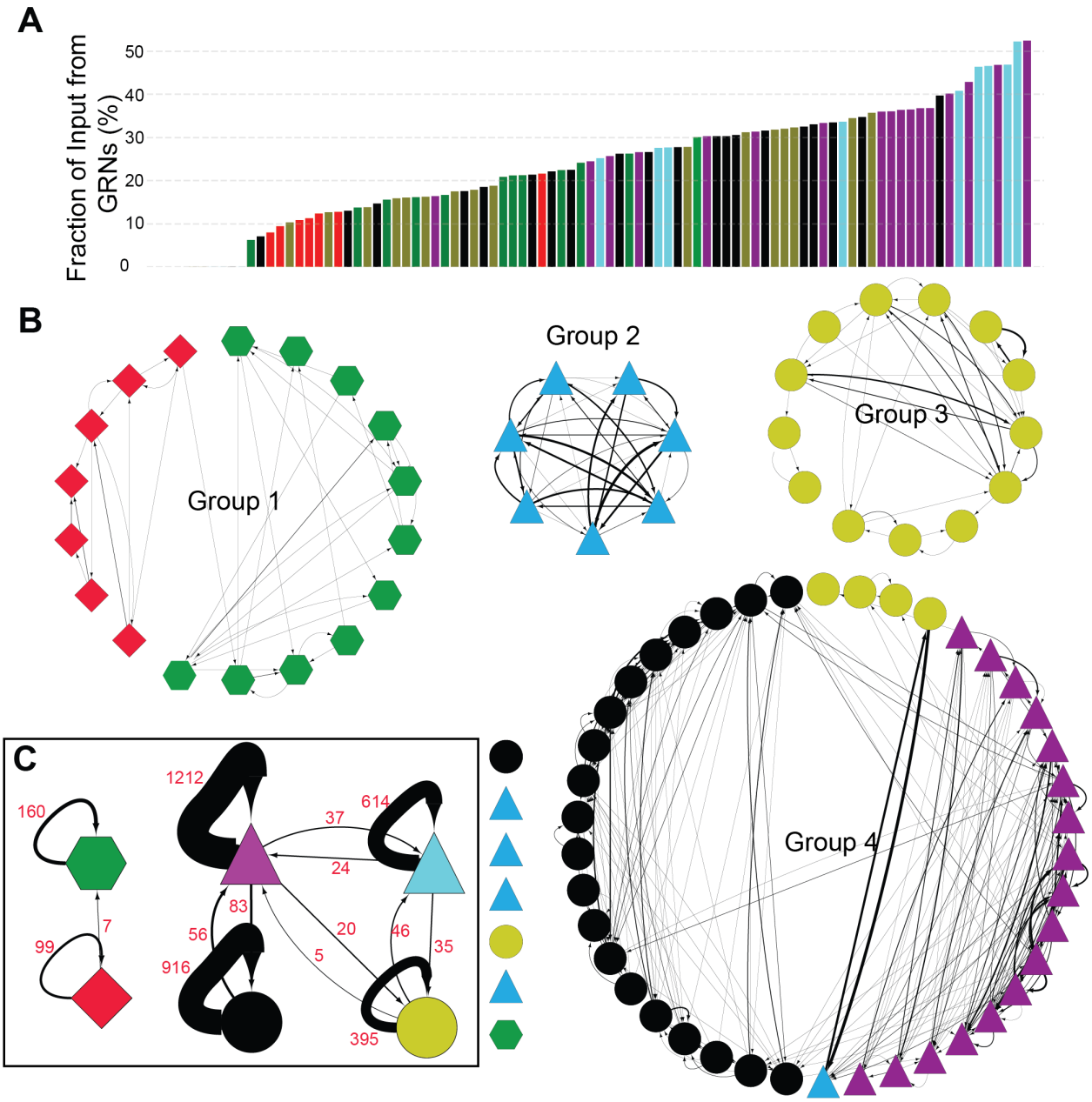
A
Fraction of Input from GRNs (%)
0
10
20
30
40
50
B
Group 1
Group 2
Group 3
Group 4
C
160
1212
37
614
24
7
99
83
56
916
20
5
46
35
395

Figure 2-3. GRNs are highly interconnected via chemical synapses.

(A) Percentage of GRN inputs to each GRN. Colors correspond to clusters established in Figure 2-2. (B) Connectivity between individual GRNs. Colors correspond to clusters established in Figure 2. Arrow thickness scales with the number of synapses comprising the connection. Only connections of at least 5 synapses are shown. (C) Connectivity between GRN clusters. Colors correspond to clusters established in Figure 2. Arrow thickness scales with the number of synapses comprising the connection, which is indicated in red.

Figure 2-4

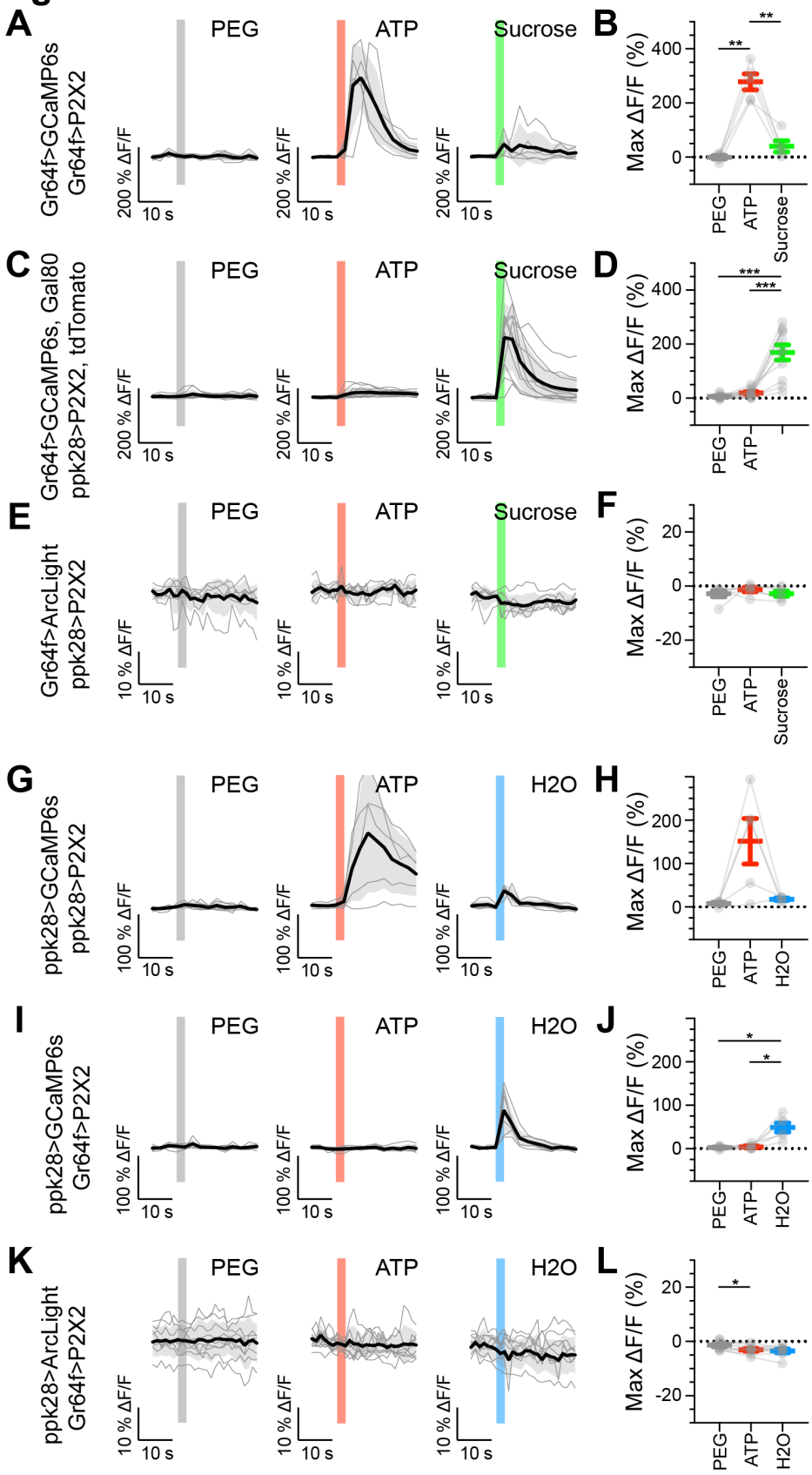
A
Gr64f>GCaMP6s
Gr64f>P2X2
PEG
ATP
Sucrose
200 % ΔF/F
10 s
B
Max ΔF/F (%)
400
200
0
**
**
PEG
ATP
Sucrose
C
Gr64f>GCaMP6s, Gal80
ppk28>P2X2, tdTomato
PEG
ATP
Sucrose
200 % ΔF/F
10 s
D
Max ΔF/F (%)
400
200
0
***
***
PEG
ATP
E
Gr64f>ArcLight
ppk28>P2X2
PEG
ATP
Sucrose
10 % ΔF/F
10 s
F
Max ΔF/F (%)
20
0
-20
PEG
ATP
Sucrose
G
ppk28>GCaMP6s
ppk28>P2X2
PEG
ATP
H2O
100 % ΔF/F
10 s
H
Max ΔF/F (%)
200
100
0
PEG
ATP
H2O
I
ppk28>GCaMP6s
Gr64f>P2X2
PEG
ATP
H2O
100 % ΔF/F
10 s
J
Max ΔF/F (%)
200
100
0
*
*
PEG
ATP
H2O
K
ppk28>ArcLight
Gr64f>P2X2
PEG
ATP
H2O
10 % ΔF/F
10 s
L
Max ΔF/F (%)
20
0
-20
*
PEG
ATP
H2O

Figure 2-4. Sugar and water GRNs do not activate each other.

(A, B) Calcium responses of sugar GRNs expressing P2X2 and GCaMP6s to proboscis presentation of PEG as a negative control, ATP to activate P2X2, or sucrose as a positive control. GCaMP6s fluorescence traces (∆F/F) (A) and maximum ∆F/F post stimulus presentation (B), n = 5. Sugar GRNs responded to ATP, but the response to subsequent sucrose presentation was attenuated. (C, D) GCaMP6s responses of sugar GRNs in flies expressing P2X2 in water GRNs to PEG, ATP, and sucrose delivery, ∆F/F traces (C) and maximum ∆F/F graph (D), n = 11. (E, F) ArcLight responses of sugar GRNs in flies expressing P2X2 in water GRNs, ∆F/F traces (E) and maximum ∆F/F graph (F), n = 6. (G, H) Calcium responses of water GRNs expressing P2X2 and GCaMP6s to proboscis delivery of PEG (negative control), ATP, and water (positive control), ∆F/F traces (G) and maximum ∆F/F graph (H), n = 5. Water GRNs responded to ATP presentation, but the subsequent response to water was diminished. (I, J) GCaMP6s responses of water GRNs in flies expressing P2X2 in sugar GRNs to PEG, ATP, and water, ∆F/F traces (I) and maximum ∆F/F graph (J), n = 6. (K, L) ArcLight responses of water GRNs in flies expressing P2X2 in sugar GRNs to PEG, ATP, and water, ∆F/F traces (K) and maximum ∆F/F graph (L), n = 9.

For all traces, period of stimulus presentation is indicated by shaded bars. Traces of individual flies to the first of three taste stimulations (shown in Supplemental Figures 2-4.2, 2-4.3 and 2-4.11) are shown in grey, the average in black, with the SEM indicated by the grey shaded area. Repeated measures ANOVA with Tukey's multiple comparisons test, *$p<0.05$, **$p<0.01$, ***$p<0.001$.

Supplemental Figure 2-4.1

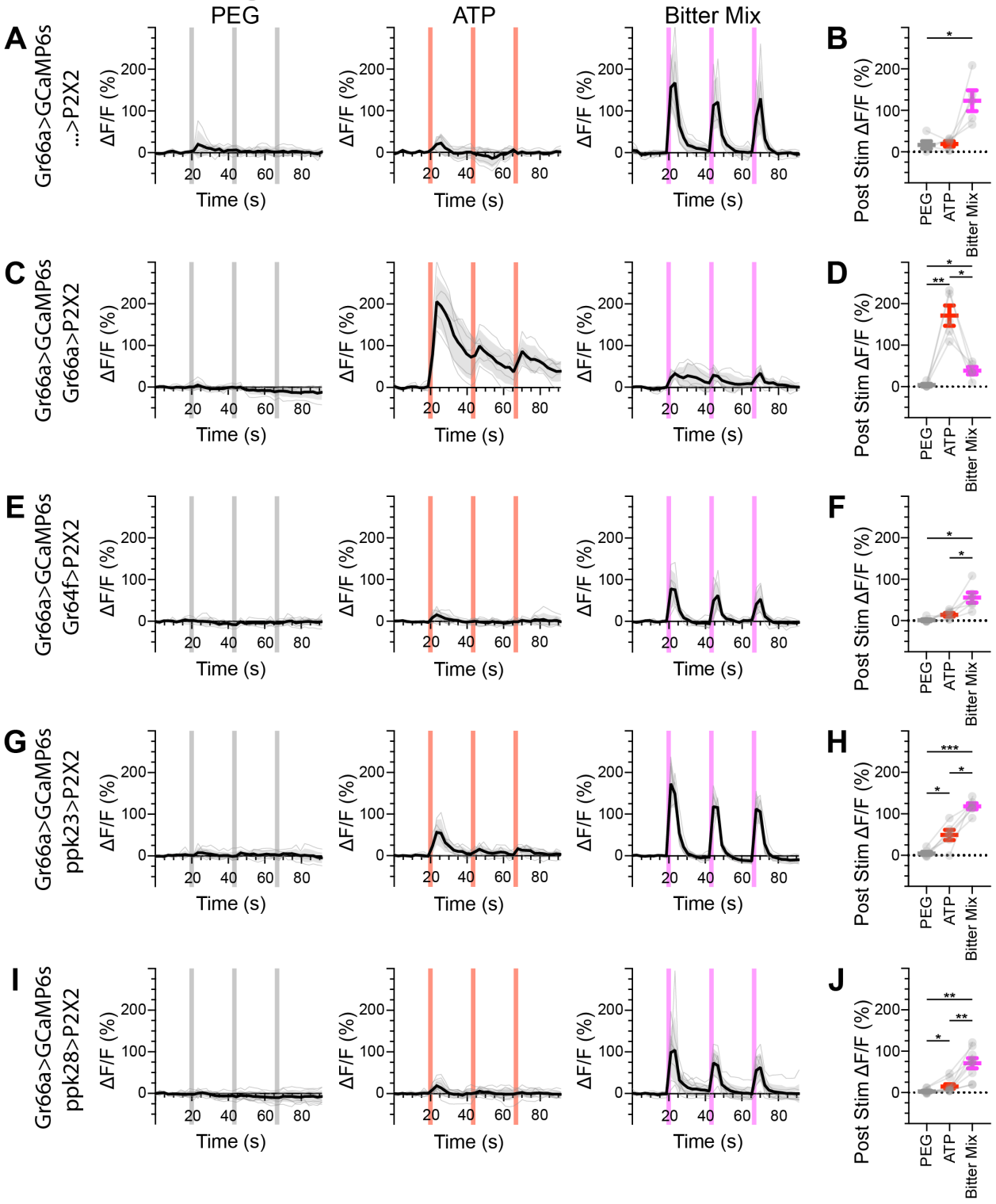

Supplemental Figure 2-4.1. Bitter GRNs do not respond to the activation of other GRN classes in fed flies.

(A, B) Calcium responses of bitter GRNs expressing GCaMP6s in a UAS-P2X2 background to proboscis presentation of PEG as a negative control, ATP, or a mixture of denatonium and caffeine, which are bitter compounds, as a positive control, GCaMP6s ∆F/F traces (A) and maximum ∆F/F graph (B), n = 5. (C, D) Calcium responses of bitter GRNs expressing GCaMP6s and P2X2 to PEG, ATP, or bitter delivery, ∆F/F traces (C) and maximum ∆F/F graph (D), n = 5. (E, F) GCaMP6s responses of bitter GRNs in flies expressing P2X2 in sugar GRNs to PEG, ATP, and bitter, ∆F/F traces (E) and maximum ∆F/F graph (F), n = 6. (G, H) GCaMP6s responses of bitter GRNs in flies expressing P2X2 in high salt GRNs to PEG, ATP, or bitter presentation, ∆F/F traces (E) and maximum ∆F/F graph (F), n = 6. (I, J) GCaMP6s responses of bitter GRNs in flies expressing P2X2 in water GRNs to delivery of PEG, ATP, or bitter to the proboscis, ∆F/F traces (I) and maximum ∆F/F graph (J), n = 9.

Period of stimulus presentation is indicated by shaded bars, 3 stimulations/fly. Traces of individual flies are shown in grey, the average in black, with the SEM indicated by the grey shaded area. Repeated measures ANOVA with Tukey's multiple comparisons test, *$p<0.05$, **$p<0.01$, ***$p<0.001$.

Supplemental Figure 2-4.2

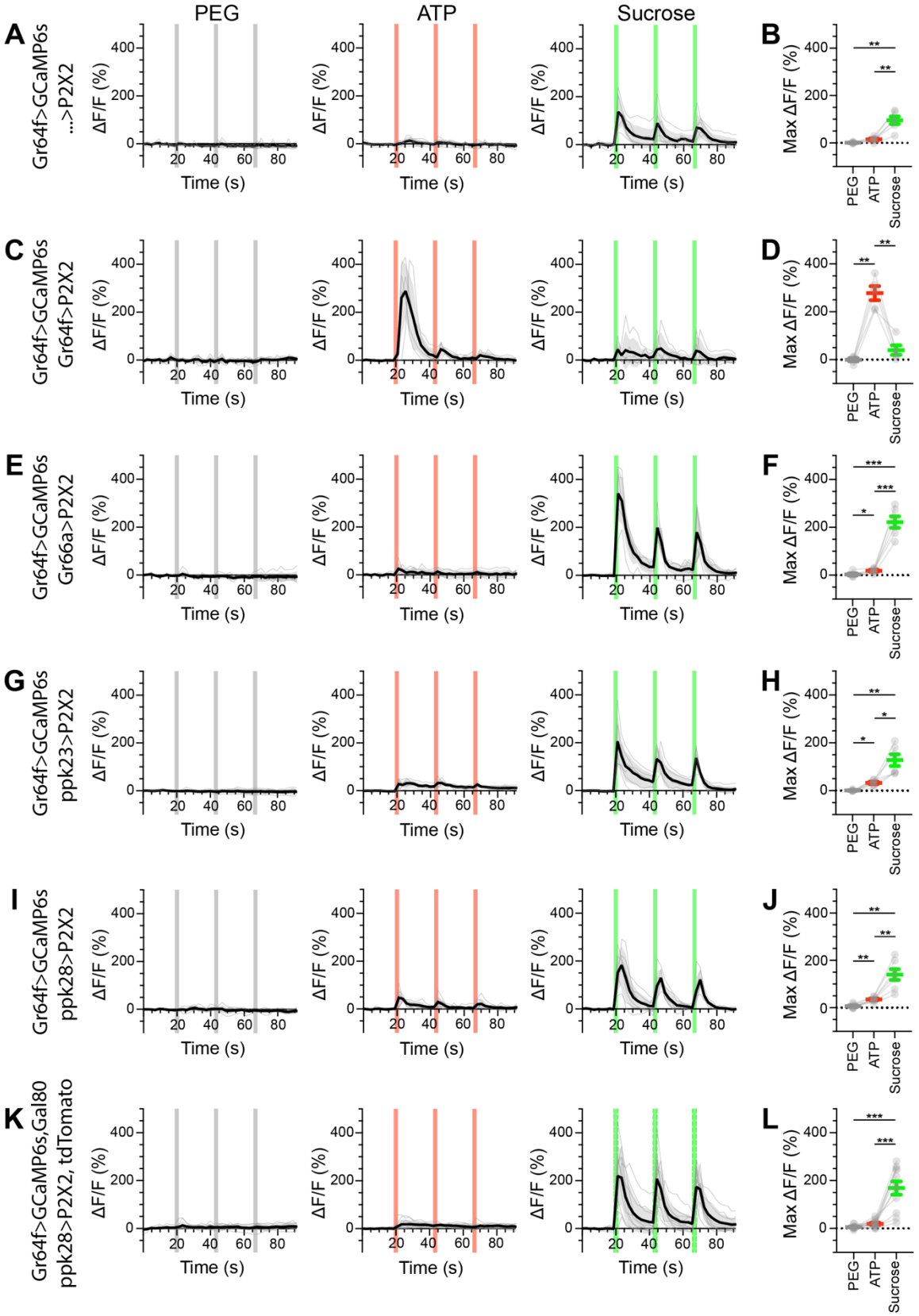

Supplemental Figure 2-4.2. Sugar GRNs do not respond to the activation of other GRN classes in fed flies.

(A, B) Calcium responses of sugar GRNs expressing GCaMP6s in a UAS-P2X2 background to proboscis presentation of PEG as a negative control, ATP, or sucrose as a positive control, GCaMP6s ΔF/F traces (A) and maximum ΔF/F graph (B), n = 6. (C, D) Calcium responses of sugar GRNs expressing GCaMP6s and P2X2 to PEG, ATP, or sucrose delivery, ΔF/F traces (C) and maximum ΔF/F graph (D), n = 5. (E, F) GCaMP6s responses of sugar GRNs in flies expressing P2X2 in bitter GRNs to PEG, ATP, and sucrose, ΔF/F traces (E) and maximum ΔF/F graph (F), n = 6. (G, H) GCaMP6s responses of sugar GRNs in flies expressing P2X2 in high salt GRNs to PEG, ATP, or sucrose to the proboscis, ΔF/F traces (G) and maximum ΔF/F graph (H), n = 6. (I, J) GCaMP6s responses of sugar GRNs in flies expressing P2X2 in water GRNs to PEG, ATP, or sucrose presentation, ΔF/F traces (I) and maximum ΔF/F graph (J), n = 7. (K, L) GCaMP6s responses of sugar GRNs in flies expressing P2X2 in water GRNs and Gal80 in sugar GRNs to inhibit P2X2 misexpression to PEG, ATP, or sucrose presentation, ΔF/F traces (K) and maximum ΔF/F plots (L), n = 11.

Period of stimulus presentation is indicated by shaded bars, 3 stimulations/fly. Data from first stimulation of C and K is shown in Figure 4A-D. Traces of individual flies are shown in grey, the average in black, with the SEM indicated by the grey shaded area. Repeated measures ANOVA with Tukey's multiple comparisons test *$p<0.05$, **$p<0.01$, ***$p<0.001$.

Supplemental Figure 2-4.3

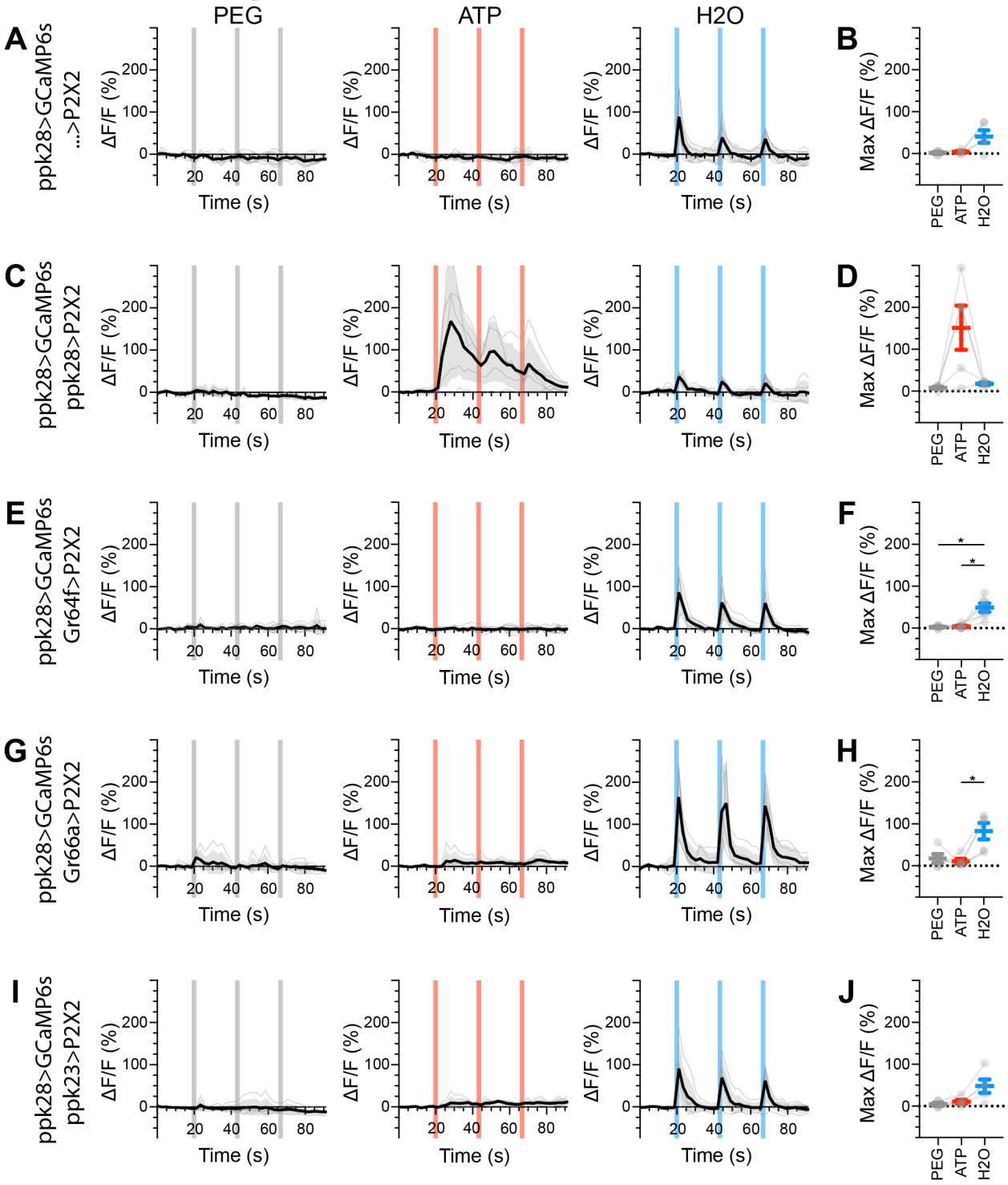

Supplemental Figure 2-4.3. Water GRNs do not respond to the activation of other GRN classes in fed flies.

(A, B) Calcium responses of water GRNs expressing GCaMP6s in a UAS-P2X2 background to proboscis presentation of PEG as a negative control, ATP, or water as a positive control, GCaMP6s ΔF/F traces (A) and maximum ΔF/F graph (B), n = 5. (C, D) Calcium responses of water GRNs expressing GCaMP6s and P2X2 to PEG, ATP, or water delivery, ΔF/F traces (C) and maximum ΔF/F graph (D), n = 5. (E, F) GCaMP6s responses of water GRNs in flies expressing P2X2 in sugar GRNs to PEG, ATP, and water, ΔF/F traces (E) and maximum ΔF/F graph (F), n = 6. (G, H) GCaMP6s responses of water GRNs in flies expressing P2X2 in bitter GRNs upon PEG, ATP, or water presentation, ΔF/F traces (G) and maximum ΔF/F graph (H), n = 5. (I, J) GCaMP6s responses of water GRNs in flies expressing P2X2 in high salt GRNs upon PEG, ATP, or water delivery, ΔF/F traces (I) and maximum ΔF/F graph (J), n = 5.

Period of stimulus presentation is indicated by shaded bars, 3 stimulations/fly. The first response in C and E is shown in Figure 4G-J. Traces of individual flies are shown in grey, the average in black, with the SEM indicated by the grey shaded area. Repeated measures ANOVA with Tukey's multiple comparisons test *$p<0.05$.

Supplemental Figure 2-4.4

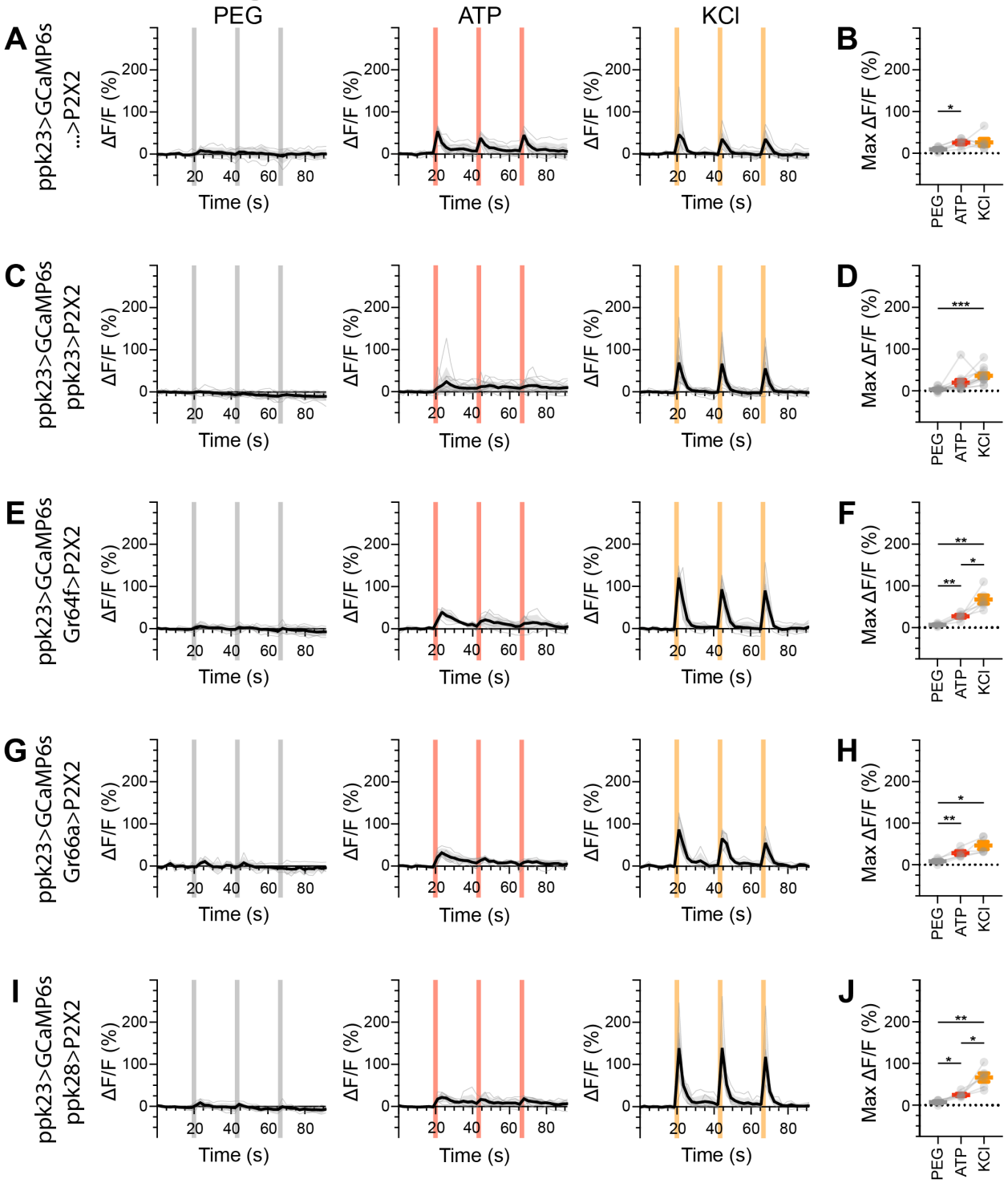

Supplemental Figure 2-4.4. High Salt GRNs do not respond to the activation of other GRN classes in fed flies.

(A, B) Calcium responses of high salt GRNs expressing GCaMP6s in a UAS-P2X2 background to proboscis presentation of PEG as a negative control, ATP, or KCl as a positive control, GCaMP6s ΔF/F traces (A) and maximum ΔF/F graph (B), n = 6. Minor responses to ATP were observed throughout, which are likely in response to the sodium counter ions contained in the ATP tastant solution. (C, D) Calcium responses of high salt GRNs expressing GCaMP6s and P2X2 to PEG, ATP, or KCl delivery, ΔF/F traces (C) and maximum ΔF/F graph (D), n = 12. (E, F) GCaMP6s responses of high salt GRNs in flies expressing P2X2 in sugar GRNs to PEG, ATP, and KCl presentation to the proboscis, ΔF/F traces (E) and maximum ΔF/F graph (F), n = 6. (G, H) GCaMP6s responses of high salt GRNs in flies expressing P2X2 in bitter GRNs to PEG, ATP, or KCl delivery, ΔF/F traces (G) and maximum ΔF/F graph (H), n = 5. (I, J) GCaMP6s responses of high salt GRNs in flies expressing P2X2 in water GRNs to PEG, ATP, or KCl presentation, ΔF/F traces (I) and maximum ΔF/F graph (J), n = 6.

Period of stimulus presentation is indicated by shaded bars, 3 stimulations/fly. Traces of individual flies are shown in grey, the average in black, with the SEM indicated by the grey shaded area. Repeated measures ANOVA with Tukey's multiple comparisons test *$p<0.05$, **$p<0.01$, ***$p<0.001$.

Supplemental Figure 2-4.5

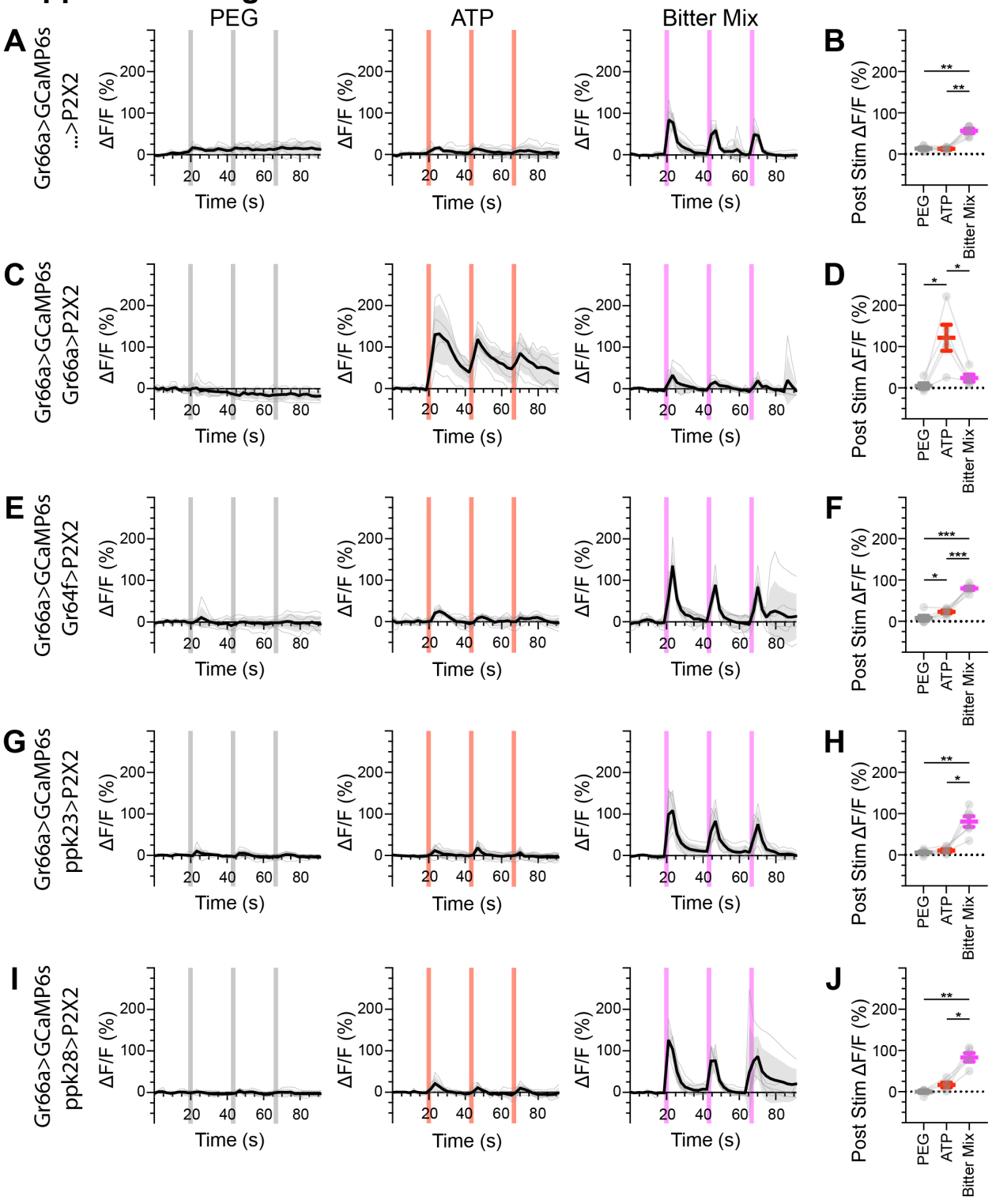

Supplemental Figure 2-4.5. Bitter GRNs do not respond to the activation of other GRN classes in food-deprived flies.

(A, B) Calcium responses of bitter GRNs expressing GCaMP6s in a UAS-P2X2 background to proboscis presentation of PEG as a negative control, ATP, or a mixture of the bitter compounds denatonium and caffeine as a positive control, GCaMP6s ΔF/F traces (A) and maximum ΔF/F graph (B), n = 6. (C, D) Calcium responses of bitter GRNs expressing GCaMP6s and P2X2 to PEG, ATP, or bitter delivery, ΔF/F traces (C) and maximum ΔF/F graph (D), n = 5. (E, F) GCaMP6s responses of bitter GRNs in flies expressing P2X2 in sugar GRNs to PEG, ATP, and bitter, ΔF/F traces (E) and maximum ΔF/F graph (F), n = 6. (G, H) GCaMP6s responses of bitter GRNs in flies expressing P2X2 in high salt GRNs to presentation of PEG, ATP, or bitter, ΔF/F traces (G) and maximum ΔF/F graph (H), n = 6. (I, J) GCaMP6s responses of bitter GRNs in flies expressing P2X2 in water GRNs to delivery of PEG, ATP, or bitter, ΔF/F traces (I) and maximum ΔF/F graph (J), n = 5.

Period of stimulus presentation is indicated by shaded bars, 3 stimulations/fly. Flies were food-deprived for 23-26 hours. Traces of individual flies are shown in grey, the average in black, with the SEM indicated by the grey shaded area. Repeated measures ANOVA with Tukey's multiple comparisons test, *p<0.05, **p<0.01, ***p<0.001.

Supplemental Figure 2-4.6

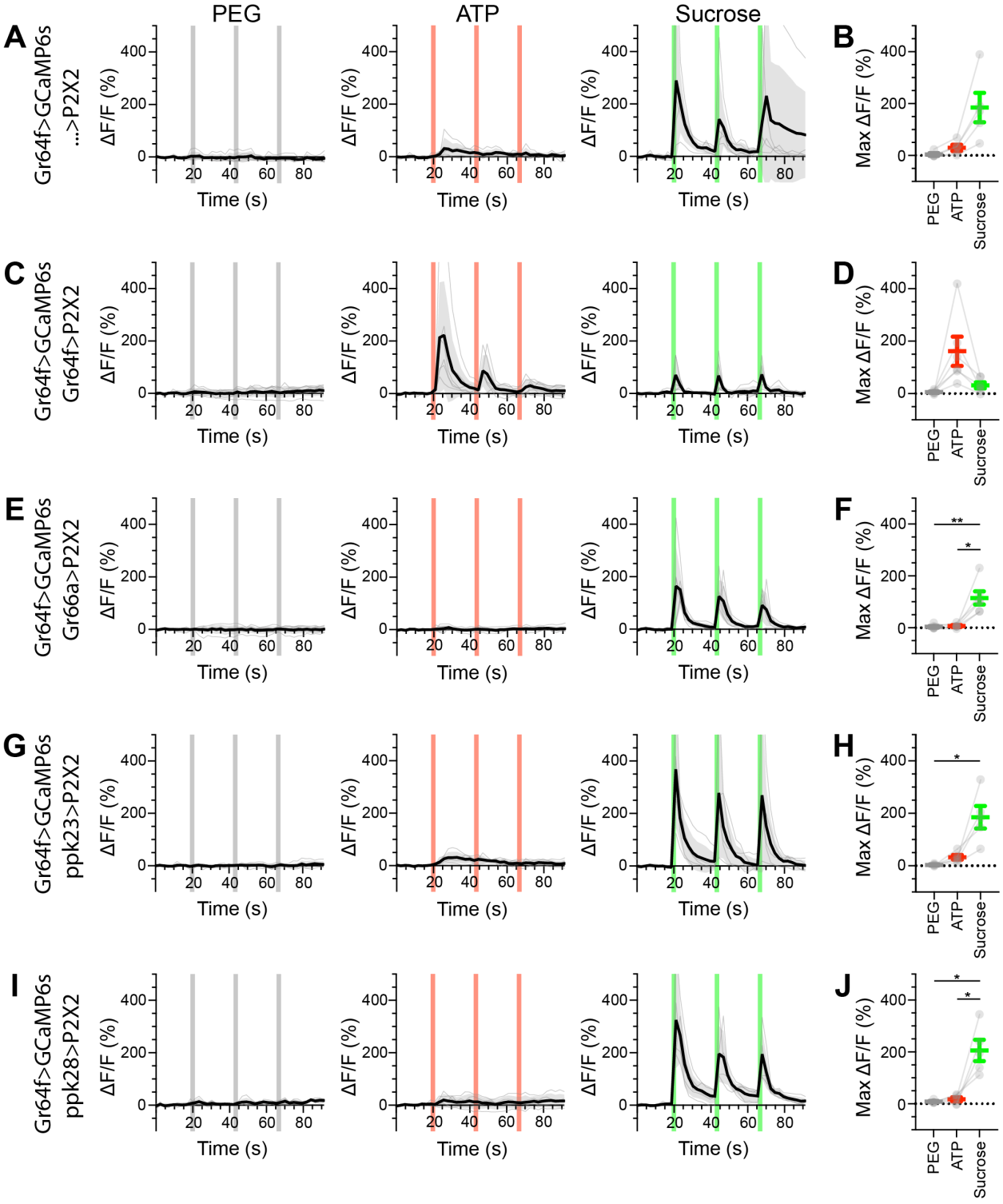

Supplemental Figure 2-4.6. Sugar GRNs do not respond to the activation of other GRN classes in food-deprived flies.

(A, B) Calcium responses of sugar GRNs expressing GCaMP6s in a UAS-P2X2 background to proboscis presentation of PEG as a negative control, ATP, or sucrose as a positive control, GCaMP6s ΔF/F traces (A) and maximum ΔF/F graph (B), n = 5. (C, D) Calcium responses of sugar GRNs expressing GCaMP6s and P2X2 to PEG, ATP, or sucrose delivery, ΔF/F traces (C) and maximum ΔF/F graph (D), n = 6. (E, F) GCaMP6s responses of sugar GRNs in flies expressing P2X2 in bitter GRNs to PEG, ATP, and sucrose, ΔF/F traces (E) and maximum ΔF/F graph (F), n = 6. (G, H) GCaMP6s responses of sugar GRNs in flies expressing P2X2 in high salt GRNs to PEG, ATP, and sucrose delivery to the proboscis, ΔF/F traces (G) and maximum ΔF/F graph (H), n = 5. (I, J) GCaMP6s responses of sugar GRNs in flies expressing P2X2 in water GRNs to PEG, ATP, and sucrose presentation to the proboscis, ΔF/F traces (I) and maximum ΔF/F graph (J), n = 5.

Period of stimulus presentation is indicated by shaded bars, 3 stimulations/fly. Flies were food-deprived for 23-26 hours. Traces of individual flies are shown in grey, the average in black, with the SEM indicated by the grey shaded area. Repeated measures ANOVA with Tukey's multiple comparisons test *$p<0.05$, **$p<0.01$.

Supplemental Figure 2-4.7

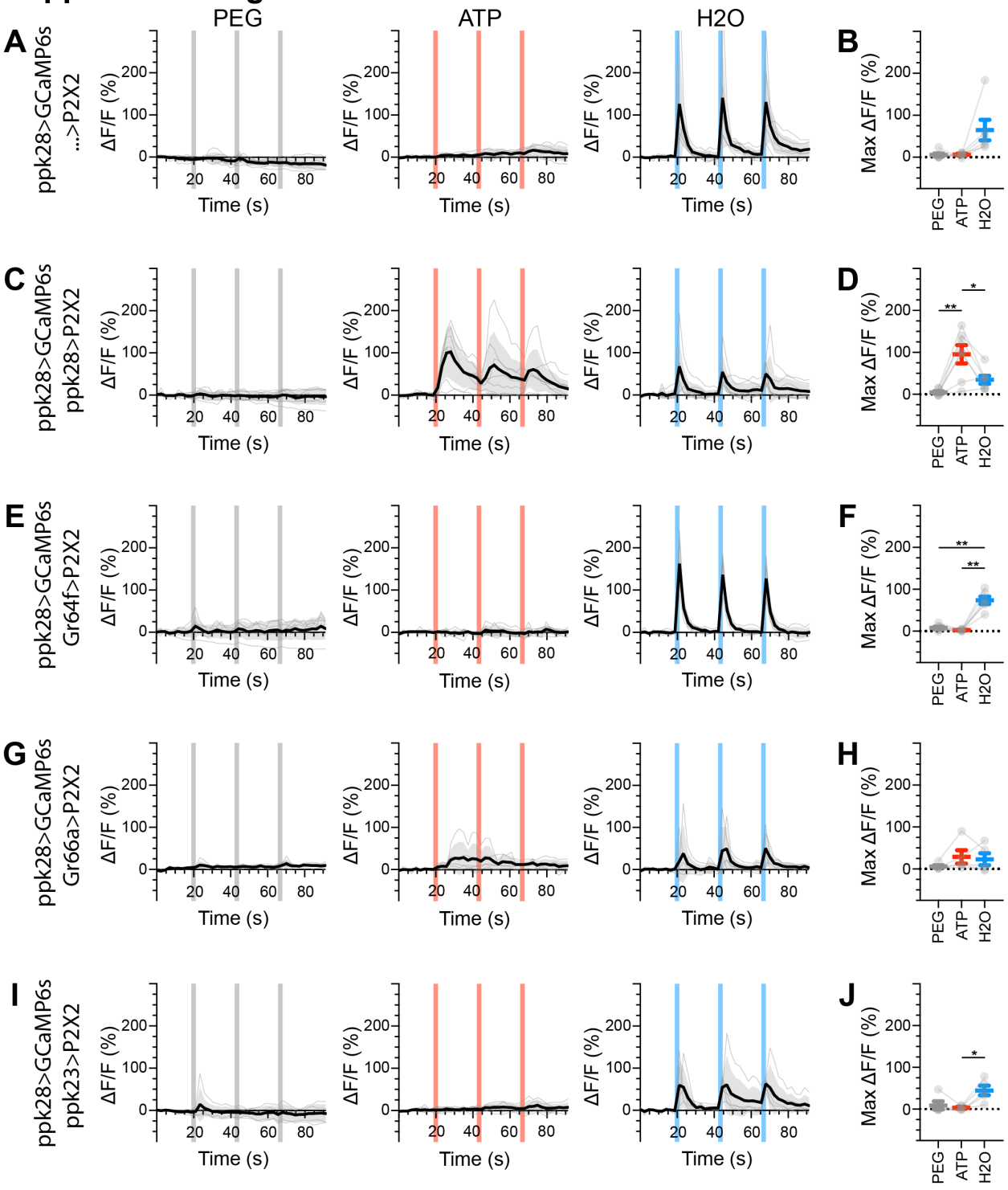

Supplemental Figure 2-4.7. Water GRNs do not respond to the activation of other GRN classes in food-deprived flies.

(A, B) Calcium responses of water GRNs expressing GCaMP6s in a UAS-P2X2 background to proboscis presentation of PEG as a negative control, ATP, or water as a positive control, GCaMP6s ΔF/F traces (A) and maximum ΔF/F graph (B), n = 6. (C, D) Calcium responses of water GRNs expressing GCaMP6s and P2X2 to PEG, ATP, or water delivery, ΔF/F traces (C) and maximum ΔF/F graph (D), n = 7. (E, F) GCaMP6s responses of water GRNs in flies expressing P2X2 in sugar GRNs to PEG, ATP, and water, ΔF/F traces (E) and maximum ΔF/F graph (F), n = 6. (G, H) GCaMP6s responses of water GRNs in flies expressing P2X2 in bitter GRNs to PEG, ATP, and water delivery, ΔF/F traces (G) and maximum ΔF/F graph (H), n = 5. (I, J) GCaMP6s responses of water GRNs in flies expressing P2X2 in high salt GRNs to PEG, ATP, and water presentation, ΔF/F traces (I) and maximum ΔF/F graph (J), n = 5.

Period of stimulus presentation is indicated by shaded bars, 3 stimulations/fly. Flies were food-deprived for 23-26 hours. Traces of individual flies are shown in grey, the average in black, with the SEM indicated by the grey shaded area. Repeated measures ANOVA with Tukey's multiple comparisons test *$p<0.05$, **$p<0.01$.

Supplemental Figure 2-4.8

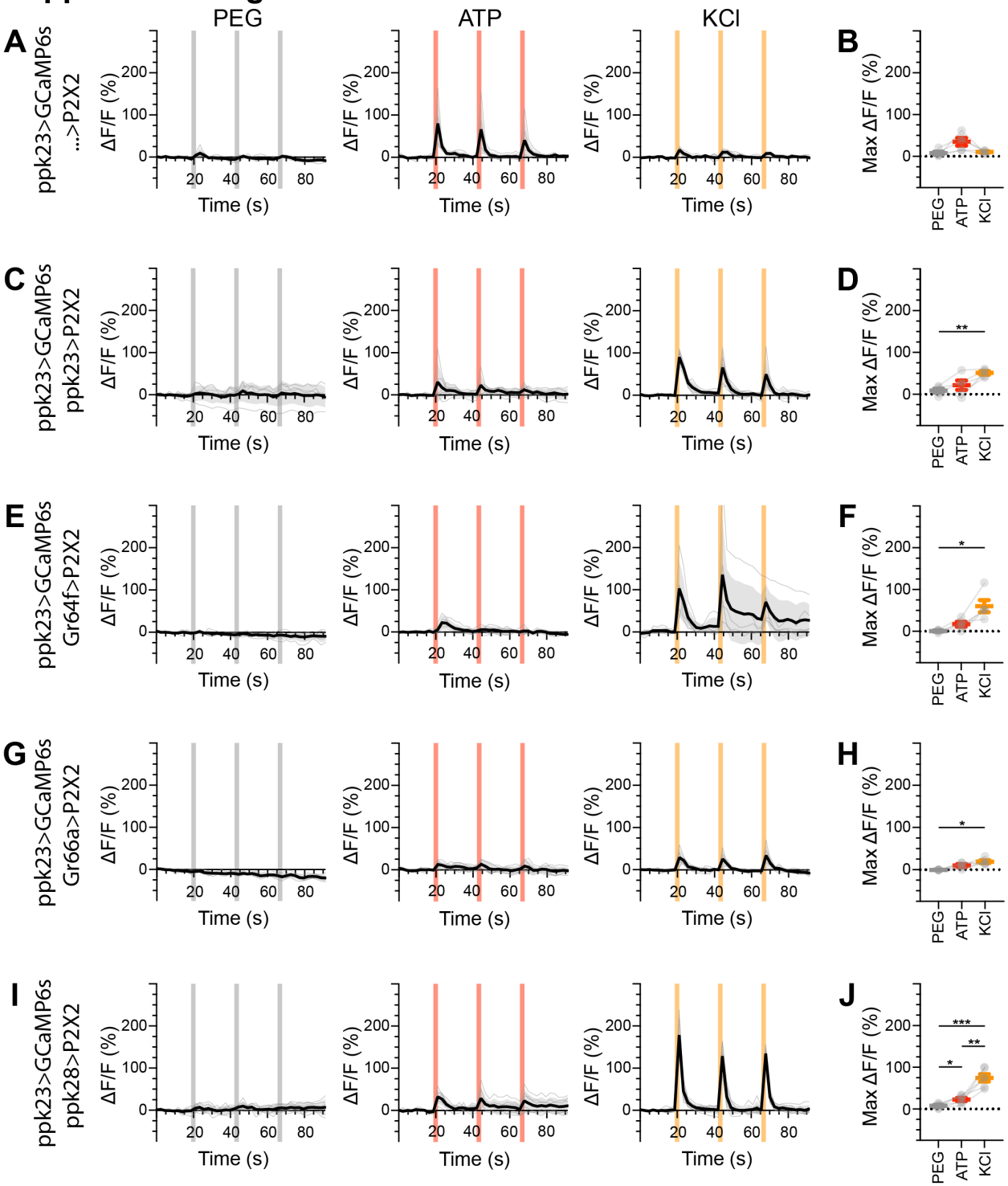

Supplemental Figure 2-4.8. High salt GRNs do not respond to the activation of other GRN classes in food-deprived flies.

(A, B) Calcium responses of high salt GRNs expressing GCaMP6s in a UAS-P2X2 background to proboscis presentation of PEG as a negative control, ATP, or KCl as a positive control, GCaMP6s ΔF/F traces (A) and maximum ΔF/F graph (B), n = 5. (C, D) Calcium responses of high salt GRNs expressing GCaMP6s and P2X2 to PEG, ATP, or KCl delivery, ΔF/F traces (C) and maximum ΔF/F graph (D), n = 5. (E, F) GCaMP6s responses of high salt GRNs in flies expressing P2X2 in sugar GRNs to PEG, ATP, and KCl delivery, ΔF/F traces (E) and maximum ΔF/F graph (F), n = 5. (G, H) GCaMP6s responses of high salt GRNs in flies expressing P2X2 in bitter GRNs to PEG, ATP, and KCl delivery to the proboscis, ΔF/F traces (G) and maximum ΔF/F graph (H), n = 5. (I, J) GCaMP6s responses of high salt GRNs in flies expressing P2X2 in water GRNs to PEG, ATP, and KCl delivery, ΔF/F traces (I) and maximum ΔF/F graph (J), n = 6.

Period of stimulus presentation is indicated by shaded bars, 3 stimulations/fly. Flies were food-deprived for 23-26 hours. Traces of individual flies are shown in grey, the average in black, with the SEM indicated by the grey shaded area. Repeated measures ANOVA with Tukey's multiple comparisons test *$p<0.05$, **$p<0.01$, ***$p<0.001$.

Supplemental Figure 2-4.9

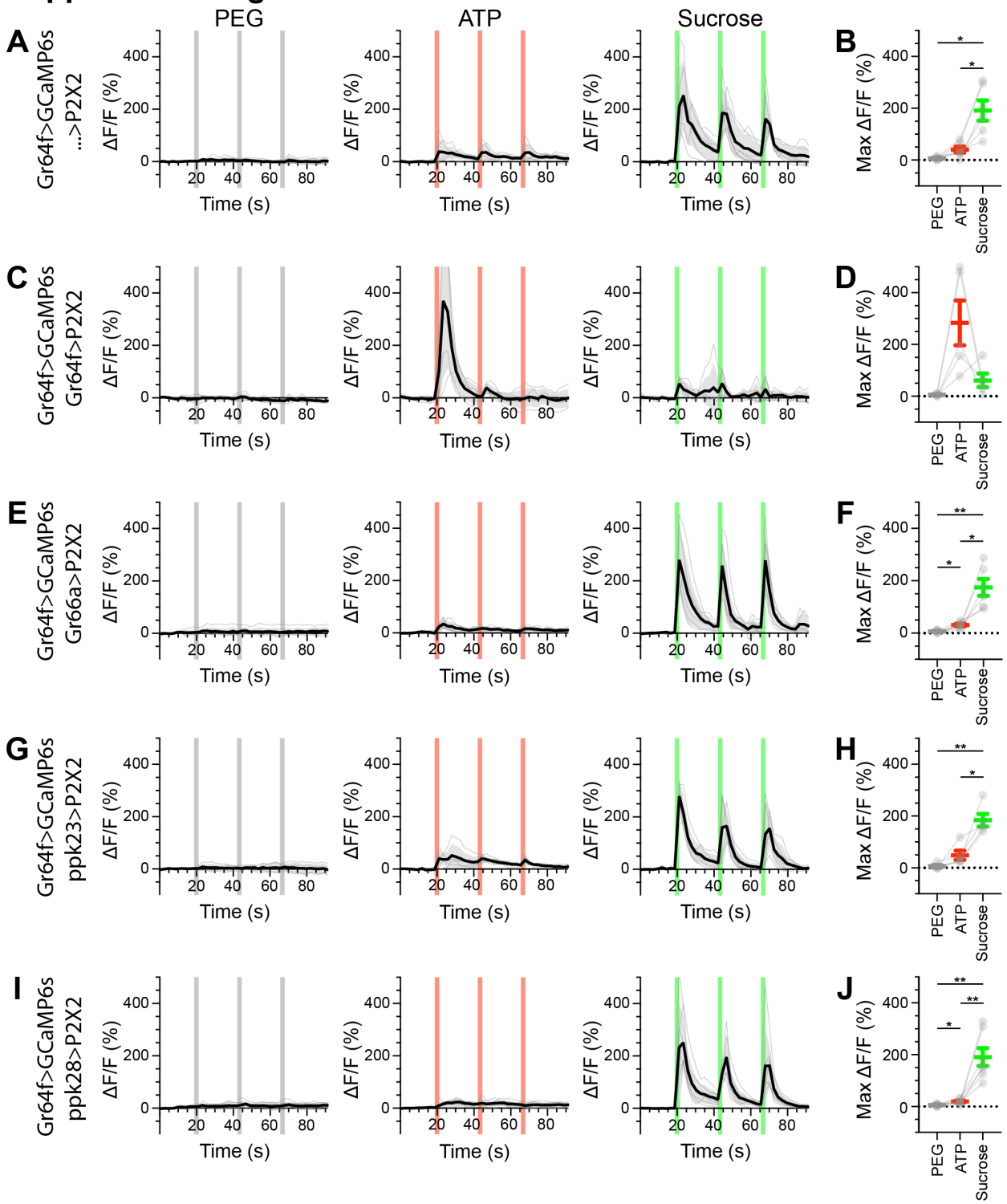

Supplemental Figure 2-4.9. Sugar GRNs do not respond to the activation of other GRN classes in pseudo-desiccated flies.

(A, B) Calcium responses of sugar GRNs expressing GCaMP6s in a UAS-P2X2 background to proboscis presentation of PEG as a negative control, ATP, or sucrose as a positive control, GCaMP6s ΔF/F traces (A) and maximum ΔF/F graph (B), n = 6. (C, D) Calcium responses of sugar GRNs expressing GCaMP6s and P2X2 to PEG, ATP, or sucrose delivery, ΔF/F traces (C) and maximum ΔF/F graph (D), n = 5. (E, F) GCaMP6s responses of sugar GRNs in flies expressing P2X2 in bitter GRNs to PEG, ATP, and sucrose, ΔF/F traces (E) and maximum ΔF/F graph (F), n = 6. (G, H) GCaMP6s responses of sugar GRNs in flies expressing P2X2 in water GRNs to PEG, ATP, or KCl presentation to the proboscis, ΔF/F traces (G) and maximum ΔF/F graph (H), n = 5. (I, J) GCaMP6s responses of sugar GRNs in flies expressing P2X2 in high salt GRNs, ΔF/F traces (I) and maximum ΔF/F graph (J), n = 7.

Period of stimulus presentation is indicated by shaded bars, 3 stimulations/fly. Dissections and imaging were performed in high osmolality AHL to simulate thirst. Traces of individual flies are shown in grey, the average in black, with the SEM indicated by the grey shaded area. Repeated measures ANOVA with Tukey's multiple comparisons test *$p<0.05$, **$p<0.01$.

Supplemental Figure 2-4.10

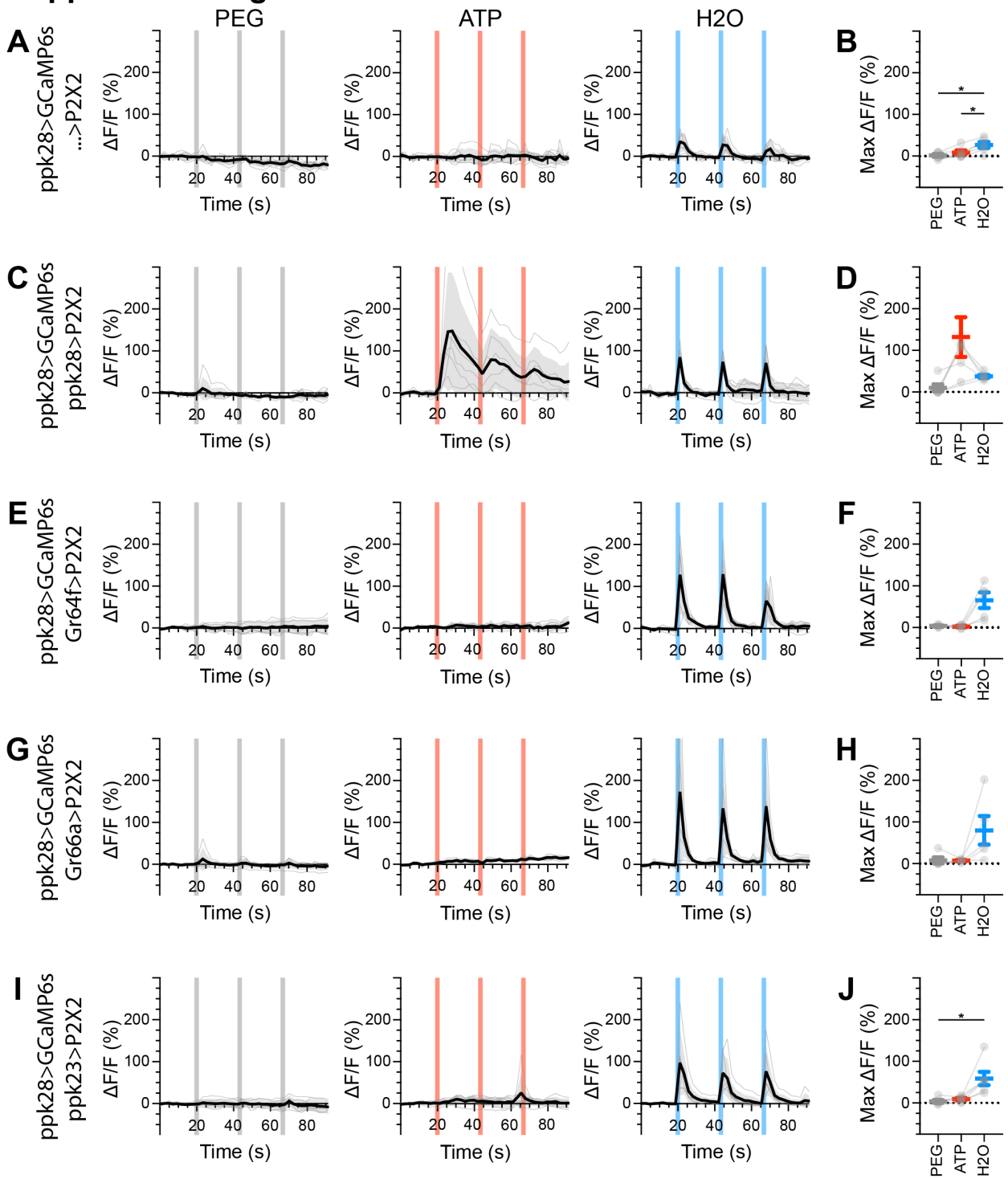

Supplemental Figure 2-4.10. Water GRNs do not respond to the activation of other GRN classes in pseudo-desiccated flies.

(A, B) Calcium responses of water GRNs expressing GCaMP6s in a UAS-P2X2 background to proboscis presentation of PEG as a negative control, ATP, or water as a positive control, GCaMP6s ΔF/F traces (A) and maximum ΔF/F graph (B), n = 6. (C, D) Calcium responses of water GRNs expressing GCaMP6s and P2X2 to PEG, ATP, or water delivery, ΔF/F traces (C) and maximum ΔF/F graph (D), n = 6. (E, F) GCaMP6s responses of water GRNs in flies expressing P2X2 in sugar GRNs to PEG, ATP, and water, ΔF/F traces (E) and maximum ΔF/F graph (F), n = 5. (G, H) GCaMP6s responses of water GRNs in flies expressing P2X2 in bitter GRNs to PEG, ATP, or water delivery, ΔF/F traces (G) and maximum ΔF/F graph (H), n = 5. (I, J) GCaMP6s responses of water GRNs in flies expressing P2X2 in high salt GRNs to PEG, ATP, or water delivery to the proboscis, ΔF/F traces (I) and maximum ΔF/F graph (J), n = 6.

Period of stimulus presentation is indicated by shaded bars, 3 stimulations/fly. Dissections and imaging were performed in high osmolality AHL to simulate thirst. Traces of individual flies are shown in grey, the average in black, with the SEM indicated by the grey shaded area. Repeated measures ANOVA with Tukey's multiple comparisons test *$p<0.05$, **$p<0.01$.

Supplemental Figure 2-4.11

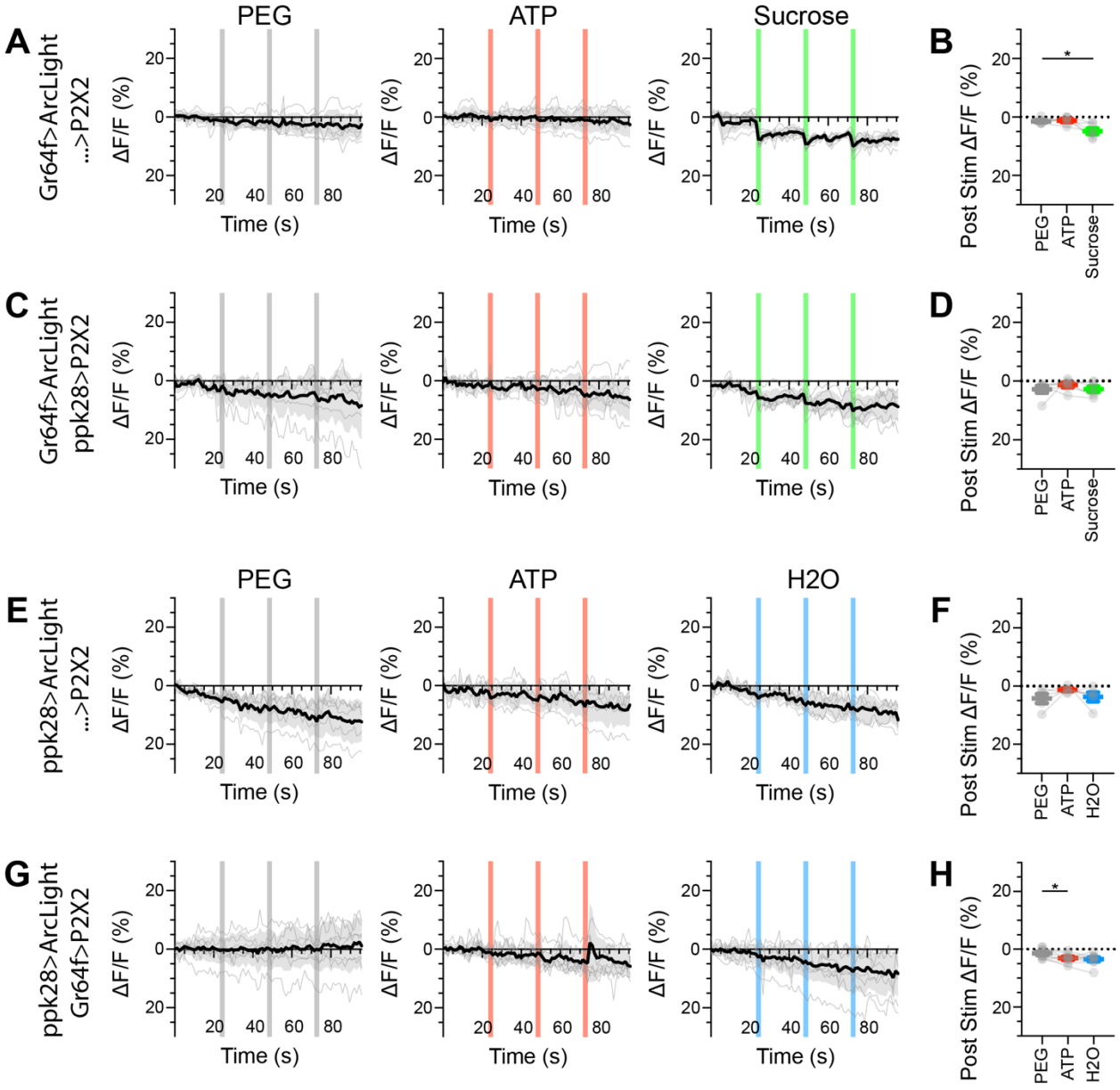

Supplemental Figure 2-4.11. Sugar and water GRNs do not show voltage responses upon reciprocal activation.

(A, B) ArcLight responses of sugar GRNs in a UAS-P2X2 background to proboscis presentation of PEG as a negative control, ATP, or sucrose as a positive control. ArcLight fluorescence traces (∆F/F) (A) and maximum ∆F/F post stimulus presentation (B), n = 6. (C, D) ArcLight responses of sugar GRNs in flies expressing P2X2 in water GRNs to PEG, ATP, and sucrose delivery, ∆F/F traces (C) and maximum ∆F/F graph (D), n = 6. (E, F) ArcLight responses of water GRNs in a UAS-P2X2 background to proboscis delivery of PEG, ATP, and water (positive control), ∆F/F traces (E) and maximum ∆F/F graph (F), n = 5. (G, H) ArcLight responses of water GRNs in flies expressing P2X2 in sugar GRNs to PEG, ATP, and water delivery, ∆F/F traces (G) and maximum ∆F/F graph (H), n = 9.

Period of stimulus presentation is indicated by shaded bars, 3 stimulations/fly. The first response in C and G is shown in Figure 2-4 E, F, K, L. Traces of individual flies to three taste stimulations are shown in grey, the average in black, with the SEM indicated by the grey shaded area. Repeated measures ANOVA with Tukey's multiple comparisons test, *$p<0.05$.

Figure 2-5

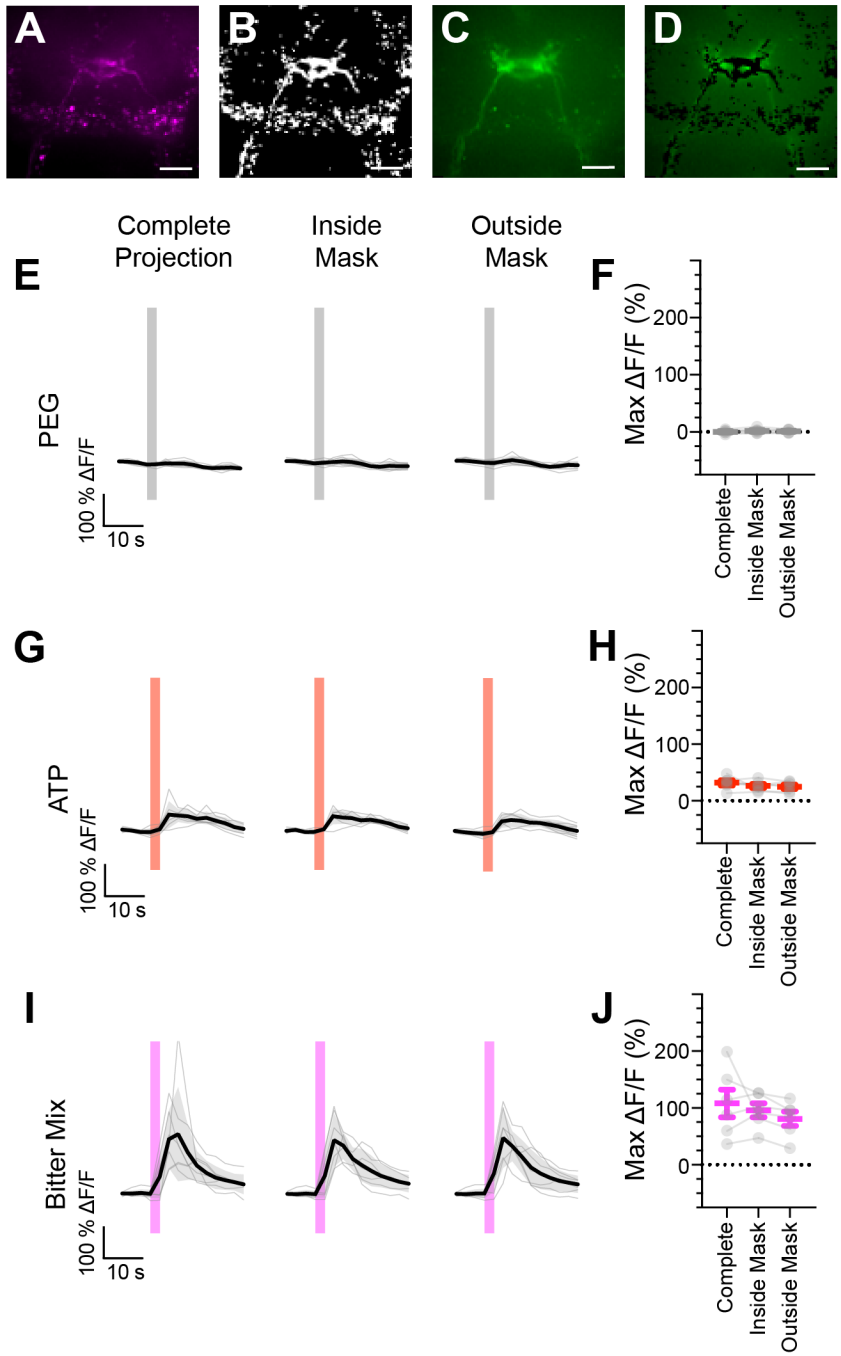
A
B
C
D
Complete Projection
Inside Mask
Outside Mask
E
PEG
100 % ΔF/F
10 s
F
Max ΔF/F (%)
200
100
0
Complete
Inside Mask
Outside Mask
G
ATP
100 % ΔF/F
10 s
H
Max ΔF/F (%)
200
100
0
Complete
Inside Mask
Outside Mask
I
Bitter Mix
100 % ΔF/F
10 s
J
Max ΔF/F (%)
200
100
0
Complete
Inside Mask
Outside Mask

Figure 2-5. Activation of a sparse subset of bitter GRNs is sufficient to cause depolarization in other bitter GRNs.

(A) Gr47a positive bitter GRNs in the SEZ of a sample fly (scale bar = 20μm) (B) Boolean mask generated based on A (scale bar = 20μm) (C) Projection pattern of all bitter GRNs in the SEZ of the same fly as A (scale bar = 20μm) (D) Bitter projection pattern with Gr47a positive GRNs excluded (scale bar = 20μm) (E-F) GCaMP6s response of all bitter GRNs in flies expressing P2X2 in Gr47a- positive bitter cells to the presentation of PEG as a negative control. Response of the entire projection (left), the area contained within the Gr47a-based mask (middle) and the projection outside the masked area (right), ΔF/F traces (E) and maximum ΔF/F graph (F). (G-H) GCaMP6s response of all bitter GRNs in flies expressing P2X2 in Gr47a- positive bitter cells to the presentation of ATP to activate P2X2. Response of the entire projection (left), the area contained within the Gr47a-based mask (middle) and the projection outside the masked area (right), ΔF/F traces (G) and maximum ΔF/F graph (H). (I-J) GCaMP6s response of all bitter GRNs in flies expressing P2X2 in Gr47a-positive bitter cells to the presentation of a mixture of the bitters caffeine and denatonium as a positive control. Response of the entire projection (left), the area contained within the Gr47a-based mask (middle) and the projection outside the masked area (right), ΔF/F traces (I) and maximum ΔF/F graph (J).

For all traces, period of stimulus presentation is indicated by shaded bars, n = 6. Traces of individual flies to the first of three taste stimulations (shown in Supplemental Figures 2-5.1) are shown in grey, the average in black, with the SEM indicated by the grey shaded area. Repeated measures ANOVA with Tukey's multiple comparisons test.

Supplemental Figure 2-5.1

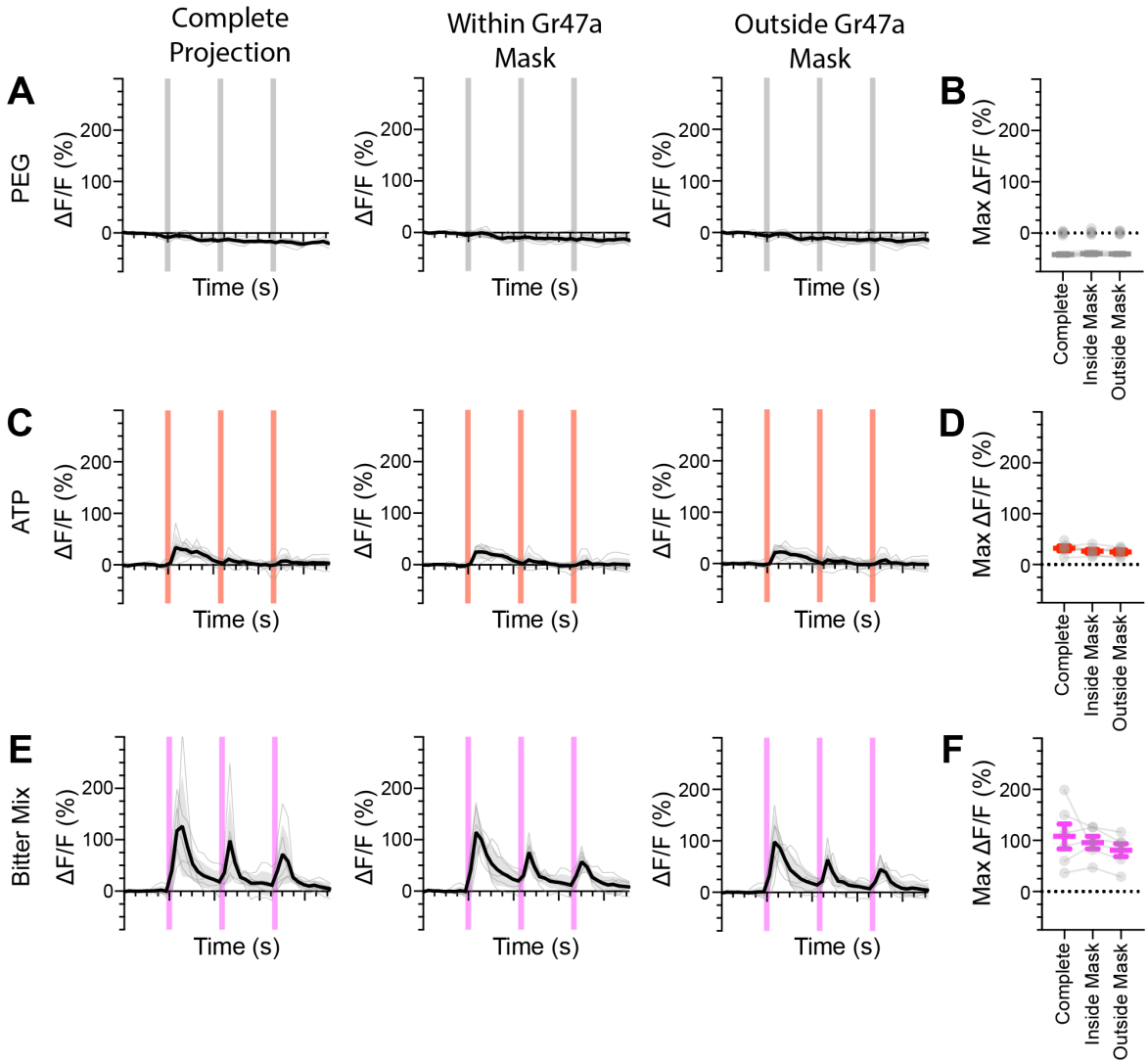

Figure 2-5.1. Bitter GRNs respond to the activation of a sparse subset of bitter neurons in fed flies.

(A-B) GCaMP6s response of all bitter GRNs in flies expressing P2X2 in Gr47a-positive bitter cells to the presentation of PEG as a negative control. Response of the entire projection (left), the area contained within the Gr47a-based mask (middle) and the projection outside the masked area (right), ΔF/F traces (A) and maximum ΔF/F graph (B). (C-D) GCaMP6s response of all bitter GRNs in flies expressing P2X2 in Gr47a-positive bitter cells to the presentation of ATP to activate P2X2. Response of the entire projection (left), the area contained within the Gr47a-based mask (middle) and the projection outside the masked area (right), ΔF/F traces (C) and maximum ΔF/F graph (D). (E-F) GCaMP6s response of all bitter GRNs in flies expressing P2X2 in Gr47a-positive bitter cells to the presentation of a mixture of caffeine and denatonium as a positive control. Response of the entire projection (left), the area contained within the Gr47a-based mask (middle) and the projection outside the masked area (right), ΔF/F traces (E) and maximum ΔF/F graph (F).

Period of stimulus presentation is indicated by shaded bars, 3 stimulations/fly. The first response throughout is shown in Figure 2-5. Traces of individual flies to three taste stimulations are shown in grey, the average in black, with the SEM indicated by the grey shaded area. Repeated measures ANOVA with Tukey's multiple comparisons test.

Figure 2-6

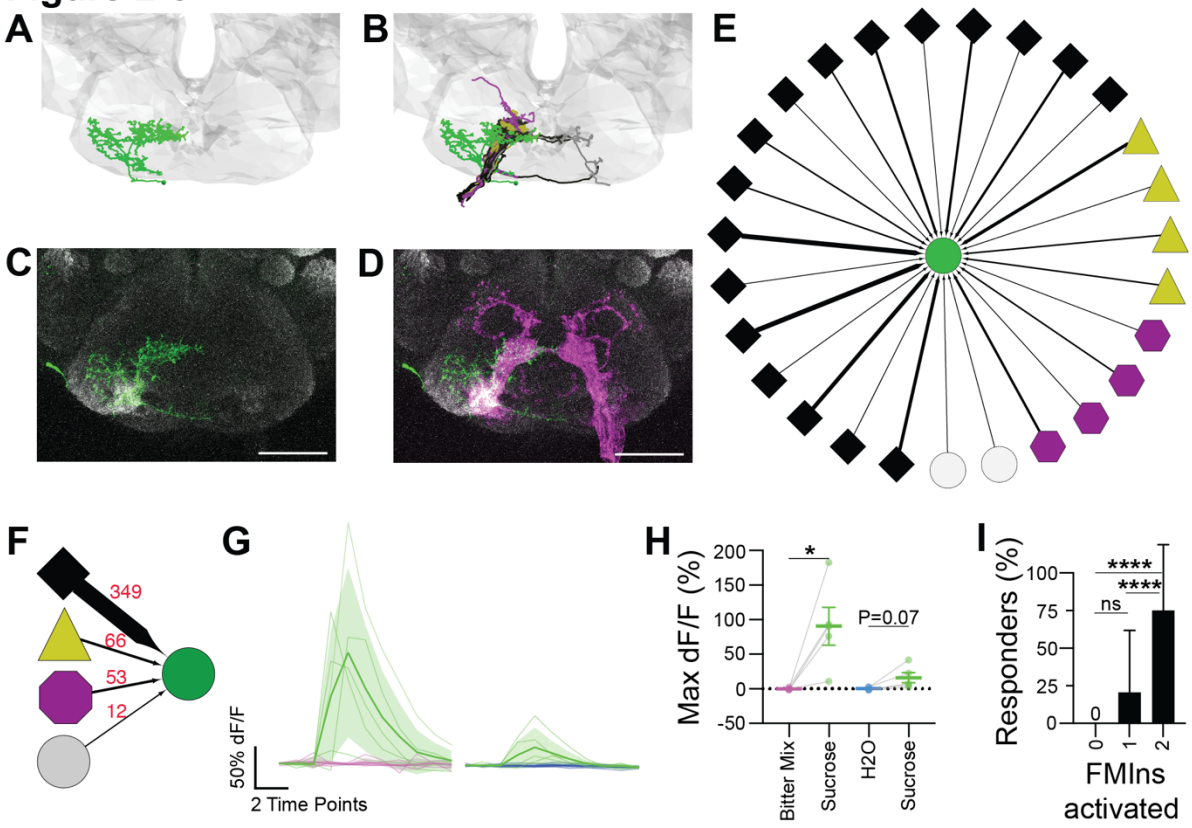
A
B
E
C
D
F
349
66
53
12
G
50% dF/F
2 Time Points
H
Max dF/F (%)
200
150
100
50
0
-50
*
P=0.07
Bitter Mix
Sucrose
H2O
Sucrose
I
Responders (%)
100
75
50
25
0
****
****
ns
0
1
2
FMIns activated

Figure 2-6. A second order gustatory neuron downstream of sugar GRNs in the EM responds selectively to sugar presentation.

(A) Reconstruction of FMIn in the FAFB dataset (B) FMIn and its GRN inputs in the EM dataset. GRN colors correspond to clusters established in Figure 2-2. (C) Light level image of a single FMIn generated by flippase 1026A mediated mosaicism from *GmR81E10-Gal4* (scale bar = 25μm) (D) FMIn (green) overlaps with sugar taste projections (magenta) in light-level imagery (scale bar = 25μm). (E) GRN inputs to FMIn identified in the EM. Colors correspond to clusters established in Figure 2-2. Arrow thickness scales with the number of synapses comprising the connection. Only connections of at least 5 synapses are shown. (F) GRN inputs to FMIn by GRN cluster. Colors correspond to clusters established in Figure 2-2. Arrow thickness scales with the number of synapses comprising the connection, which is indicated in red. Only connections of at least 5 synapses are considered. (G-H) GCaMP6s responses of FMIn cell bodies to tastant presentations to the proboscis. (G)The responses of flies presented with sucrose (green) and a bitter mixture of denatonium and caffeine (pink) are shown on the left, flies presented with sucrose and water (blue) on the right. Individual traces are shown in thin lines colored corresponding to tastant identity, averages in thicker lines with the SEM indicated by shaded areas. (H) Maximum $\Delta F/F$ graph. n=5 for each group, paired t test *p<0.5. (G) Fraction of flies performing PER to light with the number of FMIns activated using ReaChR. 0 FMIn: n = 9; 1 FMIn: n = 29; 2 FMIns: n = 36. Unpaired t test, ****p<0.0001.

Supplemental Figure 2-6.1

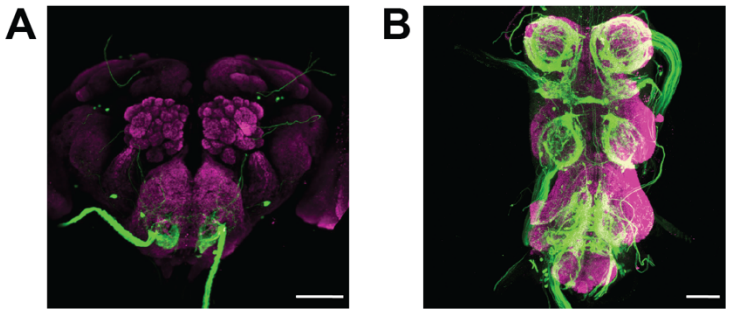

Supplemental Figure 2-6.1 Expression pattern of *GmR81E10-Gal4* in the central nervous system.

(A) Expression pattern of *GmR81E10-Gal4* in the brain (scale bar = 50 μm) (B) Expression pattern of *GmR81E10-Gal4* in the ventral nerve cord.

References

Bates AS, Manton JD, Jagannathan SR, Costa M, Schlegel P, et al. 2020. The natverse, a versatile toolbox for combining and analysing neuroanatomical data. *Elife* 9

Bogovic JA, Otsuna H, Heinrich L, Ito M, Jeter J, et al. 2020. An unbiased template of the Drosophila brain and ventral nerve cord. *PLoS One* 15: e0236495

Bradski, G. 2000. The OpenCV Library. *Dr. Dobb's Journal of Software Tools*.

Braun E, Geurten B, Egelhaaf M. 2010. Identifying prototypical components in behaviour using clustering algorithms. *PLoS One* 5: e9361

Buhmann J, Sheridan A, Malin-Mayor C, Schlegel P, Gerhard S, et al. 2021. Automatic detection of synaptic partners in a whole-brain Drosophila electron microscopy data set. *Nat Methods* 18: 771-74

Cameron P, Hiroi M, Ngai J, Scott K. 2010. The molecular basis for water taste in Drosophila. *Nature* 465: 91-5

Cao G, Platisa J, Pieribone VA, Raccuglia D, Kunst M, Nitabach MN. 2013. Genetically targeted optical electrophysiology in intact neural circuits. *Cell* 154: 904-13

Chen TW, Wardill TJ, Sun Y, Pulver SR, Renninger SL, et al. 2013. Ultrasensitive fluorescent proteins for imaging neuronal activity. *Nature* 499: 295-300

Chen Z, Wang Q, Wang Z. 2010. The amiloride-sensitive epithelial Na+ channel PPK28 is essential for drosophila gustatory water reception. *J Neurosci* 30: 6247-52

Costa M, Manton JD, Ostrovsky AD, Prohaska S, Jefferis GS. 2016. NBLAST: Rapid, Sensitive Comparison of Neuronal Structure and Construction of Neuron Family Databases. *Neuron* 91: 293-311

Dahanukar A, Foster K, van der Goes van Naters WM, Carlson JR. 2001. A Gr receptor is required for response to the sugar trehalose in taste neurons of Drosophila. *Nat Neurosci* 4: 1182-6

Dahanukar A, Lei YT, Kwon JY, Carlson JR. 2007. Two Gr genes underlie sugar reception in Drosophila. *Neuron* 56: 503-16

Gordon MD, Scott K. 2009. Motor control in a Drosophila taste circuit. *Neuron* 61: 373-84

Hampel S, Eichler K, Yamada D, Bock DD, Kamikouchi A, Seeds AM. 2020. Distinct subpopulations of mechanosensory chordotonal organ neurons elicit grooming of the fruit fly antennae. *Elife* 9

Harris DT, Kallman BR, Mullaney BC, Scott K. 2015. Representations of Taste Modality in the Drosophila Brain. *Neuron* 86: 1449-60

Hartenstein V, Omoto JJ, Ngo KT, Wong D, Kuert PA, et al. 2018. Structure and development of the subesophageal zone of the Drosophila brain. I. Segmental architecture, compartmentalization, and lineage anatomy. *J Comp Neurol* 526: 6-32

Horne JA, Langille C, McLin S, Wiederman M, Lu Z, et al. 2018. A resource for the Drosophila antennal lobe provided by the connectome of glomerulus VA1v. *Elife* 7

Huang P, Sahai-Hernandez P, Bohm RA, Welch WP, Zhang B, Nystul T. 2014. Enhancer-trap flippase lines for clonal analysis in the Drosophila ovary. *G3 (Bethesda)* 4: 1693-9

Inagaki HK, Jung Y, Hoopfer ED, Wong AM, Mishra N, et al. 2014. Optogenetic control of Drosophila using a red-shifted channelrhodopsin reveals experience-dependent influences on courtship. *Nat Methods* 11: 325-32

Jaeger AH, Stanley M, Weiss ZF, Musso PY, Chan RC, et al. 2018. A complex peripheral code for salt taste in Drosophila. *Elife* 7

Jefferis GS, Potter CJ, Chan AM, Marin EC, Rohlfing T, et al. 2007. Comprehensive maps of Drosophila higher olfactory centers: spatially segregated fruit and pheromone representation. *Cell* 128: 1187-203

Jenett A, Rubin GM, Ngo TT, Shepherd D, Murphy C, et al. 2012. A GAL4-driver line resource for Drosophila neurobiology. *Cell Rep* 2: 991-1001

Jourjine N, Mullaney BC, Mann K, Scott K. 2016. Coupled Sensing of Hunger and Thirst Signals Balances Sugar and Water Consumption. *Cell* 166: 855-66

Kwon JY, Dahanukar A, Weiss LA, Carlson JR. 2011. Molecular and cellular organization of the taste system in the Drosophila larva. *J Neurosci* 31: 15300-9

Lee T, Luo L. 1999. Mosaic Analysis with a Repressible Cell Marker for Studies of Gene Function in Neuronal Morphogenesis. *Neuron* 22: 451-61

Li F, Lindsey JW, Marin EC, Otto N, Dreher M, et al. 2020a. The connectome of the adult Drosophila mushroom body provides insights into function. *Elife* 9

Li PH, Lindsey LF, Januszewski M, Tyka M, Maitin-Shepard J, et al. 2019. Automated Reconstruction of a Serial-Section EM Drosophila Brain with Flood-Filling Networks and Local Realignment. *Microscopy and Microanalysis* 25: 1364-65

Lima SQ, Miesenbock G. 2005. Remote control of behavior through genetically targeted photostimulation of neurons. *Cell* 121: 141-52

Miroschnikow A, Schlegel P, Schoofs A, Hueckesfeld S, Li F, et al. 2018. Convergence of monosynaptic and polysynaptic sensory paths onto common motor outputs in a Drosophila feeding connectome. *Elife* 7

Miyamoto T, Slone J, Song X, Amrein H. 2012. A fructose receptor functions as a nutrient sensor in the Drosophila brain. *Cell* 151: 1113-25

Miyazaki T, Ito K. 2010. Neural architecture of the primary gustatory center of Drosophila melanogaster visualized with GAL4 and LexA enhancer-trap systems. *J Comp Neurol* 518: 4147-81

Nayak S, Singh R. 1983. Sensilla on the tarsal segments and mouthparts of adult Drosophila melanogaster meigen *Int J Insect Morphol & Embryol* 12: 273-91

Nern A, Pfeiffer BD, Svoboda K, Rubin GM. 2011. Multiple new site-specific recombinases for use in manipulating animal genomes. *Proc Natl Acad Sci U S A* 108: 14198-203

Rajashekhar KP, Singh R. 1994. Neuroarchitecture of the Tritocerebrum of Drosophila melanogaster. *J Comp Neurol* 349: 633-45

Saalfeld S, Cardona A, Hartenstein V, Tomancak P. 2009. CATMAID: collaborative annotation toolkit for massive amounts of image data. *Bioinformatics* 25: 1984-6

Schindelin J, Arganda-Carreras I, Frise E, Kaynig V, Longair M, et al. 2012. Fiji: an open-source platform for biological-image analysis. *Nat Methods* 9: 676-82

Schlegel P, Bates AS, Sturner T, Jagannathan SR, Drummond N, et al. 2021. Information flow, cell types and stereotypy in a full olfactory connectome. *Elife* 10

Schneider-Mizell CM, Gerhard S, Longair M, Kazimiers T, Li F, et al. 2016. Quantitative neuroanatomy for connectomics in Drosophila. *Elife* 5

Scott K, Brady R, Cravchik A, Morozov P, Rzhetsky A, et al. 2001. A Chemosensory Gene Family Encoding Candidate Gustatory and Olfactory Receptors in Drosophila *Cell* 104: 661-73

Shannon P, Markiel A, Ozier O, Baliga NS, Wang JT, et al. 2003. Cytoscape: a software environment for integrated models of biomolecular interaction networks. *Genome Res* 13: 2498-504

Sterne GR, Otsuna H, Dickson BJ, Scott K. 2021. Classification and genetic targeting of cell types in the primary taste and premotor center of the adult Drosophila brain. *Elife* 10

Stocker RF. 1994. The Organization of the Chemosensory System in Drosophila melanogaster: a Review *Cell Tissue Res* 275: 3-26

Takemura SY, Bharioke A, Lu Z, Nern A, Vitaladevuni S, et al. 2013. A visual motion detection circuit suggested by Drosophila connectomics. *Nature* 500: 175-81

Takemura SY, Xu CS, Lu Z, Rivlin PK, Parag T, et al. 2015. Synaptic circuits and their variations within different columns in the visual system of Drosophila. *Proc Natl Acad Sci U S A* 112: 13711-6

Thévenaz P, Ruttimann UE, Unser M. 1998. IEEE Transactions on Image Processing 7(1): 27-41

Thistle R, Cameron P, Ghorayshi A, Dennison L, Scott K. 2012. Contact chemoreceptors mediate male-male repulsion and male-female attraction during Drosophila courtship. *Cell* 149: 1140-51

Thorne N, Chromey C, Bray S, Amrein H. 2004. Taste perception and coding in Drosophila. *Curr Biol* 14: 1065-79

Tobin WF, Wilson RI, Lee WA. 2017. Wiring variations that enable and constrain neural computation in a sensory microcircuit. *Elife* 6

Tseng Q, Wang I, Duchemin-Pelletier E, Azioune A, Carpi N, et al. 2011. A new micropatterning method of soft substrates reveals that different tumorigenic signals can promote or reduce cell contraction levels. *Lab Chip* 11: 2231-40

Virtanen P, Gommers R, Oliphant TE, Haberland M, Reddy T, et al. 2020. SciPy 1.0: fundamental algorithms for scientific computing in Python. *Nat Methods* 17: 261-72

Wang JW, Wong AM, Flores J, Vosshall LB, Axel R. 2003. Two-Photon Calcium Imaging Reveals an Odor-Evoked Map of Activity in the Fly Brain. *Cell* 112: 271-82

Wang Z, Singhvi A, Kong P, Scott K. 2004. Taste representations in the Drosophila brain. *Cell* 117: 981-91

Ward JH. 1963. Hierarchical Grouping to Optimize an Objective Function. *Journal of the American Statistical Association* 58: 236-44

Weiss LA, Dahanukar A, Kwon JY, Banerjee D, Carlson JR. 2011. The molecular and cellular basis of bitter taste in Drosophila. *Neuron* 69: 258-72

Yao Z, Macara AM, Lelito KR, Minosyan TY, Shafer OT. 2012. Analysis of functional neuronal connectivity in the Drosophila brain. *J Neurophysiol* 108: 684-96

Zheng Z, Lauritzen JS, Perlman E, Robinson CG, Nichols M, et al. 2018. A Complete Electron Microscopy Volume of the Brain of Adult Drosophila melanogaster. *Cell* 174: 730-43 e22

Chapter 3: Future Perspectives

Abstract

The present work characterizes the gustatory sensory inputs to the Drosophila brain at synapse level detail. In the course of our studies, we explored the function of GRN-GRN connectivity using calcium and voltage imaging. We found no functional connections between GRNs of different modalities but found that GRNs of the same modality depolarize each other. Furthermore, we characterized the taste response of a second order neuron downstream of sugar GRNs and found it to be selectively responsive to sugar stimuli. Further study is necessary to explore the impact of connectivity between GRNs of different taste modalities. Beyond the level of GRNs, our EM studies also provide a gateway to further explore the gustatory circuit in the EM dataset. These efforts will uncover novel components of the gustatory circuitry as well as elucidate how known feeding-related neurons are connected. Ultimately, such insights will contribute to the characterization of the remaining inputs to GRNs, which are likely targets of extensive top-down modulation.

EM reconstructions of GRNs suggest potential interactions of taste modalities

In this study, we reconstructed 144 Gustatory Receptor Neurons in a whole fly brain EM volume. We manually annotated their synaptic sites and found that the pre and post synaptic sites of GRNs are interspersed. Using combined morphological and connectivity data for clustering, we were able to propose taste modality identities for reconstructed GRNs. Our studies suggested that most GRN-GRN connections exist between neurons of the same taste modality. However, we also found connectivity between proposed sugar and water GRNs, leading us to hypothesize that appetitive GRNs may be functionally connected. We explored this possibility using calcium and voltage imaging and found no functional connections between GRNs of different modalities in fed, food-deprived or pseudo-desiccated flies. We further aimed to explore the function of connections between GRNs of the same modality. For this purpose, we explored whether the activation of a small subset of bitter neurons is sufficient to depolarize other bitter neurons. Our results indicate that this is indeed the case, but further study is necessary. Finally, we characterized a second order gustatory neuron downstream of sugar GRNs in the EM to confirm our identification of GRN taste modality identity and explore the possibility of interactions between taste modalities at the level of second order neurons. We found the second order neuron to selectively respond to sugar but not water or bitter, consistent with its input in the EM. In summary, we laid a foundation for the synapse-level description of the gustatory circuit in Drosophila. Future studies will be necessary to further explore the significance of connectivity between GRNs of the same modality, higher order components of the gustatory circuit and the effect of modulation of GRNs in the brain.

Further study of GRN-GRN connectivity may uncover the function of a conserved motif in sensory circuits

While the interconnectivity of sensory neurons of the same subclass is an emerging theme across sensory modalities (Hampel et al 2020, Horne et al 2018, Miroschnikow et al 2018, Schlegel et al 2021, Takemura et al 2015, Tobin et al 2017), the function of such connectivity remains largely elusive. In our studies, we have been unable to fully address this question due to technical limitations, but it remains an endeavor with widely applicable implications. Higher resolution imaging paradigms, which could allow for the activation and imaging of distinct GRN cell populations, will be necessary to segregate activated and imaged subpopulations accurately. Furthermore, it would be intriguing to conduct experiments in which highly local de- and hyperpolarizations of taste processes can be observed. Interactions between GRNs may have an impact on very small, tightly defined compartments of the taste projection to modulate local release probabilities. Such sub-threshold interactions are not observable using our imaging paradigm.

Additionally, connectivity between GRNs could act on longer time frames than those examined in our studies. Challenging experiments in which the taste responses of GRNs are observed for extended time periods may be necessary to satisfactorily address this question. Clarity about the complete set of neurotransmitters expressed by GRNs may inform hypotheses about the timing of interactions. Furthermore, rigorous characterization of GRNs' neurotransmitter arsenal may also yield a strategy to disrupt GRN-GRN connectivity without directly impacting connections from GRNs to second

order neurons, provided that two distinct neurotransmitter systems underpin these two types of connectivity. Such insight could lead to strategies useful not only in imaging experiments to gain more insight into GRN-GRN interactions, but also in behavioral experiments to explore the biological significance of connectivity between gustatory neurons.

Further exploration of the core feeding circuit will lead to the identification of novel circuit components

To date, a complete adult feeding circuit from GRNs to the motor neurons enervating the musculature of the proboscis has not been described. Both GRNs as well as motor neurons are well studied, as are a handful of second order neurons (Bohra et al 2018, Cameron et al 2010, Gordon & Scott 2009, Jaeger et al 2018, McKellar et al 2020, Miyazaki et al 2015, Wang et al 2004). Additionally, a potential third order neuron with an extensive role in the control of feeding behavior has been proposed in Fdg (Flood et al 2013). How these components are connected in the circuit remains an elusive insight. With the present work, we have established a valuable springboard for the further exploration of the gustatory circuit in the EM dataset, which can lead to the discovery of previously unknown components of the feeding circuit as well as to the clarification of the role of already characterized feeding-related neurons.

To capitalize on this foundation, extensive further reconstruction of interneurons and motor neurons in the SEZ is necessary. This future work also has the potential to elucidate some points that have had to remain partially resolved in this study. For example, reconstruction of second order neurons in the EM, followed by identification of candidate driver lines for genetic access and subsequent characterization of taste response profiles, may help to more firmly establish the identities of GRN subclasses laid out in the present work. We have already begun this process by characterizing FMIn, but additional neurons will provide further insight. These efforts will be further aided by the use of highly specific genetic driver lines utilizing the split gal 4 system (Luan et al 2006, Sterne et al 2021). This approach allows for stable genetic access to small, defined sets of cells and will make imaging and behavioral experiments much more efficient and reproducible.

It will also be enlightening to explore whether extensive interconnections as observed among GRNs exist between neurons in higher tiers of the gustatory circuit. Furthermore, considering that GRN-GRN connectivity accounts for on average 25% of inputs to GRNs, it seems highly likely that feedback from higher feeding circuitry accounts for a part of the input to GRNs. If so, it will be fascinating to explore how feeding activity results in the modulation of sensory inputs.

EM studies will elucidate how neurons outside the core feeding circuit modulate feeding behavior

It is a well-established phenomenon that feeding decisions are impinged upon by higher brain circuits. For example, repeated pairing of a sucrose stimulus to the legs with a bitter stimulus to the proboscis results in a learned rejection behavior upon later encounters of sucrose to the legs. This behavior is dependent on the mushroom body, a region of the fly brain that is essential to learning and memory (Kirkhart & Scott 2015, Leinwand & Scott 2021). It is unclear where this learned behavior impinges upon the core

feeding circuitry to inhibit feeding. Additionally, the feeding state of flies is known to impact not only feeding behavior, but to modulate the responsiveness of gustatory neurons to tastants (Inagaki et al 2012, Inagaki et al 2014, LeDue et al 2016). It is unclear whether this modulation is mediated by an inherent sensitivity of GRNs to thirst and hunger cues, or if it is modulated by neurons monitoring the internal state of the fly, such as the ISNs (Jourjine et al 2016). Further careful study of the fly connectome as well as molecular characterization of neurons will be necessary to gain clarity on these tantalizing issues.

Due to the collaborative nature of the tracing effort in FAFB, many brain regions have been explored simultaneously by groups around the world. As we approach a complete connectome of the fly, these combined efforts can elucidate, at synaptic level detail, how long-distance connections between brain regions and larger circuits are organized. These efforts are further accelerated by new imaging volumes, further optimized for automated segmentations (Li et al 2019, Scheffer et al 2020). By characterizing the inputs of the gustatory system, we have provided insight into how one sensory modality feeds into the fly brain, contributing to the larger endeavor of deciphering the brain connectome.

References

Bohra AA, Kallman BR, Reichert H, VijayRaghavan K. 2018. Identification of a Single Pair of Interneurons for Bitter Taste Processing in the Drosophila Brain. *Curr Biol* 28: 847-58 e3

Cameron P, Hiroi M, Ngai J, Scott K. 2010. The molecular basis for water taste in Drosophila. *Nature* 465: 91-5

Flood TF, Iguchi S, Gorczyca M, White B, Ito K, Yoshihara M. 2013. A single pair of interneurons commands the Drosophila feeding motor program. *Nature* 499: 83-7

Gordon MD, Scott K. 2009. Motor control in a Drosophila taste circuit. *Neuron* 61: 373-84

Hampel S, Eichler K, Yamada D, Bock DD, Kamikouchi A, Seeds AM. 2020. Distinct subpopulations of mechanosensory chordotonal organ neurons elicit grooming of the fruit fly antennae. *Elife* 9

Horne JA, Langille C, McLin S, Wiederman M, Lu Z, et al. 2018. A resource for the Drosophila antennal lobe provided by the connectome of glomerulus VA1v. *Elife* 7

Inagaki HK, Ben-Tabou de-Leon S, Wong AM, Jagadish S, Ishimoto H, et al. 2012. Visualizing neuromodulation in vivo: TANGO-mapping of dopamine signaling reveals appetite control of sugar sensing. *Cell* 148: 583-95

Inagaki HK, Panse KM, Anderson DJ. 2014. Independent, reciprocal neuromodulatory control of sweet and bitter taste sensitivity during starvation in Drosophila. *Neuron* 84: 806-20

Jaeger AH, Stanley M, Weiss ZF, Musso PY, Chan RC, et al. 2018. A complex peripheral code for salt taste in Drosophila. *Elife* 7

Jourjine N, Mullaney BC, Mann K, Scott K. 2016. Coupled Sensing of Hunger and Thirst Signals Balances Sugar and Water Consumption. *Cell* 166: 855-66

Kirkhart C, Scott K. 2015. Gustatory learning and processing in the Drosophila mushroom bodies. *J Neurosci* 35: 5950-8

LeDue EE, Mann K, Koch E, Chu B, Dakin R, Gordon MD. 2016. Starvation-Induced Depotentiation of Bitter Taste in Drosophila. *Curr Biol* 26: 2854-61

Leinwand SG, Scott K. 2021. Juvenile hormone drives the maturation of spontaneous mushroom body neural activity and learned behavior. *Neuron* 109: 1836-47 e5

Li PH, Lindsey LF, Januszewski M, Tyka M, Maitin-Shepard J, et al. 2019. Automated Reconstruction of a Serial-Section EM Drosophila Brain with Flood-Filling Networks and Local Realignment. *Microscopy and Microanalysis* 25: 1364-65

Luan H, Peabody NC, Vinson CR, White BH. 2006. Refined spatial manipulation of neuronal function by combinatorial restriction of transgene expression. *Neuron* 52: 425-36

McKellar CE, Siwanowicz I, Dickson BJ, Simpson JH. 2020. Controlling motor neurons of every muscle for fly proboscis reaching. *Elife* 9

Miroschnikow A, Schlegel P, Schoofs A, Hueckesfeld S, Li F, et al. 2018. Convergence of monosynaptic and polysynaptic sensory paths onto common motor outputs in a Drosophila feeding connectome. *Elife* 7

Miyazaki T, Lin TY, Ito K, Lee CH, Stopfer M. 2015. A gustatory second-order neuron that connects sucrose-sensitive primary neurons and a distinct region of the gnathal ganglion in the Drosophila brain. *J Neurogenet* 29: 144-55

Scheffer LK, Xu CS, Januszewski M, Lu Z, Takemura SY, et al. 2020. A connectome and analysis of the adult Drosophila central brain. *Elife* 9

Schlegel P, Bates AS, Sturner T, Jagannathan SR, Drummond N, et al. 2021. Information flow, cell types and stereotypy in a full olfactory connectome. *Elife* 10

Sterne GR, Otsuna H, Dickson BJ, Scott K. 2021. Classification and genetic targeting of cell types in the primary taste and premotor center of the adult Drosophila brain. *Elife* 10

Takemura SY, Xu CS, Lu Z, Rivlin PK, Parag T, et al. 2015. Synaptic circuits and their variations within different columns in the visual system of Drosophila. *Proc Natl Acad Sci U S A* 112: 13711-6

Tobin WF, Wilson RI, Lee WA. 2017. Wiring variations that enable and constrain neural computation in a sensory microcircuit. *Elife* 6

Wang Z, Singhvi A, Kong P, Scott K. 2004. Taste representations in the Drosophila brain. *Cell* 117: 981-91